

TECHNICAL REPORT DOCUMENTATION PAGE

1. Report No. NURail2014-UTK-R10	2. Government Accession No.	3. Recipient's Catalog No.	
4. Title and Subtitle Seismic Performance of Stone Masonry and Unreinforced Concrete Railroad Bridge Piers		5. Report Date January 9, 2020	
		6. Performing Organization Code	
7. Author(s) Qiang Gui; Z. John Ma, Ph.D. P.E; Richard Bennett, Ph.D.; David Clarke, Ph.D, P.E.		8. Performing Organization Report No. NURail2014-UTK-R10	
9. Performing Organization Name and Address Center for Transportation Research The University of Tennessee, Knoxville 309 Conference Center Building Knoxville, TN 37996-4133		10. Work Unit No.	
		11. Contract or Grant No. USDOT Grant# DTRT13-G-UTC52	
12. Sponsoring Agency Name and Address National University Rail (NURail) Center University of Illinois at Urbana-Champaign 1239B Newmark Engineering Laboratory, MC-250 205 N. Mathews Ave Urbana, IL 61801		13. Type of Report and Period Covered Final Report (2014-2019)	
		14. Sponsoring Agency Code	
15. Supplementary Notes			
16. Abstract Numerous railroad bridge structures in the United States were constructed more than 100 years ago. With railroad infrastructure aging quickly, there is a push to reuse existing substructures while replacing entire superstructures. Often, these substructures are unreinforced concrete (URC) or unreinforced masonry (URM). In order for these URC or URM elements to be accepted for an extended design life, they must be evaluated for their ability to withstand seismic loading. The research objective of this project is to investigate the mechanism of the behavior, especially failure modes, of the URM and URC piers that are subject to earthquake loads and propose mitigation or retrofit methods for these types of structures.			
17. Key Words Transportation, Railroad Bridges, Bridges, Railroad Transportation, Freight Transportation, Rail Infrastructure		18. Distribution Statement No restrictions.	
19. Security Classif. (of this report) Unclassified	20. Security Classif. (of this page) Unclassified	21. No. of Pages 144	22. Price



National University Rail Center - NURail
US DOT OST-R Tier 1 University Transportation Center

NURail Project ID: NURail2014-UTK-R10

Seismic Performance of Stone Masonry and Unreinforced Concrete Railroad Bridge Piers

By

Qiang Gui

PhD student

Department of Civil and Environmental Engineering

University of Tennessee Knoxville (UTK)

qgui@vols.utk.edu

Z. John Ma

Professor

Department of Civil and Environmental Engineering

University of Tennessee Knoxville (UTK)

zma2@utk.edu

Richard Bennett

Professor and Director of Engineering Fundamentals

Department of Civil and Environmental Engineering

University of Tennessee Knoxville (UTK)

rbennet2@utk.edu

David Clarke

Research Associate Professor and Director

Center for Transportation Research

University of Tennessee Knoxville (UTK)

dclarke@utk.edu

January 9, 2020

Grant Number: DTRT13-G-UTC52 (Grant 2)

DISCLAIMER

Funding for this research was provided by the NURail Center, University of Illinois at Urbana - Champaign under Grant No. DTRT13-G-UTC52 of the U.S. Department of Transportation, Office of the Assistant Secretary for Research & Technology (OST-R), University Transportation Centers Program. The contents of this report reflect the views of the authors, who are responsible for the facts and the accuracy of the information presented herein. This document is disseminated under the sponsorship of the U.S. Department of Transportation's University Transportation Centers Program, in the interest of information exchange. The U.S. Government assumes no liability for the contents or use thereof.

ACKNOWLEDGMENTS

This research was supported by the National University Rail (NURail) Center, a US DOT OST-R Tier 1 University Transportation Center. The financial support provided by the Center for Transportation Research and the Department of Civil and Environmental Engineering at University of Tennessee, Knoxville is much appreciated.



TECHNICAL SUMMARY

Title:

Seismic Performance of Stone Masonry and Unreinforced Concrete Railroad Bridge Piers

Introduction

Numerous railroad bridge structures in the United States were constructed more than 100 years ago. With railroad infrastructure aging quickly, there is a push to reuse existing substructures while replacing entire superstructures. Often, these substructures are unreinforced concrete (URC) or unreinforced masonry (URM). In order for these URC or URM elements to be accepted for an extended design life, they must be evaluated for their ability to withstand seismic loading.

The research objective of this project is to investigate the mechanism of the behavior, especially failure modes, of the URM and URC piers that are subject to earthquake loads and propose mitigation or retrofit methods for these types of structures.

Compared to highway bridges, railroad bridges typically have better seismic performance. The track system is considered a contributor to this better performance because it can act as a restraint against horizontal movement of the superstructure during earthquakes.

Based on the observation on the URC and URM railroad bridge piers in previous earthquakes, we find that the behavior of this type of pier is prone to include sliding and rocking, which are typical rigid body motions. Thus, this study proposes to simplify the railroad piers into a single-body or into stacked multi-body rigid block systems with a horizontal restraint at the top and understand the behavior of this type of system when subjected to various ground motions.

Approach and Methodology

First, we conducted a literature review to investigate the typical damage modes of the existing URM and URC railroad bridge piers in past earthquakes, and we found that railroad bridges performed well in past earthquakes. The track system, which restrains the horizontal movement of the pier top subject to earthquake loading, contributes to this better performance. The theoretical analysis on this restraining effect has not been addressed in previous studies where only full-scale tests were conducted.

Then, in order to quantify the equivalent spring stiffness of the restraining effect, a structure modeling scheme was proposed in SAP2000 using a nonlinear link element to simulate the behavior of bearings and ballast structure under lateral pushing. The experimental data from previous studies were used to calibrate and verify the proposed modeling scheme. Then this scheme was used to investigate the influence of the lateral stiffness and rotational stiffness of the substructure on the performance of bridge structure, with rail track intact, under lateral pushover load.

Based on observations of the URC/URM railroad bridge piers in previous earthquakes, we found that the behavior of these types of piers is prone to include sliding and rocking, which are typical for rigid body motions. Therefore, this study proposes to simplify the railroad piers into a single-body or stacked dual-body rigid block system with a horizontal restraint at the top. We will examine the behavior of this type of system when subjected to various ground motions. A series of rigid-body dynamic tests were conducted by using the teaching shaking-table facilitated in the High Bay Lab at the University of Tennessee. The restraining effect was verified by the testing data.

Conclusions

The major conclusions are summarized below:

1. We synthesized and summarized the performance records found in the published literature and databases of old URM and URC railroad bridge piers in past earthquakes. The recorded damages are tabulated in Appendix A. We found that old railroad bridge structures had historically performed well in earthquakes. However, as minimal as the damage appeared, it is highly possible the damage will be severe, which means the bridges were severely damaged or collapsed, and this affected railroad traffic after the earthquakes.
2. Typical failure modes of URM and URC railroad bridge piers under earthquake loads include: (1) integral horizontal or vertical displacement or tilting integrally; (2) horizontal cracking along construction joints in URC piers; (3) cracking of mortar joints in brick or stone masonry piers; (4) sliding along the horizontal run-through cracks; (5) tilting of the

upper portion of piers after the formation of horizontal run-through cracks; (6) coping stone failure, e.g., loosened, displaced or torn; and (7) anchorage failure between bearings and piers. This result is expected to benefit the evaluation of the theoretical analytical results and the selection of the retrofit measures.

3. To quantify the track's influence on the lateral behavior of a railroad bridge system under lateral load at the end of a span, we implemented a nonlinear three-dimensional model analyses for both the ballast bridge and the open-deck girder bridge in SAP2000, and we validated our results based on experimental research discovered in the literature. This leads to several conclusions: (1) The SAP2000 model is proposed in this study by using the link element to simulate the nonlinear behavior of bearings and ballast. The model results reach a reasonable agreement with the previous full-scale field experimental results on both open-deck and ballast railroad bridges regarding the fundamental frequency and mode type and the force-displacement behavior before the ultimate state. (2) For the open-deck girder bridge model, the secant stiffness of the bridge system increases with the increase of the lateral stiffness of the substructure; the model with higher pier stiffness has a smaller ultimate displacement. We found that the failure of the bridge system is governed by the bearing capacity for a stiffer substructure and by the rail steel failure for a substructure with less lateral stiffness. (3) For open-deck bridge models, the rotational stiffness of the substructure has minor impact on the secant lateral stiffness of the bridge system. The stress of the rail steel remains at a low level. At the ultimate state the excessive bearing deformation is observed. (4) For ballast bridge models, the secant stiffness of the bridge system increases when the lateral stiffness of the substructure increases. Due to the existence of ballast between the rail track and the bridge girder, the lateral displacement and tensile stress of the rail steel remains small. The bridge system reaches the ultimate state when the bearing reaches the lateral displacement capacity. (5) For ballast bridge models, as the rotational stiffness of the substructure decreases, the secant lateral stiffness of the bridge structure system decreases. Meanwhile, the ultimate load and corresponding system lateral displacement at ultimate state increases. The bridge system reaches the ultimate state due to the excessive lateral deformation of the bearing. (6) A range of secant stiffness is obtained for both open-deck and ballasted bridges with the rail intact between each span subject to lateral load.

4. URM and URC piers are inherently weak under seismic loading due to the presence of mortar joints or construction joints. As mentioned earlier, the major damage modes are relative sliding between the top and bottom portions of the piers and rocking of the top portion of the piers. In order to limit the relative movement between the top and bottom portions, the effective and relatively easy-to-deploy retrofit method, among the methods reviewed in this study, may be the external prestressing method that stresses the plain piers vertically with external prestressing cables.

Recommendations

In this study, we propose the following recommendations:

1. Researchers should employ large-scale or full-scale experiment studies by using the shaking table method or the quasi-static cyclic loading method. A preliminary testing design for a large-scale quasi-static cyclic load experiment is attached in Appendix B.
2. Similar to the rail track system, the performance of the bridge bearings influences the railroad bridge seismic performance. Researchers should investigate the mechanism of various types of railroad bridge bearings subject to the dynamic load. The preliminary literature review on this topic is summarized in Appendix C.

Primary Contact

Z. John Ma
Professor
Department of Civil and Environmental Engineering
University of Tennessee Knoxville (UTK)
zma2@utk.edu

David Clarke
Research Associate Professor and Director
Center for Transportation Research
University of Tennessee Knoxville (UTK)
dclarke@utk.edu

NURail Center
217-244-4999
nurail@illinois.edu
<http://www.nurailcenter.org/>

TABLE OF CONTENTS

1. INTRODUCTION.....	1
1.1 Motivation.....	1
1.2 Goals and Methodology.....	1
1.3 Structure of the Report.....	2
2. SEISMIC PERFORMANCE OF UNREINFORCED MASONRY (URM) AND UNREINFORCED CONCRETE (URC) RAILROAD BRIDGE PIERS: STATE-OF-THE-ART	2
2.1 Introduction.....	2
2.2 Previous Seismic Research on Railroad Bridges	4
2.3 Seismic Performance of URM and URC Railroad Bridges Piers in Past Earthquakes.....	9
2.4 Seismic Design.....	16
2.4.1 AREMA MRE 2018	16
2.4.2 AASHTO LRFD Bridge Design Specifications 2017	18
2.4.3 AREMA MRE 1907	22
2.4.4 Code for Seismic Design of Railway Engineering (GB50111-2006 [2009 Edition]) in China	23
2.5 Seismic Assessment.....	27
2.6 Seismic Retrofit	30
2.7 Conclusions and Recommendations	34
3. RESTRAINING EFFECT OF RAIL TRACK STRUCTURE ON THE PERFORMANCE OF RAILROAD BRIDGE UNDER LATERAL LOAD	35
3.1 Introduction.....	35
3.2 Modeling Based on Previous Experimental Studies.....	37
3.2.1 Modeling for Uppal et al. (2000) testing	37
3.2.2 Modeling for Maragakis et al. (2001) testing	43
3.3 Results and Model Verification	46
3.3.1 Natural frequencies and modal analysis	46
3.3.2 Load-displacement curve	47

3.4 Discussion	51
3.4.1 Influence of lateral stiffness of substructure	52
3.4.2 Influence of rotational stiffness of substructure.....	60
3.5 Conclusions.....	66
4. SHAKING TABLE EXPERIMENT RESULTS AND DISCUSSION	67
4.1 Introduction.....	67
4.2 Testing Program.....	68
4.3 Testing Result and Discussion	75
4.3.1 Coefficient of friction	75
4.3.2 Failure mode under sinusoidal input.....	75
4.3.3 Restraining effect	77
4.4 Conclusions.....	77
5. CONTRIBUTIONS AND RECOMMENDATIONS	78
REFERENCES	80
APPENDICES	87
APPENDIX A. SUMMARY OF RECORDED DAMAGES OF URM AND URC RAILROAD BRIDGE PIERS IN PAST EARTHQUAKES.....	88
APPENDIX B. PRELIMINARY QUASI-STATIC CYCLIC LOADING TESTING PLAN	101
B.1 Specimens.....	101
B.2 Lateral Loading System	110
B.3 Vertical Loading System.....	110
B.4 Bearing System	110
B.5 Rail System	111
B.6 Footing and Anchorage System	113
B.7 Instrument System.....	114
B.8 Loading Protocol	118
B.9 Prototype Pier	119
REFERENCES:	123

APPENDIX C. SUMMARY OF PREVIOUS EXPERIMENTAL STUDIES ON BRIDGE BEARING	124
REFERENCES:	126
APPENDIX D. TEAM MEMBERS	127

LIST OF TABLES

Table 2.1 Summary of the Dynamic Experimental Results by UNR (Sandirasegaram 1997)	7
Table 2.2 Minimum Analysis Requirements for Seismic Effects (AASHTO 2017).....	19
Table 2.3 Response Modification Factors for Substructures (AASHTO 2017)	21
Table 2.4 Response Modification Factors for Connections (AASHTO 2017).....	21
Table 2.5 Seismic Design Checking Requirements (NRA China 2009)	25
Table 3.1 Frequencies and Mode Types of First Three Vibration Modals	47
Table 3.2 Influence of Substructure Lateral Stiffness on System Secant Stiffness for Open-deck Bridge Models	54
Table 3.3 Influence of Substructure Lateral Stiffness on System Secant Stiffness for Ballast Bridge Models.....	58
Table 3.4 Influence of Substructure Rotational Stiffness on System Secant Stiffness for Open-deck Bridge Models	62
Table 3.5 Influence of Substructure Rotational Stiffness on System Secant Stiffness for Ballast Bridge Models.....	65
Table 4.1 Instrumentation List	69
Table 4.2 Geometries of Blocks.....	71
Table 4.3 Test Matrix.....	72
Table 4.4 Failure Mode Results of Single-body Specimens without Restraint under Sinusoidal Waves.....	76
Table B.1 Weigh Proportions of Cement and Sand for Mortar (Baker 1917).....	102
Table B.2 Properties of Masonry Used for Specimen Strength Estimation	102
Table B.3 Types of Stone Units	103
Table B.4 Testing Matrix	104
Table B.5 Estimated Failure Mode and Ultimate Strength of Specimen 1 and 2.....	110
Table B.6 Instrument List (Specimen 1 and 3)	114
Table B.7 Instrument List (Specimen 2 and 4)	115
Table B.8 Instrument List (Specimen 5).....	117
Table B.9 Instrument List (Specimen 6).....	118

Table B.10 Targeted Deformation Amplitude in Each Step..... 118
Table B.11 Compressive Strength of Material Samples..... 121

LIST OF FIGURES

Figure 2.1 Rail Track Mileage and Number of Class I Rail Carriers, United States, 1830-2012 (Rodrigue 2015)	3
Figure 2.2 Damaged Railroad Bridge and the Crack at the Pier (Abé and Shimamura 2014)	6
Figure 2.3 Locations of damaged URM and URC railroad bridge piers in fault line map	12
Figure 2.4 Displacement of Piers of the Pajaro River Bridge after 1906 San Francisco Earthquake (Duryea and ASCE 1907)	13
Figure 2.5 Cracking Damage at the Base of a URC Pier of Pajaro Bridge after 1906 San Francisco Earthquake (Duryea and ASCE 1907)	13
Figure 2.6 Cracking Damage of a URM Pier of Dos Pueblos Viaduct after 1925 Santa Barbara Earthquake (Kirkbride 1927)	14
Figure 2.7 Sliding at a URC Pier of Kuzuryu River Bridge after 1948 Fukui Earthquake (Far East Command 1949)	14
Figure 2.8 Tilting of Upper Partition of URC Piers of Dou River Railway Bridge after 1976 Tangshan Earthquake (Chen 1978)	15
Figure 2.9 Damage at the Coping stone of a URC Pier of Pajaro Bridge after 1906 San Francisco Earthquake (Duryea and ASCE 1907)	15
Figure 2.10 Anchorage Failure at the Bearing of a URC Pier of Bridge 14.5 after 1964 Alaska Earthquake (McCulloch and Bonilla 1970)	16
Figure 2.11 Typical Cross-section Layout of Steel Jacketing Retrofit (Priestley et al. 1996)	31
Figure 2.12 Typical Layout of Concrete Jacketing Retrofit (Priestley et al. 1996)	32
Figure 2.13 Construction of the RC Jacket Retrofitting at a URM Pier of the Illinois Central Railroad Cairo Bridge over the Ohio River (Modjeski and Masters 1953)	33
Figure 2.14 External Prestressing Retrofit at a URC Railroad Bridge Pier in New Zealand (Walsh 2002)	34
Figure 3.1 Plan View of Lateral Push Tests on the Cincinnati Bridge (Uppal et al. 2000)	38
Figure 3.2 Correlation between SAP2000 Model and Physical Bridge (Pier 16 of Cincinnati bridge)	39
Figure 3.3 Constitutive Law of Rail Steel in Modeling	40
Figure 3.4 Stiffness of Ballast under Lateral Load in Modeling (after Kerr, 1980)	42

Figure 3.5 Stiffness of Bearing under Lateral Load in Testing and in Modeling for the Cincinnati Bridge	43
Figure 3.6 Typical Pier Condition in the Cincinnati Bridge (Uppal et al. 2000).....	44
Figure 3.7 Plan-view Layout of Lateral Push Tests of the California Bridge (Maragakis et al. 2001)	45
Figure 3.8 Stiffness of Bearing under Lateral Load in Testing and in Modeling for the California Bridge	45
Figure 3.9. Constitutive Law of Plain Concrete in Modeling	46
Figure 3.10 Load vs. Displacement of Modeling Results (Cincinnati Bridge)	48
Figure 3.11 Comparison of Experimental and Modeling Results (Span 16 @abutment, Cincinnati Bridge).....	49
Figure 3.12 Comparison of Experimental and Modeling Results (Span 17 @pier 16, Cincinnati Bridge).....	50
Figure 3.13 Load vs. Displacement of Modeling Results (California Bridge).....	51
Figure 3.14 Comparison of Experimental and Modeling Results (East span, California Bridge)	52
Figure 3.15 Influence of Lateral Stiffness of Substructure on Load vs. Displacement (open-deck bridge)	53
Figure 3.16 Influence of Lateral Stiffness of Substructure on Tensile Stress in Rail (Open-deck Bridge)	53
Figure 3.17 Relationship between Substructure Lateral Stiffness and Secant Stiffness for Open-deck Bridge System	54
Figure 3.18 Influence of Lateral Stiffness of Substructure on Displacement at Different Position (Open-deck Bridge)	56
Figure 3.19 Influence of Lateral Stiffness of Substructure on Load vs. Displacement (ballast bridge)	57
Figure 3.20 Influence of Lateral Stiffness of Substructure on Tensile Stress in Rail (Ballast Bridge).....	57
Figure 3.21 Relationship between Substructure Lateral Stiffness and Secant Stiffness for Ballast Bridge System.....	58
Figure 3.22 Influence of Lateral Stiffness of Substructure on Displacement at Different Position (Ballast Bridge).....	59
Figure 3.23 Torsion with Respect to Pier Centerline Axis	60

Figure 3.24 Influence of Torsional Stiffness of Substructure on Load vs. Displacement (Open-deck Bridge)	61
Figure 3.25 Influence of Torsional Stiffness of Substructure on Tensile Stress in Rail (Open-deck Bridge)	61
Figure 3.26 Relationship between Substructure Rotational Stiffness and Secant Stiffness for Open-deck Bridge System.....	62
Figure 3.27 Influence of Rotational Stiffness of Substructure on Displacement at Different Position (Open-deck Bridge).....	63
Figure 3.28 Influence of Torsional Stiffness of Substructure on Load vs. Displacement (Ballast Bridge).....	64
Figure 3.29 Influence of Torsional Stiffness of Substructure on Tensile Stress in Rail (Ballast Bridge).....	64
Figure 3.30 Relationship between Substructure Rotational Stiffness and Secant Stiffness for Ballast Bridge System	65
Figure 3.31 Influence of Rotational Stiffness of Substructure on Displacement at Different Position (Ballast Bridge)	66
Figure 4.1 a) Single-body and b) Dual-body Prismatic Block Systems	68
Figure 4.2 Example application of Tracker 5.0.5 in this study.....	70
Figure 4.3 Frame for Spring Restraint Attachment and Testing Setup.....	70
Figure 4.4 a) Ground Acceleration Time History and b) FFT Power Spectrum of NORTHR_MUL009 Record.....	73
Figure 4.5 a) Ground Acceleration Time History and b) FFT Power Spectrum of IMPVALL_E06140 Record.....	74
Figure 4.6 a) Ground Acceleration Time History and b) FFT Power Spectrum of GAZLI_GAZ000 Record.....	74
Figure 4.7 Coefficient of Friction Measurement Setup	75
Figure 4.8 Force-displacement Data for Coefficient of Friction Measurement.....	76
Figure 4.9 Response Time-history Comparison for X-direction Tip Displacement of Dual-body System w/ and w/o Horizontal Restraint under Earthquake NORTHR_MUL009, 1 in.=25.4 mm.....	78
Figure B.1 Elevation and Lateral View of Specimen	103
Figure B.2 Unit Layout in Courses with Even Number.....	104
Figure B.3 Unit Layout in Courses with Odd Number	104

Figure B.4 Loading Direction	105
Figure B.5 Proposed Test Setup for Specimen 1 and 3	106
Figure B.6 Proposed Test Setup for Specimen 2 and 4	107
Figure B.7 Proposed Test Setup for Specimen 5	108
Figure B.8 Proposed Test Setup for Specimen 6	109
Figure B.9 Proposed Bearing for Specimen 5 and 6.....	111
Figure B.10 Dimension of commonly used rail (S-10020).....	112
Figure B.11 A36/A572-50 Steel I Beam S 3 x 5.7 lb (3.00" x .170" x 2.33").....	112
Figure B.12 Layout of common used rail-spike system	113
Figure B.13 Layout of commonly used rail-fastening system.....	113
Figure B.14 Instrument Layout of Specimen 1 and 3	114
Figure B.15 Instrument Layout of Specimen 2 and 4.....	115
Figure B.16 Instrument Layout of Specimen 5.....	116
Figure B.17 Instrument Layout of Specimen 6.....	117
Figure B.18 Proposed Loading History	119
Figure B.19 Elevation and Lateral Views of a Pier of Cairo RR Bridge.....	120
Figure B.20 Layout and Dimension of Masonry Courses	121
Figure B.21 Bearing Details	122
Figure B.22 Bearing Anchorage Details.....	122

1. INTRODUCTION

1.1 Motivation

The railroad infrastructure in the United States includes many bridges that are 100 years old or older (U.S. Govt. Accountability Office 2007). A common approach to bridge replacement is to reuse the existing substructure while replacing the superstructure. Often, the substructure is unreinforced masonry (URM) or unreinforced concrete (URC) piers. In order to use the URM and URC piers in an extended design life, they must be evaluated for their ability to withstand seismic loading.

1.2 Goals and Methodology

The objective of this project is to investigate the behavior and failure modes of URM and URC piers subject to earthquake loads and propose mitigation or retrofit methods for these structural elements.

A literature review was conducted to investigate the behavior and damage patterns of URM and URC railroad bridge piers in past earthquakes. It was found that railroad bridges generally performed well in past earthquakes. The track system, which restrains the horizontal movement of the pier top, is considered to contribute to the good performance. The theoretical analysis on this restraining effect has not been addressed in previous studies.

To quantify an equivalent spring stiffness of the restraining effect, we proposed a structure modeling scheme in SAP2000. It uses nonlinear link elements to simulate the behavior of the bearings and the ballast track structure under lateral forces. Experimental data from previous studies is used to calibrate and verify the proposed modeling scheme. This model is employed to investigate the influence of lateral stiffness and rotational stiffness of the substructure on the performance of the bridge structure under lateral pushover load with rail track intact.

Based on observations of previous earthquakes and their impact on URC/URM railroad bridge piers, where the piers slide and rock, this study proposes to simplify the railroad piers into single-body or stacked dual-body rigid block systems with horizontal restraints at the top. It then examines the behavior of these systems when subjected to various ground motions. A series of rigid-body dynamic tests were conducted, and the restraining effect was verified by the testing data.

1.3 Structure of the Report

Section 2 presents the literature review of previous studies on seismic performance of railroad bridges; seismic performance of existing URM and URC railroad bridge piers; failure modes of URM and URC piers (tabulated in Appendix A); and seismic design, assessment, and retrofit requirements in the major codes around the world.

Section 3 develops the numerical investigation of the equivalent spring stiffness of the restraining effect of the rail track system. A structural analysis model of the rail track structure under lateral pushing load treats the rail as a continuous beam with spring support at each anchor position between the rail and ties. The connection between the ties and the bridge superstructure is modeled as a rigid link for open deck railroad bridges and as a spring link for ballasted deck railroad bridges. The proposed model is verified with the data from previous full-scale field testing. A parametric study is conducted for a range of the stiffness of the rail track structure under lateral loading.

Section 4 describes the experimental investigation of the dynamic response of column shaped rigid body specimens with a spring restraint on the top. Several parameters are considered in the test matrix: stiffness of restraint spring, height/breadth ratio, ground excitations and single-body or multi-body configurations. The testing results are discussed.

Lastly, Section 5 summarizes the contributions and recommendations of this study.

2. SEISMIC PERFORMANCE OF UNREINFORCED MASONRY (URM) AND UNREINFORCED CONCRETE (URC) RAILROAD BRIDGE PIERS: STATE-OF-THE-ART

2.1 Introduction

In 1830, the first U.S. railroad for commercial transport of passengers and freight opened, built by the Baltimore & Ohio Railroad (America's Library 2015). After 185 years, the railroad network in the U.S. has reached approximately 140,000 miles (Rodrigue 2015). It has played an important role in the development of the United States, and it dominated the transportation market before the construction of modern highways.

Railroad mileage peaked in 1916 with 254,000 route-miles (Rodrigue 2015), as shown in **Figure 2.1**. From the 1920s, the industry entered a long period of decline. The vast majority of railroad bridges surviving today were constructed between 1890 and 1930 (Solomon 2008). According to a 1993 bridge survey by Federal Railroad Administration (FRA), more than half of the U.S. railroad bridges were built before 1920 (U.S. Govt. Accountability Office 2007).

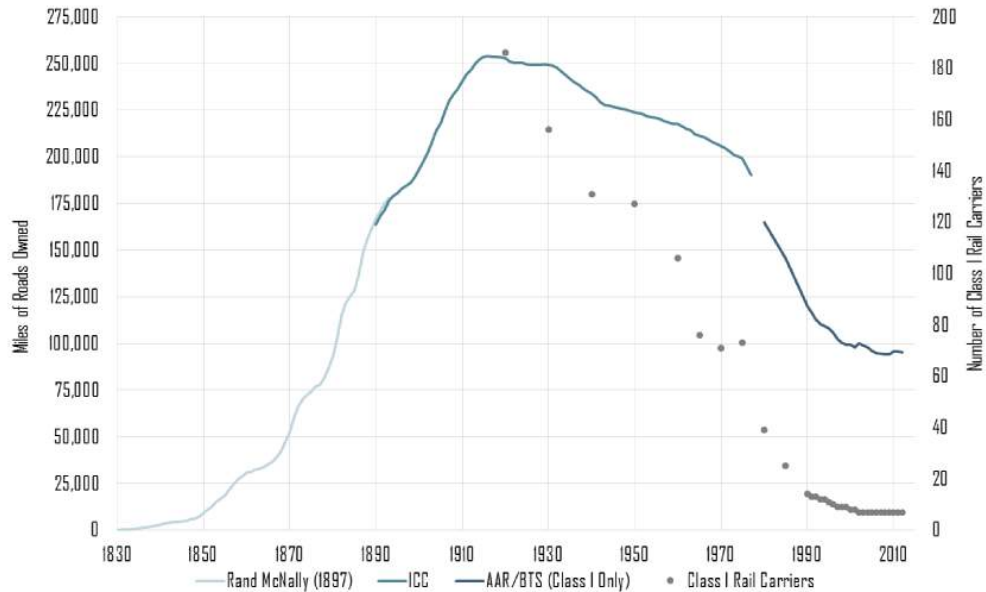


Figure 2.1 Rail Track Mileage and Number of Class I Rail Carriers, United States, 1830-2012 (Rodrigue 2015)

In 1887, the Pennsylvania Railroad began to replace wooden bridges with masonry structures on its east-west Main Line. After that, masonry viaducts dominated the structural type of railroad bridges in North America until the emergence of concrete structures in the first decade of the twentieth century (Tyrrell 1911). The advantages of masonry bridges are that they are solidly built, requiring minimal maintenance under normal conditions; they can withstand the continued increase of axle weights and train speeds; and they are less likely to be washed out (Solomon 2008). This may explain why, as old building material, masonry structures represent 20% of the 76,000 railroad bridges in the U.S. (U.S. Govt. Accountability Office 2007).

Because of the important role of the railroad network, it would be a disaster if the railroad system were damaged or disrupted by an earthquake. Based on research into railroad bridges in the Mid-American region, Day and Barkan (2003) point out that the total length of all bridges in the areas potentially exposed to damaging Peak Ground Acceleration levels (2% probability of experiencing greater than 0.2 g in the next 50 years) is about 306,800 ft. (58 mi.). Eight bridges across the Ohio and Mississippi Rivers carry about 245 million revenue tons of freight per year, accounting for 11.4% of the national total rail freight originating in the United States. Thus, sufficient seismic research on railroad bridges should be conducted to protect railroad bridges and networks properly in order to prevent devastation on national operations caused by bridge failures after earthquakes.

2.2 Previous Seismic Research on Railroad Bridges

The U.S. railroad community has undertaken several efforts related to seismic research in the past 25 years. In 1993, the American Railway Engineering and Maintenance-of-Way Association (AREMA) established a stand-alone committee (AREMA Committee 9) to develop seismic design guidelines specific to railway structures. In 1997, the U.S. Department of Transportation and the Japanese Ministry of Transport signed an agreement to improve the general understanding of the behavior of railway structures in earthquakes and reduce the potential for casualties, damage, and traffic disruption (Prucz and Otter 2002).

Many of these efforts focus on the seismic performance of railroad systems in past earthquakes. Byers investigated railroad damage in 20 notable earthquakes with magnitudes greater than 6 (Byers 1996). He demonstrated that the most frequent reason for damage was soil movement caused by liquefaction or lateral spreading at stream banks, and shaking. Since 1940, Byers (1996) says the seismic performance of railroad bridges is superior to highway bridges.

Prucz and Otter (2002) constructed a database of about 3,500 railway structures located in earthquake-prone areas. The bridge data include information on each bridge's structural characteristics (i.e., type, length, height, number of spans, and span length) as well as information on seismic performance. This study includes a general description of the performance of railway structures during the 1886 Charleston Earthquake, the 1906 San Francisco Earthquake, and the 1964 Alaska Earthquake, all of which caused extensive damage. It found that damage to railroad bridges has been relatively limited. Several factors that contribute to this good seismic response to ground shaking include: (1) proper selection of structure type and configuration, as well as sound design; (2) characteristics such as simplicity, symmetry, and regularity; and (3) proper consideration of details such as the bearing seat. Current railroad bridge design and construction practices typically follow these requirements.

Byers summarized seismic damages to railroads around the world in 93 earthquakes from 1886 through 2003 (Byers 2003). He collected more than 580 photographs that illustrate damage to railroad systems after earthquakes. Data related to railroad damage and earthquake characteristics as well as the sources of the data were listed in a spreadsheet. The type and severity of damage are also included in this spreadsheet. Researchers can use this database to further analyze and improve understanding of railroad structure response to seismic activity.

Based on his 2003 database, Byers (2004) analyzed the characteristics of damaging earthquakes, railroad damage mechanisms, and effects on operations and recovery by

introducing examples from numerous earthquakes. Damage that affected railroad operations after earthquakes included derailments and damage to bridges, tunnels, tracks and roadbed, railroad buildings and signals, and communication facilities. He concluded that: (1) railroads are apt to suffer from severe impact when they span active faults; (2) generally speaking, a comprehensive recovery plan might be a more economical solution to reduce impact of earthquakes than retrofitting.

In 2001, three significant earthquakes occurred around the world: the magnitude (M) 7.7 Gujarat Earthquake, the M6.8 Nisqually Earthquake, and the M8.4 Atico Earthquake. Byers examined the damage to railroad infrastructure, track, roadbed, bridges, tunnels, and buildings during these strong shocks (Byers 2004). He reported the following: track and roadbed damage resulted from settlement, slides, and rock falls; damage to railroad bridges included minor displacement of steel girder spans, cracking of joints in masonry piers and arches, separation of wing walls from abutments, collapse of masonry spandrel walls of arches, rotation and displacement of a framed dump bent in a timber trestle, and movement of piers of an open bascule span that prevented closing of the span; and that damage to tunnels was minor. Byers pointed out that, with appropriate operating restrictions, cracking along mortar joints within masonry piers and large displacement between abutment and roadbed might not significantly impact the safe operation of trains after earthquakes.

Abé and Shimamura reported on the performance of railway bridges along the Shinkansen line during the 2011 Tohoku Earthquake and several aftershocks (Abé and Shimamura 2014). Bridge structures of the Shinkansen line were retrofitted and upgraded to the updated seismic design code after severe structural damage was observed in the 1995 Kobe Earthquake. With this strategy, bridge damage was reduced considerably and the time for recovery of service operation was decreased correspondingly. No major damage is reported for structures that had been retrofitted to the post-1995 earthquake code. Despite this design code a severe crack along the bed joint was observed at a brick masonry pier (shown in **Figure 2.2**). Excessive deformations of rail tracks were also observed at this bridge. A structural monitoring and an alarm system detected this behavior during the shock and gave warning.

Several studies have focused on seismic experimental and theoretical research into railroad bridges. Sharma et al. examined the design criteria used for railway bridges during the past century and analyzed their beneficial effects on the seismic performance for railway bridges (Sharma et al. 1994). The values of longitudinal force for open deck spans with various spans by chronological railroad design code were normalized to equivalent acceleration (g). Sharma et al. concluded that the design equivalent acceleration values for longitudinal forces based on railway design criteria were generally higher than 0.4g, the maximum value of Effective Peak Acceleration (EPA) in the

western regions of the continent. The contribution to longitudinal resistance from the rail track structure was discussed since the track provides an additional restraint and a



Figure 2.2 Damaged Railroad Bridge and the Crack at the Pier (Abé and Shimamura 2014)

mechanism for transferring seismic loads to roadbeds and helps relieve the substructure of carrying all of the seismic load demand.

Railroad bridges had better seismic performance during past earthquakes than highway bridges (Byers 1996, Cook et al. 2006). The track system contributed to this improved performance because it acts as a restraint against horizontal movement of the superstructure during earthquakes (AREMA 2018). To verify this assumption, a series of field tests were conducted from 1994 to 2000 in the U.S.

- (1) From 1994 to 1995, two full-scale field tests on a railroad ballast deck through-plate girder (TPG) bridge were conducted by the Association of American Railroads (AAR), the California Department of Transportation (Caltrans), and the University of Nevada Reno (UNR). One of the tests was designed to quantify the beneficial effects of the dynamic response of the bridge of the connection that the rails provide between the structure and the adjacent roadbed (Maragakis et al. 1996; Sandirasegaram 1997). The bridge was excited in both the transverse and longitudinal directions by a dynamic shaker, with rails intact and rails cut at the abutments, respectively. Natural frequencies and the corresponding mode shapes and modal damping values were identified based on the analysis of the field data from the resonance tests (as shown in **Table 2.1**).

The authors concluded that: (a) in all cases, cutting the rails resulted in lower natural frequencies, which indicates a softer system; (b) no significant effects on the modal damping values were observed, with the exception of the modal

damping of the fundamental transverse frequency; and (c) in the longitudinal direction, disconnecting the rails resulted in a sudden decrease of the vibrations that were transmitted to the roadbed. The authors mentioned that the effect of cutting the rails may be more significant for open deck bridges than for ballast bridges.

The other test was designed to identify the ultimate capacity of the deck-abutment connections in the lateral direction (Maragakis et al. 2001). The track structure (i.e., the rails, ties and ballast, and the ballast pan) were cut completely free at the west abutment and the part of the deck above the central pier. The east abutment was left in its as-built condition with the ties, rails, ballast, and ballast pan intact.

Table 2.1 Summary of the Dynamic Experimental Results by UNR (Sandirasegaram 1997)

Mode	Rail Uncut		Rail Cut	
	Frequency	Damping	Frequency	Damping
First Transverse Mode	4.93	2.15	4.80	2.3
Second Transverse Mode	6.75	4.50	-	-
First Longitudinal Mode	6.56	5.00	5.95	5.33
First Vertical Mode	6.06	1.65	5.55	1.45

Lateral force was applied to the bridge directly over the bearings at the abutments. Force-displacement diagrams were obtained at both ends of the bridge. We may conclude that for this bridge: (a) the ultimate capacity at the as-built end was 45% greater than that at the free end, which could be explained by the presence of the ballast pan (tie-plate), ballast, ties, and rails; (b) the ultimate strength of the steel bearings is controlled by the tensile strength of the anchor bolts plus the friction force on the sliding surface; and (c) due to the additional strength that the railway elements provide, the seismic retrofitting requirements of this type of railway bridge could be less than those of highway bridges.

- (2) In 1998, the Transportation Technology Center, Inc. (TTCI) deployed a field test on a 5-span 62-ft, open-deck deck plate girder (DPG) steel bridge subjected to lateral and longitudinal loading (Otter et al. 1999a; Uppal et al. 2000). The objectives were: (a) to quantify the total resistance of these spans; and the contribution of the rail to this total resistance; and (b) to investigate the

contribution of anchor bolts, friction and continuity of the track structure to the bridge's resistance.

The authors concluded that: (a) the lateral resistance of this type of railroad bridge exceeds some of the most severe requirements used in seismic design of bridges; (b) the resistance to lateral displacement was provided primarily by anchor bolts, frictional and locking forces, and the continuous rail; and (c) the resistance of the approach abutment could be reduced by vertical uplift or liquefaction.

- (3) In 2000, TTCI conducted a field test on two open deck I-beam railroad spans to examine the resistance to longitudinal movement provided by the track structure (Doe et al. 2001; Uppal et al. 2001). The intermediate span was tested to quantify the resistance between rail and bridge deck and the resistance between bridge deck and span. In addition, this test measured the resistance to longitudinal movement offered by friction between plates, hook-bolts, and box anchoring of bridge ties. Displacement measurements were taken at the interfaces of the rail to tie, tie to beam, and beam to pier. The conclusion is that for this bridge: (a) the coefficient of friction for resistance against longitudinal movement with the flat bearings greased and rails disconnected was 0.21; (b) the coefficient of friction between rail and bridge deck was 0.24 when the ties were box-anchored for this test and everything else was loose; (c) the coefficient of friction between bridge deck and span was 0.37 when rails were anchored but hook bolts were loose; (d) the coefficient of friction for the whole deck span system was 0.49 when ties and hook bolts were tightened. They concluded that properly anchored rail and bridge decks can provide significant resistance to ground motion, which may be enough to eliminate the need for seismic retrofit of many railroad bridges.

The Mid-America Earthquake (MAE) center conducted a study on seismic evaluation of a railroad bridge spanning the Mississippi River in Memphis, Tennessee (Foutch and Yun 2001). This bridge was built in 1894 on deep, soft soil within the New Madrid seismic zone. Six stone masonry piers with caisson foundation support a five span steel truss superstructure. A three-dimensional model of this bridge was built using SAP 2000 software. Using this model, mode analysis and elastic response analysis were carried out. The results showed that the first order period of transverse mode was 3.05 seconds; the first order period of vertical mode was 1.16 seconds; and the first order period of longitudinal mode was 1.19 seconds. The elastic analysis showed that under M7.5 earthquake excitation in tri-axial ground motions the most vulnerable components of the bridge are the bearings and the stone piers instead of superstructure members. The authors also investigated the possible failure mechanisms of the piers. They include: stone layers sliding along a horizontal plane, overturning of the upper portion of the piers, and overturning at the base with toe crushing. Based on the results of modeling for

longitudinal and transverse directions by Drain 2DX software, a set of hazard curves were developed. The researchers found that for these stone piers, longitudinal response is governed by tilting under a shock with a return period of 473 years, and transverse direction is governed by sliding under a shock with a return period of 1575 years. Further experiments are needed to verify the analytical results above.

2.3 Seismic Performance of URM and URC Railroad Bridges Piers in Past Earthquakes

The historical performance of URM and URC railroad bridge piers in past earthquakes can provide a better understanding of the seismic behavior of these bridge elements. The published literature that recorded historical earthquakes and their destructive effect on railroad structures was reviewed.

In this part of the study, I: (1) synthesize and compile all the resources; (2) extract and summarize the seismic performance of URM and URC piers in past earthquakes; and (3) analyze the typical failure modes for these piers under seismic excitation.

Typically, the U.S. Geographic Survey or American Society of Civil Engineers (ASCE) recorded the condition of railroad structures following earthquakes in their investigation reports. For example, the effects of the 1906 San Francisco Earthquake on engineering infrastructure were investigated and reported by experts from ASCE in 1907 (Duryea and ASCE 1907). Although six railroad companies were operating within the area of destruction, the damage to railroad structures was much less than that for buildings and highway infrastructure. The typical damage to railroad structures was from the large displacement caused by the movement of active faults. For example, the railroad bridge across the Pajaro River that spanned an active fault line was affected severely by movement along the fault. The shocks moved all four URC piers and two abutments and increased the distance between the east and west abutments by 3.5 ft.

Other damages to the piers of this railroad bridge that were caused by inertial force and displacement are discussed in the following section. In this study, we review reports from U.S. Geological Survey, including the special report on the effects of 1964 Alaska Earthquake on the railroad system (McCulloch and Bonilla 1970).

Another resource for this part of study comes from the published papers by seismic experts investigating after major earthquakes. For example, the destructive effects of the 2011 Tohoku Earthquake on the railroad infrastructure was reported in the journal paper by Abé and Shimamura (Abé and Shimamura 2014). The damage to railroad structures in the Gujarat Earthquake, the Nisqually Earthquake and the Atico Earthquake were described by Byers (Byers 2004).

Based on the database used in this study, 139 of 4351 performance records report as damaged: 23 with light damage; 29 with modest damage; and 87 with severe damage. Light damage means the damage did not affect traffic after earthquakes. Moderate damage means the structures had their integrity but damage affected traffic. Severe damage means the structures lost their integrity or collapsed. These data show that, historically, railroad bridges performed well in earthquakes. However, when damage occurred, it was likely to be severe.

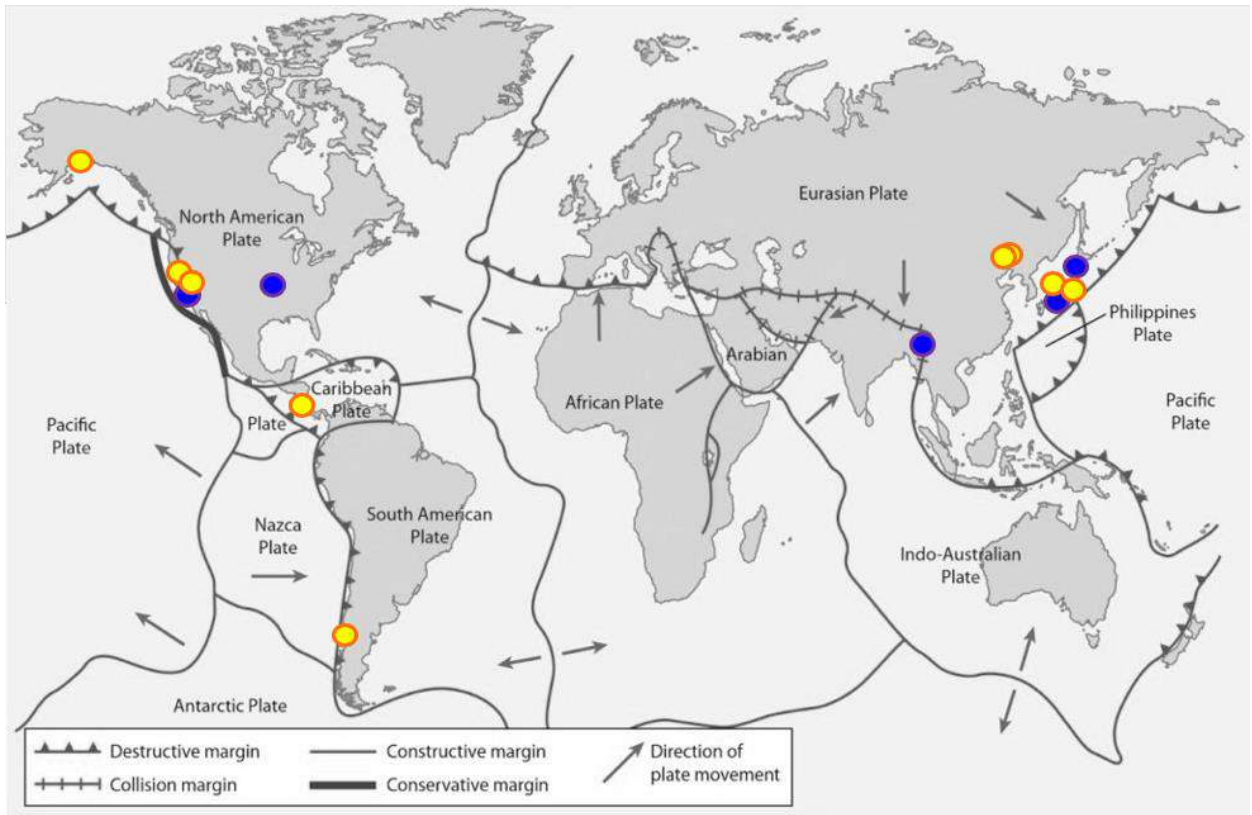
Five URM pier damage records and nine URC pier damage records were in the database. Appendix A summarizes damages to URM and URC railroad bridges from past earthquakes, according to data from the literature. **Figure 2.3** shows the locations of all five URM pier damage records and nine URC pier damage records. The locations of damage records were overlapped with the major fault lines (www.usgs.gov). This illustrates the correlation between the damage and bridge distance from fault lines. Records show that most damage occurred in bridges very close to major fault lines. There are three exceptions: two piers damaged in the Tangshan, China 1976 earthquake were close to a minor fault line in northeast China. One pier in the Charleston, Missouri 1895 earthquake was close to the New Madrid minor fault line. The definition on destructive margin, collision margin, constructive margin and conservative margin, which are not introduced in this report, can be found at <https://maxwatsongeography.wordpress.com/section-a/hazardous-environments/fault-linesplate-boundaries/>.

Typical failure modes of URM and URC railroad piers can be generalized as follows:

- (1) Integral displacement: horizontal, vertical or tilt - This is a typical failure mode for the bridge spanning an active fault in an earthquake. An example of this mode is the Pajaro River railroad bridge in the 1906 San Francisco earthquake. A fault line crosses this bridge near the west end. Earth movement along the fault line increased the distance between the east and west abutments by 3.5 ft. and moved all 5 piers from their original position, as shown in **Figure 2.4**.
- (2) Horizontal crack along construction joint in plain concrete piers - This is a typical failure mode for plain concrete piers. An example of this mode is the Pajaro River railroad bridge in the 1906 San Francisco earthquake (Duryea and ASCE 1907), as shown in **Figure 2.5**. Since the construction joints are the inherent defects within unreinforced concrete piers, cracking will occur when the tensile stress exceeds the ultimate tensile strength at these inherent defects.
- (3) Cracking of joints in brick or stone masonry piers - This is a typical failure for unreinforced masonry piers since the joints between masonry units are the weak

points in these piers. Examples of this mode are the Dos Pueblos bridge on the Southern Pacific Railroad in the 1925 Santa Barbara Earthquake (Byers 2003) and a brick masonry railroad pier on the Shinkansen line in the 2001 Tohoku Earthquake, as shown in **Figure 2.6**, respectively. Similar to the construction joints in URC piers, weak bonding between the mortar and masonry units will lead to cracking when the bond is stressed.

- (4) Sliding along the horizontal run-through cracks - An example of this mode is the Kuzuryu River railroad bridge in the 1948 Fukui earthquake (Far East Command 1949), as shown in **Figure 2.7**. The cracks initiated at the construction joints in URC piers and bed joints in URM piers. These joints are the inherent weak points of these structures. With intense shocks, run-through cracks develop along the weak bond between the blocks. The upper and lower parts slide along these run-through cracks when the horizontal earthquake load exceeded the friction resistance between the two parts.
- (5) Tilting of upper portion of piers after the horizontal run-through cracks appeared - An example of this failure mode occurred at the piers of the Dou River railway bridge in the 1976 Tangshan Earthquake (Chen 1978), as shown in **Figure 2.8**. The upper portion of damaged piers tilted or rocked due to the excessive overturning moment. The tilted part may either return to the vertical position or remain tilted (as in the example of the Dou River railway bridge). Either condition can affect train operations after an earthquake because of the excessive displacement of the superstructure.
- (6) Coping stone (pier cap): loosened, displaced, torn - An example of this mode is the Pajaro River railroad bridge in the 1906 San Francisco earthquake, as shown in **Figure 2.9**. The bond between the coping stone and main body of the pier may become the weakest part within the substructure system. Displacement may occur under high shear force conditions.
- (7) Anchorage failure between bearings and piers - An example of this failure mode is Bridge 14.5 in the 1964 Alaska earthquake (McCulloch and Bonilla 1970), as shown in Figure 2.10. Anchor bolts are the typical connection between the bearing and the pier. Thus, the anchorage strength is important when the bridge experiences high-level horizontal or vertical seismic excitation.



URM ●

Year	Earthquake	Location	M
1891	Mino–Owari Earthquake	Japan	8.0
1895	Charleston Earthquake	MO, USA	6.8
1897	Assam Earthquake	India	8.0
1925	Santa Barbara Earthquake	CA, USA	6.8
2011	Tōhoku Earthquake	Japan	9.1

URC ●

Year	Earthquake	Location	M
1906	San Francisco Earthquake	CA, USA	7.9
1948	Fukui Earthquake	Japan	7.3
1976	Tangshan Earthquake	China	7.8
1960	Valdivia Earthquake	Chile	9.5
1964	Alaska Earthquake	AK, USA	9.2
1978	Miyagi Earthquake	Japan	7.7
1989	Loma Prieta Earthquake	CA, USA	6.9
1991	Limon Earthquake	Costa Rica	7.7

Figure 2.3 Locations of damaged URM and URC railroad bridge piers in fault line map

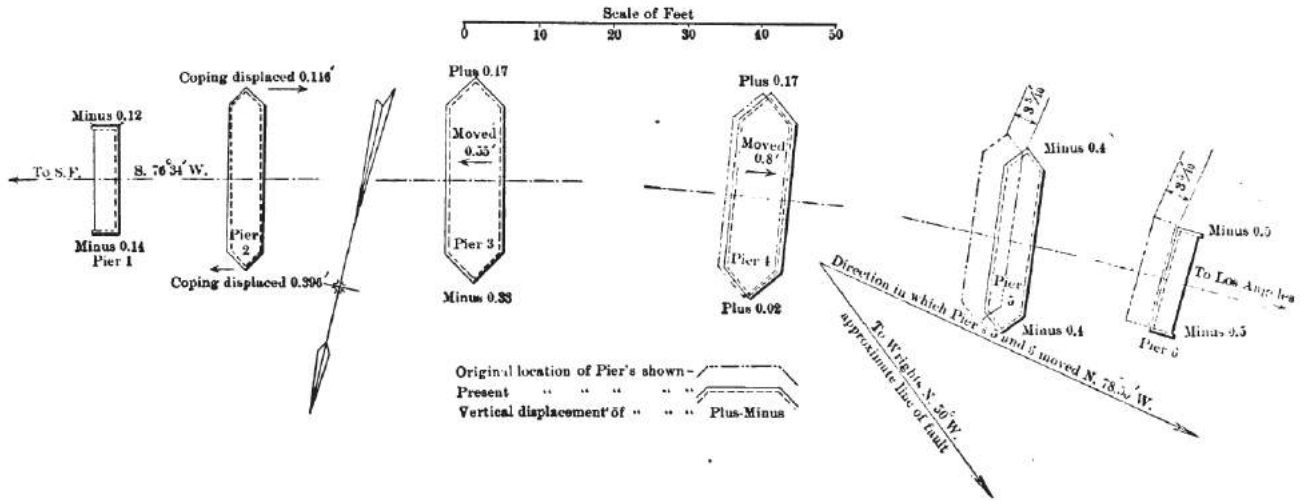


Figure 2.4 Displacement of Piers of the Pajaro River Bridge after the 1906 San Francisco Earthquake (Duryea and ASCE 1907)

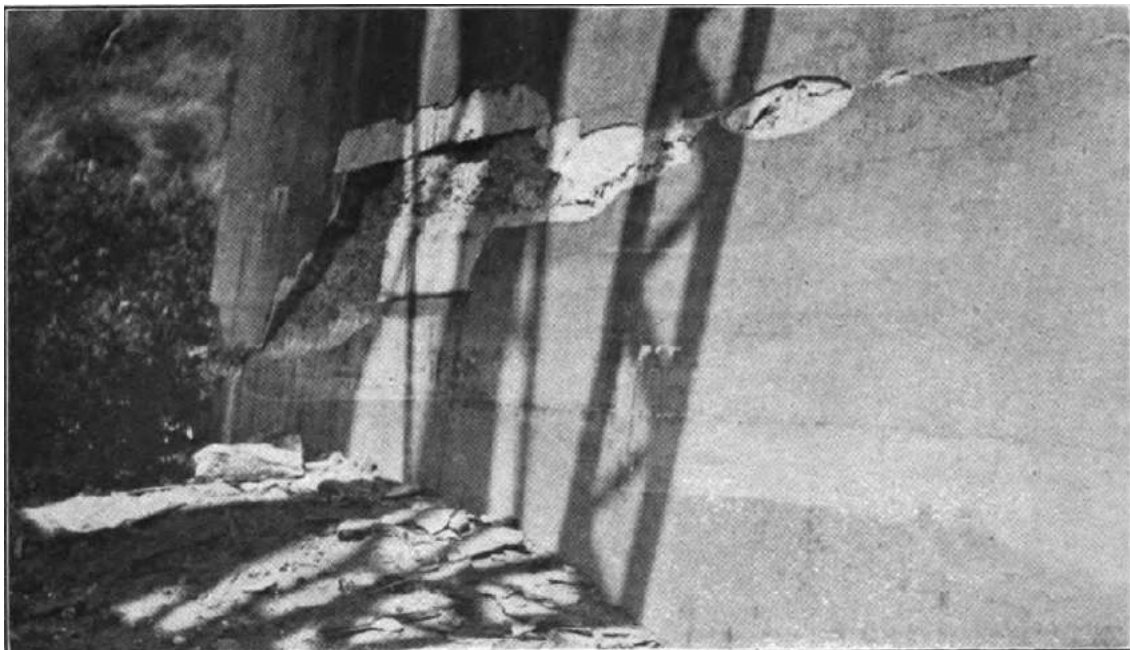


Figure 2.5 Cracking Damage at the Base of a URC Pier of Pajaro Bridge after the 1906 San Francisco Earthquake (Duryea and ASCE 1907)



Figure 2.6 Cracking Damage of a URM Pier of Dos Pueblos Viaduct after the 1925 Santa Barbara Earthquake (Kirkbride 1927)

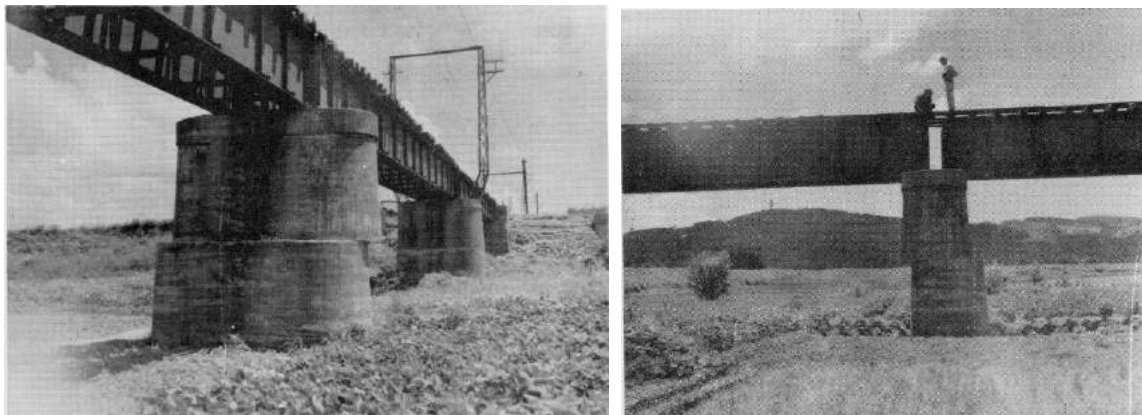


Figure 2.7 Sliding at a URC Pier of Kuzuryu River Bridge after the 1948 Fukui Earthquake (Far East Command 1949)



Figure 2.8 Tilting of Upper Partition of URC Piers of Dou River Railway Bridge after the 1976 Tangshan Earthquake (Chen 1978)

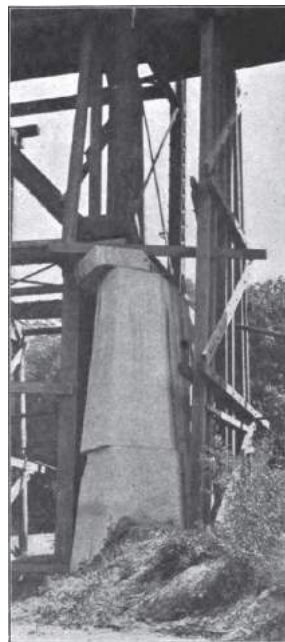


Figure 2.9 Damage at the Coping stone of a URC Pier of Pajaro Bridge after the 1906 San Francisco Earthquake (Duryea and ASCE 1907)

2.4 Seismic Design

In 1941, an earthquake load was first listed as a design load in section 3.2.1 of the bridge design code by the American Association of State Highway and Transportation Officials (AASHTO) (AASHTO 1941). However, there were no practical requirements to calculate seismic load and check the corresponding stresses. Following several major earthquakes in the past half century, AASHTO's seismic design provision for bridges was developed and improved, introducing stricter requirements.

In 1993, the American Railway Engineering and Maintenance-of-Way Association (AREMA) established a stand-alone committee (AREMA Committee 9) to develop seismic design guidelines specific to railroad structures. In 1994, guidelines for the design of railroad bridges under seismic forces were introduced in Chapter 9 of AREMA's Manual for Railway Engineering (MRE) (Moreu and LaFave 2012).

Current provisions for seismic design for bridges by AREMA and AASHTO are discussed below.



Figure 2.10 Anchorage Failure at the Bearing of a URC Pier of Bridge 14.5 after the 1964 Alaska Earthquake (McCulloch and Bonilla 1970)

2.4.1 AREMA MRE 2018

Chapter 9 of MRE provides guidelines for seismic design of railroad bridges, along with commentaries and references (AREMA 2018).

General requirements: Three-level performance criteria must be satisfied in the bridge design process: serviceability limit state, ultimate limit state, and survivability limit state.

The serviceability limit state requires the critical members to remain in the elastic range under ground motion of 50-100 years average return period. Earthquake damage to bridges will not affect the safe operation of trains under restricted speeds.

The ultimate limit state requires that the strength and stability of the critical members will not be exceeded under ground motion with 200-500 years average return period. The integrity of the bridge structure should be preserved during this state. Ductility of the structure is required to minimize damage and the loss of use due to the large displacement caused by seismic excitation. Running trains need to stop under this level of ground motion until bridge inspections are completed.

The survivability limit state requires the structural survival of the bridge under ground motion with 1000-2400 years average return period. Further ductility capacity of the structure may be required to avoid collapse. Running trains need to stop under this level of ground motion until bridge inspections are completed.

Analysis: The methods recommended by MRE include Equivalent Lateral Force (ELF) Procedure and Modal Analysis (MA) Procedure. Typically, ELF is recommended for the analysis of regular bridges while MA is for the analysis of multi-span irregular bridges.

Design forces: To get the final seismic design loads, MRE allows combining the loads in each of the two principal directions of the structure using one of the following: (1) the square root of the sum of the squares (SRSS) method; and (2) an alternate method that includes combination of the forces in principle direction 1 with 30% of the forces from principle direction 2, and combination of the forces in principle direction 2 with 30% of the forces from principle direction 1.

The seismic design loads for the ultimate limit state and survivability limit state could be computed by increasing the forces under the serviceability limit state by the ratio of the Base Acceleration Coefficients which is determined per the formula and base acceleration maps in Section 1.3.2.3.

For the bridge design of concrete structures, the load combination formula is **1.0D+1.0E+1.0B+1.0PS+1.0EQ** and load factor design shall be used. For the bridge design of steel structures, the combination formula is **D+E+B+PS+EQ**, and allowable stress design shall be used. In the combination formulas, D, E, B, PS, and EQ stand for dead load, earth pressure, buoyancy, secondary forces from prestressing and earthquake load, respectively.

Response Limits: For bridge design of concrete structures, the design strength of each member shall follow the requirements in MRE Chapter 8, Concrete structures and foundations. For bridge design of steel structures, the allowable stresses for each member shall follow the requirements in MRE Chapter 15, Steel structures. Each member under design loads of three-level limit state shall be checked to satisfy the limit requirements in MRE.

Detailing considerations: To satisfy the performance criteria under the ultimate limit state and the survivability limit state, MRE lists corresponding requirements to guarantee the continuity, ductility, and redundancy of the bridge structure. Continuously welded rails (CWR) that satisfy certain requirements are considered to be a redundant load path for seismic load and to increase the damping improving the energy dissipating capacity of the structure.

Summary: The bridge seismic design approach specified in MRE 2012 contains no requirements on the response limit for URM or URC bridge piers. Thus, it is difficult to determine if the strength of URM or URC bridge piers matches the seismic criteria under the three-level limit state. Since URM or URC piers contain no reinforcement, old piers cannot be considered as structures with proper ductility capacity per the ductility provisions in MRE. Furthermore, it may be doubtful to utilize load factor design in analysis of old piers.

2.4.2 AASHTO LRFD Bridge Design Specifications 2017

AASHTO's requirements for the seismic design of highway bridges are in Section 3.10, 3.4, and 4.7 of the 2017 edition of LRFD bridge design specifications (AASHTO 2017).

General requirements: One-level force-based design criteria are adopted in the specifications. Earthquake ground motions with a 7% probability of exceedance in 75 years, i.e., a return period of about 1000 years, are defined as the design earthquake. Under this earthquake load, bridge structures satisfy the performance that have a low probability of collapse but may suffer significant damage and disruption to service. Higher performance levels may be adopted but need to be authorized by the bridge owner.

Based on the comments in the specifications, bridges are designed to resist small to moderate earthquakes within the elastic behavior range of the structural components. Collapse of bridge structures should be prevented during large earthquakes.

The specifications could provide adequate strength capacity to resist design force demands. However, the displacement capacity that is critical in the limit states is not under supervision by a designer. The comments in the specifications mention that bridges

designed by the force-based method should be checked by displacement-based methods such as the *AASHTO Guide Specifications for LRFD Seismic Design* (AASHTO 2011), especially for high seismic zones.

Analysis: The requirements for the dynamic analysis method under earthquake loads are specified in Article 4.7.4 and summarized in Table 4.7.4.3.1-1 (shown in **Table 2.2**) in the specifications. Seismic analysis is not required for single-span bridges in all seismic zones and multi-span bridges in low seismic zones (Seismic Zone 1). Generally, uniform load elastic method (UL) and single-mode elastic method (SM) are recommended for regular bridges and multimode elastic method (MM) is recommended for irregular bridges. For critical bridges in high seismic zones, either elastic or inelastic time history method (TH) may be required, based on seismic zone identification.

Design forces: Two load cases are considered during the combination of the seismic effect in two perpendicular horizontal directions. Load case 1 consists of 100 percent of the absolute value of the elastic seismic forces resulting from the seismic loading in the longitudinal direction, combined with 30 percent of the absolute value of the elastic seismic forces resulting from the seismic loading in the transverse direction. Similarly, load case 2 consists of 100 percent of the absolute value of the elastic seismic forces resulting from the seismic loading in the transverse direction; combined with 30 percent of the absolute value of the elastic seismic forces resulting from the seismic loading in the longitudinal direction.

Earthquake load is considered in the “Extreme Event I” load combination in the AASHTO 2017 LRFD bridge design specifications. The total factored force effect for bridge piers under this combination is:

Table 2.2 Minimum Analysis Requirements for Seismic Effects (AASHTO 2017)

Seismic zone	Single-span bridges	Multi-span bridges					
		Other bridges		Essential bridges		Critical bridges	
		regular	irregular	regular	irregular	regular	irregular
1		*	*	*	*	*	*
2	No seismic analysis required	SM/UL	SM	SM/UL	MM	MM	MM
3		SM/UL	MM	MM	MM	MM	TH
4		SM/UL	MM	MM	MM	TH	TH

$$Q = \sum \eta_i \gamma_i Q_i$$

$$= \eta_{DC} \gamma_p DC + \eta_{LL} \gamma_{EQ} LL + \eta_{WA} \times 1.0 \times WA + \eta_{FR} \times 1.0 \times FR + \eta_{EQ} \times 1.0 \times EQ$$

where:

η_i = load modifier specified in article 1.3.2, $\eta_i = \eta_D \eta_R \eta_I$, for the Extreme Event limit state, $\eta_{DC}, \eta_{LL}, \eta_{WA}, \eta_{FR}, \eta_{EQ}$ are taken as 1.0

η_D = a factor relation to ductility, as specified in Article 1.3.3, for the Extreme Event limit state $\eta_D = 1.0$

η_R = a factor relating to redundancy as specified in Article 1.3.4 for the Extreme Event limit state $\eta_R = 1.0$

η_I = a factor relating to perational classification as specified in Article 1.3.5, for the Extreme Event limit state $\eta_I = 1.0$

γ_p = load factors for permanent loads, γ_p were taken as 1.0 in this example

γ_{EQ} = load factor for live load applied simultaneously with seismic loads, γ_{EQ} could be taken as 0.5 for a common condition according to Article C.3.4.1

DC = dead load of structural components and nonstructural attachments

LL = vehicular live load

WA = water load and stream pressure, in this example: only buoyancy was considered

FR = friction load, in this example: friction load was neglected

EQ = earthquake load

AASHTO 2017 LRFD bridge design specifications require that seismic design force for individual components and connections of bridges be determined by dividing the elastic forces obtained from the analysis by the appropriate Response Modification Factor (R) (ACI et al. 2003) specified in Table 3.10.7.1-1 and Table 3.10.7.1-2 (shown in **Table 2.3** and **Table 2.4**). The R-factors are obtained by assuming that the individual components will yield and develop a ductile mechanism under the calculated design seismic loads. Thus, detailing considerations need to be guaranteed to make sure that the mechanism is formed without brittle behavior.

Response Limits: For concrete and steel structures design, the response limits must follow the requirements in Sections 5 and 6, respectively.

Table 2.3 Response Modification Factors for Substructures (AASHTO 2017)

Substructure	Operational category		
	Critical	Essential	Other
Wall-type piers (larger dimension)	1.5	1.5	2.0
Reinforced concrete pile bents			
• Vertical piles only	1.5	2.0	3.0
• With batter piles	1.5	1.5	2.0
Single columns	1.5	2.0	3.0
Steel or composite steel and concrete pile bents			
• Vertical pile only	1.5	3.5	5.0
• With batter piles	1.5	2.0	3.0
Multiple column bents	1.5	3.5	5.0

Table 2.4 Response Modification Factors for Connections (AASHTO 2017)

Connection	All Operational Categories
Superstructure to abutment	0.8
Expansion joints with a span of the structure	0.8
Columns, piers, or pile bents to cap beam or superstructure	1.0
Columns or piers to foundations	1.0

Detailing considerations: To guarantee the ductility and redundancy of bridges under seismic loading, AASHTO provides several requirements on the detailing design, e.g., the minimum support lengths of bearing seats, detailing of the expansion joints and restrainers, design of the abutments, hold-down devices and shear keys, etc. Furthermore,

AASHTO published guidelines on the design and application of the seismically isolated bridges in 1991 (AASHTO 1991).

Summary: The current edition of AASHTO's bridge design code is based on the research findings and engineering experience of recent years. The requirements are not applicable for URM or URC piers built a century ago. For example, the ductility concept that is fundamental in the current code is based on the post-yield behavior of reinforced concrete members. Since no reinforcement was embedded in the old piers, they cannot be analyzed as components with ductility capacity. Meanwhile, no requirements are provided for the response limits on the URM and URC members in the current code.

2.4.3 AREMA MRE 1907

As mentioned previously, since currently more than half of the railroad bridges in U.S. were built before 1920, it is reasonable to review the design code for railroad bridges of a century ago to build a solid foundation for the analysis of these historical piers.

The first edition of the MRE by AREMA was published in 1900, the same year AREMA was established, and its contents have been refreshed or renewed annually. In 1907, the specifications for design loads of railroad bridges were first listed in MRE section "Iron and Steel Structures" (AREMA 1907). Some significant differences from the current code are summarized below:

Live load: The minimum live load for each track is specified to be Cooper's E-40. This requirement was changed to E60 in the 1920 edition, E72 in the 1935 edition, and E80 in the 1967 edition. The current code specifies E80.

Lateral load: The lateral load on the loaded chord was specified at 200 lbs. per linear foot plus 10 percent of the specified train load on one track. The lateral load on the unloaded chord was specified to be 200 lbs. per linear foot.

Wind load: Substructures must be designed for a lateral force of 50 lbs. per sq. ft. on one and one-half times the vertical projection of the structure unloaded; or 30 lbs. per sq. ft. on the same surface plus 400 lbs. per linear ft. of the structure applied 7 ft. above the rail for assumed wind load on train when the structure is either fully loaded or unloaded on either track with empty cars assumed to weigh 1200 lbs. per linear ft., whichever gives the larger load.

Longitudinal load: Substructures must be designed for a longitudinal force of 20 percent of the live load, applied to the rail.

Besides the design load, the analysis method and response limit are different from the design of railroad piers of a century ago. According to treatises and textbooks of that era (Baker 1909; Derleth 1907; Ketchum 1921), safety checking for railroad bridge piers could be generalized as follows:

- (1) Calculate the forces to be resisted.
- (2) Determine load cases.
- (3) Calculate overturning moments and resistance moments under each load case in both directions.
- (4) Examine the safety factors against overturning under each load case in both directions.
- (5) Calculate sliding forces and resistance to sliding under each load case in both directions.
- (6) Examine the safety factors against sliding under each load case in both directions.
- (7) Calculate maximum and minimum “intensities of pressure”, i.e. stresses, on subfoundation under each load case in both directions.
- (8) Check the safety factors of maximum stress under each load case in both directions to avoid crushing of the substructure at the edge of the subfoundation.
- (9) Check the safety factors of minimum stress under each load case in both directions to avoid the uplift of the substructure at the edge of the subfoundation.

According to this process, we find that the design of old URM and URC piers includes safety factors for overturning and sliding at critical sections and the allowable stress check for masonry or concrete material at the base of the substructures. The analysis is under elastic behavior, which is different from the ultimate strength analysis used in current codes. “Over-engineered” design was typical in that era. For example, the safety factors against overturning and sliding are typically taken to be 3.0 or more (International Correspondence Schools 1908). This explains the strong appearance of old URM and URC piers.

2.4.4 Code for Seismic Design of Railway Engineering (GB50111-2006 [2009 Edition]) in China

The first edition of the seismic design code for railway engineering in China was published in 1977. This code was amended and supplemented comprehensively in 1987 and 2006. After 30 years of development, the seismic design concept in the Chinese code has gradually changed from strength-based design to displacement-based design with ductility design consideration (Ni 2005). In 2009, to satisfy the rapid development of high-speed rail (HSR) in China, several supplements to the requirements on seismic design of HSR bridges were adopted in GB50111-2006 (2009 Edition) (NRA China 2009). This was adopted by *Code for Design of High Speed Railway* (TB10621-2014) in

2014 (NRA China 2014). The experiences summarized from the M8.0 2008 Sichuan earthquake have been integrated into GB50111-2006 (2009 Edition).

General requirements: In GB50111-2006 (2009 Edition), railway bridges are categorized into four seismic protection levels:

Level A: Significant bridges with a long span or complex structural type or difficulty in recovering from severe earthquake damage.

Level B: (1) for a regular speed railroad, simple support concrete girder bridges with span ≥ 48 m (158 ft.), simple support steel girder bridges with span ≥ 64 m (210 ft.), continuous concrete girder bridges with main span ≥ 80 m (263 ft.), continuous steel girder bridges with main span ≥ 96 m (315 ft.); (2) for High-speed Rail (HSR), bridges with span ≥ 40 m (131 ft.); (3) bridges with pier height ≥ 40 m (131 ft.); (4) normal water depth ≥ 8 m (26 ft.); (5) regular bridges with long span or complex structural type or difficulty to recover from severe earthquake damage.

Level C: (1) HSR bridges except those defined in Level B; (2) bridges with pier heights from 30 m (99 ft.) to 40 m (131 ft.); and (3) bridges with normal water depth from 5 m (17 ft.) to 8 m (26 ft.).

Level D includes: all other railway bridges not defined in Levels A, B, or C.

According to GB50111-2006 (2009 Edition), railroad bridges are designed to withstand three levels of earthquake motion: low-level earthquake, design earthquake, and high-level earthquake. The return periods of the three-level earthquake are 50,475 and 2475 years respectively. The requirements for the performance of railroad bridges under these three earthquake motions are:

After a low-level earthquake, bridges must retain design operational functions without damage or with little damage. Structures must work in the elastic range.

After a design earthquake, bridges must recover design operational functions in a short period with repairable damage. Structures might work in the inelastic, exceeding elastic limits, range.

After a high-level earthquake, bridges must survive without integral collapse. After emergency repairs, bridges must be able to support a train under restricted speeds.

The requirements for seismic design checking are listed in **Table 2.5**. Specifically: (1) checks on a strength, eccentricity and stability are required for low-level earthquake; (2)

connection detail must be checked for the design earthquake; (3) Ductility checks may be required for the high-level earthquake.

Analysis: For simply supported bridges, the seismic analysis can be made by single pier modeling that considers the mass effect from the superstructure or whole bridge modeling considering the stiffness effect from the superstructure.

For low-level earthquake design, the response spectrum method is recommended for Level B bridges. Besides the response spectrum method, the time-history analysis method is recommended for Level B and C bridges and new structural type bridges.

For design earthquake design, the static analysis method is recommended. The response spectrum method should be used to design bearings in continuous bridges.

Table 2.5 Seismic Design Checking Requirements (NRA China 2009)

Type		low-level earthquake	Design earthquake	high-level earthquake
simple support girder bridges	plain concrete	pier and foundation: checking on strength, eccentricity and stability	checking on connection details	no requirement on checking, casing reinforcements are required
	reinforced concrete	pier and foundation: checking on strength and stability	checking on connection details	checking on ductility by using simplified method
Other girder bridges and Level B bridges		pier and foundation: checking on strength, eccentricity and stability	checking on connection details	for reinforced concrete piers: checking on ductility and maximum displacement by using non-linear time-history response analysis method

For high-level earthquake design, simplified time-history analysis method is recommended for the reinforced concrete piers of simply supported bridges. The nonlinear time-history analysis method is recommended for Level B bridges and new structural type bridges.

Design forces: Calculation of horizontal seismic loadings in both longitudinal and transverse directions is required during the seismic checking process. For cantilever structures and prestressed concrete rigid frame bridges with design intensity of 9 degrees, the vertical seismic load must be considered. The vertical seismic load value is either 7% of the sum of dead load and live load, or the result of dynamic analysis by 65% of the fundamental horizontal acceleration (a). However, the combination of seismic loads in longitudinal and transverse directions is not considered in GB50111-2006 (2009 Edition).

The critical combinations of the seismic loads with other loads, i.e. self-weight, earth pressure, hydrostatic pressure, buoyancy force, live load, centrifugal force and earth pressure by live load, must be checked under both with-train and without-train conditions. For the with-train condition: (1) seismic load in longitudinal direction caused by live load is not considered; (2) 50% of the seismic load in transverse direction caused by live load is applied at 2 meters above the top of rail.

Response limits: The requirements for the response limits of railroad structures are included in *Code for Design on Subsoil and Foundation of Railway Bridge and Culvert* (TB10002.5-2005). The allowable stress method is adopted in TB10002.5-2005.

Detailing considerations: The requirements for detail design provided in GB50111-2006 (2009 Edition) guarantee the ductility of the bridge piers. For example, the maximum longitudinal reinforcement ratio, minimum diameter of stirrups, minimum transverse reinforcement ratio, and maximum stirrup spacing are recommended both within and outside the plastic hinge zone. The detailing of welding and hooking are suggested as well.

The nonlinear time-history analysis method is recommended for checking after a high-level earthquake. Based on the results from the time-history analysis, the ductility ratio is calculated using the following equation:

$$\mu_u = \frac{\Delta_{\max}}{\Delta_y} < [\mu_u]$$

Where:

μ_u = displacement ductility ratio

$[\mu_u]$ = limit on displacement ductility ratio, set to be 4.8

Δ_{\max} = maximum displacement of the piers under nonlinear response analysis

Δ_y = yield displacement of the piers

2.5 Seismic Assessment

As mentioned previously, railroad bridges have historically performed well in earthquakes, suffering little or no damage. However, due to limited knowledge about earthquake characteristics and bridge seismic behavior, URM and URC bridge piers designed and built a century ago may not have adequate capacity, e.g. strength and deformation, to resist shocks in the future despite surviving previous earthquakes. Considering the uncertainty of earthquake location and intensity, future seismic damage to the piers is unpredictable. Thus, it is necessary to evaluate the strength and deformation capacity of old piers using proper seismic assessment approaches.

Interest in seismic research and corresponding retrofit methods increased after the severe damage to highway bridges in the 1971 San Fernando Earthquake. In 1983, the Applied Technology Council (ATC) issued guidelines for seismic retrofitting for highway bridges (ATC 1983). Meanwhile, more research was carried out in the 1980s (ACI et al. 2007). The earlier guidelines and approaches for seismic assessment and retrofit of bridges were based solely on strength-based methods without considering the inelastic behavior of the structure after yield and the deformation demand on the bridges. Damage in the Loma Prieta and Northridge Earthquakes raised concern from the bridge community on this issue.

Over the past three decades, researchers have been pursuing comprehensive assessment methods that can consider both the strength and deformation capacities at component and structure levels. In this procedure, the deformation-based approach and the energy-based approach were adopted as guidelines for the seismic assessment and retrofit successively in the 1990s (ACI et al. 2007).

Recently, seismic engineering societies have broadly accepted the performance-based evaluation method. AASHTO and AREMA have adopted the concept in their guidelines and design code. In this method, instead of placing sole emphasis on the ultimate capacities of structures at maximum design seismic loading, the capacities of bridges are evaluated for multiple earthquake levels. Design or retrofit will satisfy multiple performance objectives under diverse seismic hazard levels. For example, under low-intensity and frequent seismic loading, elastic behavior may be needed for structures to

satisfy the performance with need to repair. Under moderately-intensive seismic loading, inelastic behavior and limited repairable damage may be allowed. Under severely-intensive earthquakes, the ultimate capacity needs to be evaluated and the bridge retrofitted to avoid collapse.

The seismic evaluation procedure for a bridge includes: (1) evaluation of the seismic demand on the structural components; (2) evaluation of the capacity of each component; and (3) examination of the demand-capacity ratio and identifying the potential damage in the components and structural system (ACI et al. 2007).

The common analytical methods of seismic demand evaluation are reviewed and introduced below:

Linear elastic analysis methods (AASHTO 2017; AREMA 2018): The common linear elastic analysis methods include the single-mode response spectrum method, the multimode response spectrum method, and the linear time-history analysis method. For simple or regular bridges whose structural response can be represented approximately with the fundamental vibration mode dynamic model, the single-mode response spectrum method is adequate to obtain the seismic demand. For irregular bridges where single-mode response is not adequate to represent the structural response under seismic excitation, the multimode response spectrum and linear time-history analysis methods are required. Force demands are obtained from the linear elastic analysis by these methods. The force demands are reduced by a response modification factor R (as shown in **Table 2.3** and **Table 2.4**) to account for the ductility of the analyzed components in AASHTO's LRFD 2017 design code.

Nonlinear analysis methods (ASCE and FEMA 2000): The common nonlinear analysis methods include the limit analysis method, the pushover analysis method paired with linear dynamic analyses, and the acceleration time-history analysis method. The limit analysis and pushover methods pertain to static nonlinear procedures. The limit analysis method is developed using the virtual work principle. In limit analysis, the location of plastic hinges needs to be assumed appropriately to obtain a reasonable mechanism after yield. But this limits the application of this method to complex structures because it is difficult to find a proper collapse mechanism. The pushover analysis method is used to estimate member demands, the monotonic force-displacement relationship, and the displacement capacity of the structural system. However, this method may result in unrealistic seismic demands in members if misassumptions are made about the boundary condition, deck stiffness, and coherence of the ground motions (ACI et al. 2007). The acceleration time-history method is a more complex, nonlinear analysis approach, but it could approach the real response of the structures if reasonable simplifications are used.

Evaluating the actual capacities of the components and structural system is another significant part of the demand-capacity ratio procedure. It can be accomplished in the following steps (ACI et al. 2007; Priestley et al. 1996):

- (1) Identify the actual properties of the material: To obtain the real capacities of components, it is important to use the actual material properties in the analysis. As the material properties in the design codes are conservative with the reliability consideration, the properties from codes cannot be used directly in the seismic capacity analysis of structures. It is preferred to obtain the actual strength from material testing on the existing piers. However, several adjustments on the material strength may be taken based on the recommendations in relevant literature. For example, a 50% increase in the concrete design strength and 10% overstrength in the yield strength of reinforcement is suggested to estimate the actual strength in ATC-32 (Nutt et al. 2000). The adjustment parameters are 70% and 10% for concrete and reinforcement, respectively, in MCEER/ATC-49 (ATC MCEER Joint Venture and NCHRP 2003).
- (2) Calculate the flexural capacities of individual components based on moment-curvature analyses: Actual material properties, stress-strain relationships of concrete and reinforcements with consideration on the confinement effect and strain-hardening behavior need to be used.
- (3) Calculate the lower-bound shear capacities of individual components based on specified material properties: Although there is no consensus within the engineering community which shear capacity equation is the best, most provide conservative estimates for the shear capacity of members tested in the laboratory (ACI et al. 2007). Thus, it is reasonable to estimate the shear capacity of members using the smallest result from these suggested equations.
- (4) Evaluate the anchorage of reinforcement and shear strength of joints
- (5) Determine strengths of footings, pile-cap connections, and piles
- (6) Determine the bridge response by considering the bridge as an individual framing system

Based on the results of demand and capacity analyses, the demand-capacity ratio can be determined and evaluated. The critical sections should be located where the demand-capacity ratios exceed unity. Appropriate retrofit measures could be applied to these critical sections based on the seismic assessment results.

2.6 Seismic Retrofit

After the seismic assessment analyses, two decisions need to be made at the beginning of a bridge seismic retrofit: (1) whether the critical sections with damage risk are worth retrofitting and (2) which level the bridges should be retrofitted to (Priestley et al. 1996). These two issues must be analyzed in light of the available financial resources and cost-effectiveness analysis. Since these issues are at least partially in the domain of economics, they are not discussed as major topics in this research. The engineered retrofit design, measures, and implementation for URM and URC railroad bridge piers are the major topics in this research, while cost-effectiveness analysis will be discussed preliminarily.

The retrofit design sections in current codes are reviewed and summarized below:

- (1) AREMA MRE 2018: The purposes of retrofit schemes are listed in the code (AREMA 2018): (1) change the dynamic response to reduce the global seismic demand in a structure; (2) strengthen components to increase the local seismic capacity; (3) provide alternate paths for seismic loading to improve the redundancy of a structural system; (4) provide restrainers, extended bearing seats, and other devices to accommodate displacements; (5) design non-critical components to post-yield response to increase the ductility of a structure and relieve the seismic stresses of critical components. These considerations represent the requirements on seismic demand, seismic capacity, ductility, and redundancy to the bridge seismic retrofit design. However, there are no more detailed design guidelines for bridge retrofit in the MRE.
- (2) FHWA Seismic retrofitting Manual for Highway Bridges: The performance-based retrofit philosophy is used in the design requirements in the FHWA manual (Buckle et al. 2006). Performance criteria are given for two earthquake ground motions with different return periods, 100 and 1,000 years. A higher level of performance is required for the event with the shorter return period (the lower level earthquake ground motion) than for the longer return period (the upper level earthquake ground motion). Criteria are recommended according to bridge importance and anticipated service life, with more rigorous performance being required for important, relatively new bridges, and a lesser level for standard bridges nearing the end of their useful life. Retrofitting measures are designed according to an assigned Seismic Retrofit Category (SRC). Bridges in Category A need not be retrofitted whereas those in Categories B, C and D require successively more rigorous consideration and retrofitting as required.

Retrofit measures and implementation for bridge piers are reviewed and summarized as below:

- (1) Steel jacketing (Priestley et al. 1996): In this measure, two half shells of steel plate are placed around the pier. The gap between the steel and pier is filled with cement grout. This measure is applicable to circular and rectangular columns (as shown in **Figure 2.11**). The jacket increases the reinforcement ratio of the cross-section, also providing effective confinement to the core concrete pier. This measure can improve the seismic capacity effectively. U.S. bridges treated in this manner behaved well during the 1994 Northridge Earthquake.

Concrete jacketing (Priestley et al. 1996): In this measure, a reinforced concrete jacket is placed around the pier (as shown in **Figure 2.12**). This improves the seismic capacity, e.g. flexural strength and shear strength, and ductility of the piers. In the U.S., this measure has been used in several railroad retrofit projects on piers with under-reinforcement. For example, from 1949 to 1952, the concrete jacketing approach was used in retrofitting the substructure of the Illinois Central Railroad Cairo Bridge over the Ohio River (Modjeski and Masters 1953). This project included replacement of all six truss spans and retrofitting three stone masonry piers. These masonry piers were built in 1889 and developed cracks along the mortar joints after the 1895 M6.6 Charleston Earthquake. The piers were strengthened by placing a 2 ft. thick concrete jacket reaching up to bottom of the stone coping. This concrete jacket was attached with expansion anchors to alternate stone courses by a pattern of anchors approximately 4 ft. on centers. Reinforcements consisted of $\frac{3}{4}$ in. diameter bars with horizontal bars at 12 in. centers and vertical bars at 18 in. centers. This retrofit is shown in **Figure 2.13**.

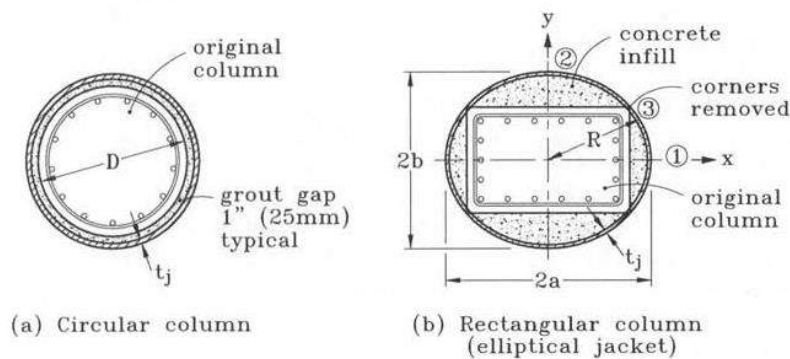


Figure 2.11 Typical Cross-section Layout of Steel Jacketing Retrofit (Priestley et al. 1996)

- (2) Composite-Material Jackets: Retrofit could be made using carbon-FRP (Fiber Reinforced Polymer) or Glass-FRP bonded to the column with epoxy. This

approach has been proved effective in laboratory tests (Priestley et al. 1996). This measure could provide confinement for the core concrete and increase the ductile behavior of the piers. However, debonding of the epoxy adhesives may lead a durability issues for FRP retrofitted piers (Au and Büyüköztürk 2006). In 2011, Choi et al. conducted a study on the application of FRP-steel plate (FSP) for retrofitting plain concrete piers in Korea (Choi et al. 2011). FSP is a type of sandwich composite consisting of a steel plate between two FRP plates. With the steel plate, this hybrid material could be fixed to the pier body by durable anchoring instead of adhesive layers. An effective retrofit scheme with FSP material is developed in this study to restrict joint cracking and improve displacement capacity and strength in bending.

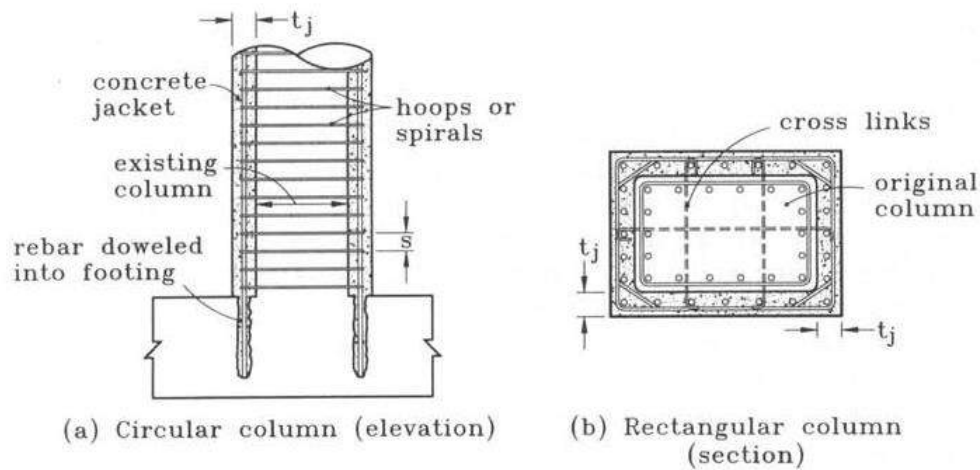


Figure 2.12 Typical Layout of Concrete Jacketing Retrofit (Priestley et al. 1996)



Figure 2.13 Construction of the RC Jacket Retrofitting at a URM Pier of the Illinois Central Railroad Cairo Bridge over the Ohio River (Modjeski and Masters 1953)

- (3) External prestressing: URM and URC piers have inherent weakness under seismic load due to the presence of mortar joints or construction joints. These piers may be severely damaged by an earthquake when loads produce tensile stress. A retrofit measure by stressing the plain piers vertically with external prestressing cables has been utilized in New Zealand railroad bridges (Walsh 2002). As shown in **Figure 2.14**, caps are built at the top and bottom of the old piers. Prestressing strands protected by steel ducts are placed and prestressed between the top and bottom caps. The prestressing forces the mass piers into controlled compression loading, reducing the possibility of tension stresses developing during earthquakes.
- (4) Reinforced shotcrete overlay, grouted reinforcing bars within drilled cores (Abrams et al. 2007): Abrams et al. conducted several model tests on retrofit schemes for URM brick wall piers. The tests evaluated reinforced shotcrete overlay and grouted reinforcing bars within drilled cores. The results indicated that reinforced shotcrete is an effective retrofit approach due to deformation capacity and energy-dissipation through yielding of the reinforcement. Grouted reinforcing bars within drilled cores provided a moderate improvement to the lateral resistance capacity of URM piers due to the insufficient anchorage of the

grout core. The slip of the core in its cavity resists the yield of the embedded steel bars and limits the ductile behavior of the piers.



Figure 2.14 External Prestressing Retrofit at a URC Railroad Bridge Pier in New Zealand (Walsh 2002)

2.7 Conclusions and Recommendations

URM and URC railroad bridge structures built up to a century ago still serve a considerable percentage of in-service U.S. railroad bridges. Research, literature, and provisions in code about seismic performance of URM and URC railroad bridges are reviewed to explore reasonable research approaches for evaluating the resistance capacity of these bridges in future earthquakes. The findings are summarized below:

- (1) Previous seismic research on railroad bridges has concentrated in two areas: seismic performance of piers in past earthquakes and seismic experimental and theoretical research. However, these studies did not focus on URM and URC railroad piers.
- (2) In this study, the performance records of old URM and URC railroad bridge piers in past earthquakes are synthesized and summarized. Recorded damages are tabulated in Appendix A. Records show that old railroad bridge structures performed well in earthquakes. However, if damage appeared, it was highly possible to be severe. Typical failure modes of URM and URC bridge piers under earthquake loads include: (1) integral displacement in horizontal or vertical

directions or integral tilting; (2) horizontal cracks along construction joints in URC piers; (3) cracking of mortar joints in brick or stone masonry piers; (4) sliding along the horizontal run-through cracks; (5) tilting of the upper portion of piers after horizontal run-through cracks form; (6) coping stone failure, e.g., loosened, displaced, or torn; (7) anchorage failure between bearings and piers. These failure modes are considered in evaluation of theoretical analytical results and selection of retrofit measures.

- (3) The design of old URM and URC railroad bridge piers was based on an elastic analysis approach. The process included checks of the safety factors of overturning and sliding at critical sections and the allowable stress of masonry or concrete material at the base of the substructures. This design philosophy is different from requirements in current design codes such as AREMA MRE, AASHTO LRFD Specifications and Chinese GB50111-2006. These codes have no requirements for the response limits of URM and URC structures. Thus, further studies need to be carried out to determine a proper approach for evaluating the actual capacity of old piers under seismic loading.
- (4) Performance-based evaluation method is broadly accepted by seismic engineering societies. Multi-level performance objectives under diverse seismic hazard levels are considered in the capacity evaluation of bridge structures. Different analysis methods, e.g., single-mode or multimode response spectrum method, linear time-history analysis method, limit analysis method, pushover analysis, and non-linear time-history analysis method could be used in seismic demand evaluation of URM and URC piers. The proper method should be selected by considering structural regularity, assumptions on the boundary condition and structural stiffness, and calculation capacity, etc. Based on review of current seismic retrofit provisions in codes, it is reasonable to employ retrofit schemes with multi-level performance criteria, according to the importance and service life of the bridges. It might be appropriate to use the performance criteria in the design provision of the AREMA MRE. Further theoretical or experimental research may need to be implemented to determine proper measures specified for URC and URM railroad bridge piers.

3. RESTRAINING EFFECT OF RAIL TRACK STRUCTURE ON THE PERFORMANCE OF RAILROAD BRIDGE UNDER LATERAL LOAD

3.1 Introduction

Railroad bridges typically have better seismic performance as compared to highway bridges (Byers 1996, Cook et al. 2006). The track system was considered as a contributor

to this better performance because it can act as a restraint against horizontal movement of the superstructure during earthquakes (AREMA 2018).

From 1994 to 1995, two full-scale field tests on a railroad ballast deck through-plate girder bridge with jointed rail track were conducted by AAR, Caltrans, and UNR. One of the tests evaluated the impact of the continuity of the rail track structure between the deck and adjacent roadbed on the dynamic response of the bridge superstructure (Maragakis et al. 1996; Sandirasegaram 1997). The other test investigated the static ultimate capacity of the deck-abutment connections when the bridge superstructure was pushed in the lateral direction (Maragakis et al. 2001).

In 1998, a field test on a 5-span 18.9-m (62-ft), open-deck deck-plate-girder (DPG) steel bridge with jointed rail track subjected to lateral and longitudinal loading was conducted by the Transportation Technology Center, Inc. (TTCI) (Otter et al. 1999a; Uppal et al. 2000). The resistance to lateral and longitudinal displacement provided by anchor bolts, frictional and locking forces, and the continuous rail was identified in the test.

In 2000, a field test on two open-deck I-beam railroad spans to examine the resistance to longitudinal movement provided by the track structure was conducted by TTCI (Doe et al. 2001; Uppal et al. 2001). Several critical friction properties that contribute to the resistance of longitudinal movement of the bridge superstructure were investigated separately, including the coefficient of friction between rails and ties, the coefficient of friction between ties and the bridge girder, and the coefficient of friction between the girder bearings and pier head.

These full-scale field experiments systematically studied the restraint effect on the horizontal movement of bridge superstructure from the rail track structure for both ballast deck bridges and open deck bridges. However, the restraint effect of the rail track structure on the performance of bridge piers was not explored. Meanwhile, there exists a need to analyze these field experiments theoretically by using numerical approaches.

In this study, a structural analysis model of the rail track structure under lateral pushing load was developed by treating the rail as a continuous beam with support at each anchor position between rail and ties. The connection between the ties and the bridge superstructure was modeled as a rigid link element for open deck railroad bridges and as a spring link element for ballasted deck railroad bridges. The proposed model was implemented for ballast-deck and open-deck girder bridges and verified with the data from the previous field testing. A parametric study was conducted to investigate a range of the stiffness of the rail track structure under lateral loading.

Several studies were conducted on the numerical modeling methods to investigate the behavior of the rail track system. For instance, Dong et al. (1994) developed a two-

dimensional finite element model of a long track consisting of rail, tie, and ballast to study the dynamic interactions between trains and rail track. With the calculation capacity limitation at that time, the tie was modeled as a lumped mass and the ballast was modeled as a one-dimensional linear spring element. A nonlinear wheel-rail contact model was proposed by using a set of vertical contact spring elements distributed between the wheel and rail. Since the concern of the study is on the wheel loading applied onto the track structure, the discussions were carried out on the influence of the axle weight and wheel rotation speed, the ballast stiffness in the wheel loading direction.

In Ganesh Babu and Sujatha's study (2010), the finite element models of a 1.95-meter rail track section with consideration of subgrade, ballast and rail pad parameters were developed to investigate the influence of prestressed and wood crossies on the ground vibrations excited by cyclic axle loads. The FE model was developed in three-dimensions, however the material properties of the track components, e.g. rails, concrete and wood ties, ballast and subgrade, are assumed to be linear elastic. There are also other similar studies that investigate the behavior of the rail track system by the finite element method. However, they are concerned with either the interaction of the vehicle, wheel and track or the evaluation of different types of crossies. The numerical modeling that evaluates the effect of rail track structure on the behavior of bridge superstructures and substructures has not been thoroughly studied. This study proposes a three-dimensional numerical analysis approach in SAP2000 that investigates the interaction between the rail track and the bridge structure by considering the nonlinear properties of steel and concrete materials as well as the nonlinear behavior of the ballast and bearings subjected to lateral loads. The modeling considerations are introduced below.

3.2 Modeling Based on Previous Experimental Studies

3.2.1 Modeling for Uppal et al. (2000) testing

3.2.1.1 Introduction of the testing and continuities of rail track along the bridge in the modeling

Uppal et al. (2000) tested a single-track open deck bridge in Cincinnati, Ohio (referred to as the Cincinnati Bridge). The bridge had seven spans with identical 18.9-m (62-ft) riveted steel deck-plate-girders. The spans rested on flat-plate bearings and were supported by concrete piers. Five tests, including three lateral pushes and two longitudinal pushes, were implemented on these seven bridge spans. The layout of this testing program is shown in **Figure 3.1**.

In this study, the leftmost three spans, spans 16, 17 and 18 in **Figure 3.1** are modeled. The rail and guardrail are continuous between span 16 and the embankment at the

abutment, are continuous between spans 16 and 17 at pier 16 and are discontinuous between spans 17 and 18 at pier 17. The modeling considerations of the components and their connections for this bridge system are discussed below. As an example, the correlation between the model and the physical bridge at pier 16 of the Cincinnati Bridge is illustrated in **Figure 3.2**.

3.2.1.2 Rail track and guardrail track

The American Railway Engineering and Maintenance-of-Way Association (AREMA) standard rail with 196.4 kg/m (132 lb/ft) unit weight was used as the rail track for the Cincinnati Bridge. AREMA standard rail with 148.8 kg/m (100 lb/ft) was used as the guardrail. ASTM A499 (ASTM International 2015) Grade 50 steel was used for the rail and guardrail. The rails are modeled as wide flange sections with cross-sectional properties of the actual rail section. The rail material properties include: yield strength 344.7 MPa (50 ksi), ultimate tensile strength 551.6 MPa (80 ksi), Poisson’s ratio 0.3 and modulus elasticity 200 GPa (29000 ksi). The stress-strain curve of the steel which includes the elasticity stage and post-yield hardening stage is shown in **Figure 3.3**.

The three-dimensional frame element, which can consider the effects of biaxial bending, torsion, axial deformation and biaxial shear deformations, in SAP2000 is used for the simulation of the rail steels. The element sizes range from 305 mm to 457 mm (1 to 1.5 ft.) depending on the length of the member in the model.

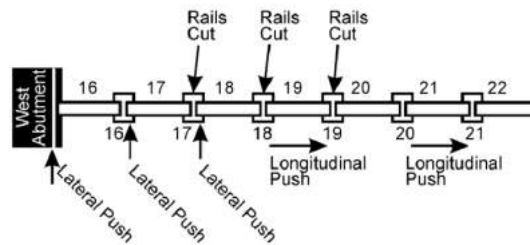
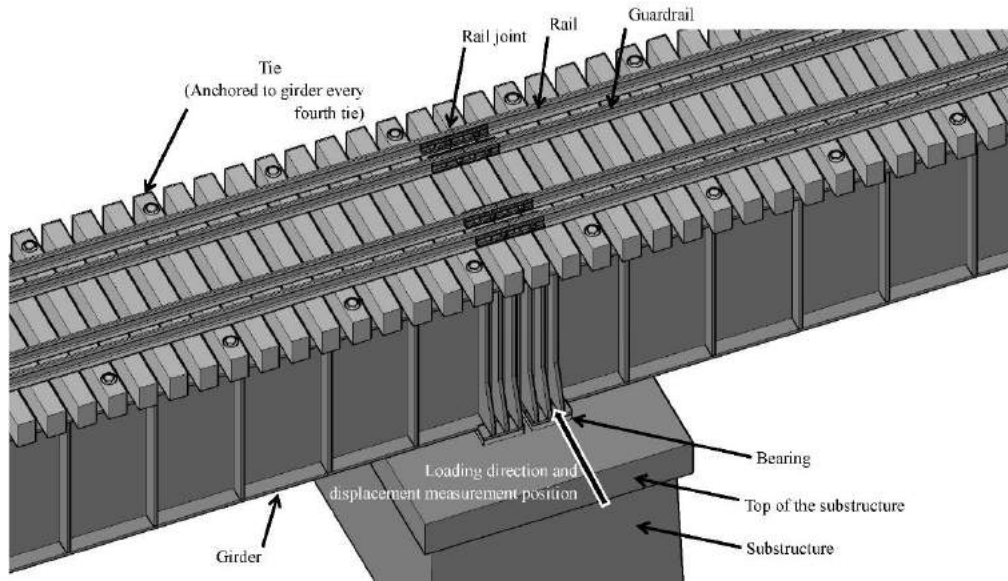
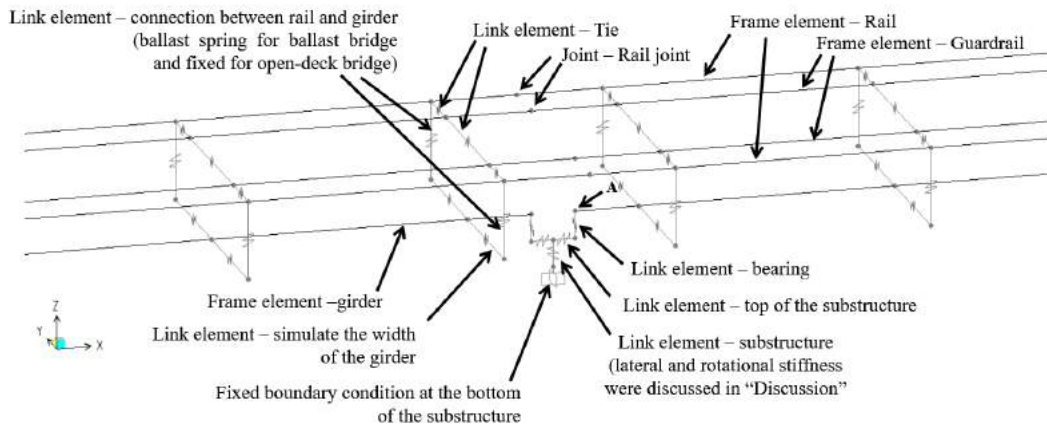


Figure 3.1 Plan View of Lateral Push Tests on the Cincinnati Bridge (Uppal et al. 2000)



a) Physical bridge components



Joint A: The end of the girder, also the position of lateral loading and lateral displacement measurement.

b) SAP2000 model

Figure 3.2 Correlation between SAP2000 Model and Physical Bridge (Pier 16 of the Cincinnati Bridge)

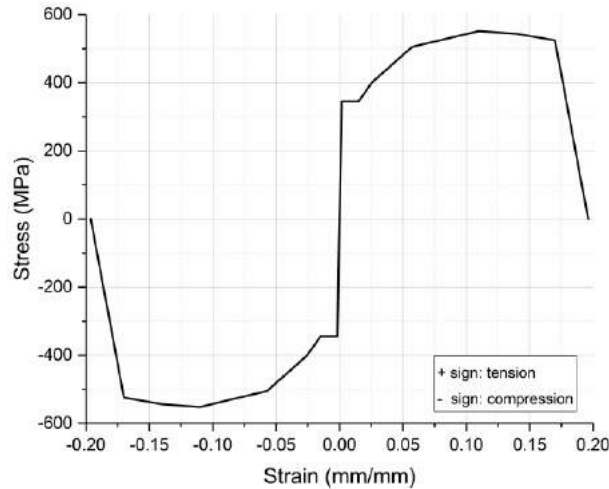


Figure 3.3 Constitutive Law of Rail Steel in Modeling

3.2.1.3 Rail joints

Because of how rail joints are configured, they are physically able to transfer only a portion of the axial force and the moment between adjacent rail ends. However, few studies are available to indicate the range for this internal force transfer ratio of rail joints, which may be caused by the variations of joint types for different rail sizes and the variations of joint fasten levels. In this study, this release percentage in the model is calibrated by using the experimental load-displacement curves of the field testing. In the models, the joints of the rail track and the guardrail track are assumed to be located at the middle of adjacent bridge girder ends and they transfer half of the axial force and the bending moment. This is realized in the models by releasing 50 percent of the fixity at the ends of adjacent frame elements connected by the rail joint.

3.2.1.4 Timber ties

The bridge used timber crossties measuring 203 mm (8 in.) wide by 303 mm (13 in.) deep on 356 mm (14 in.) centers. In the model, the spacing between two adjacent ties is 1.42 m (56 in.) to represent the rail being anchored to every fourth tie, which has regular 0.36 m (14 in.) spacing on the bridge deck.

The three-dimensional frame element is used to simulate timber ties. The element sizes range from 305 mm to 457 mm (1 to 1.5 ft.). The timber is an orthotropic material (Green et al. 1999) that has independent mechanical properties in the three perpendicular axes: longitudinal (parallel to the grain), radial (perpendicular to the grain in the radial direction) and tangential (perpendicular to the grain, tangent to the growth rings). The longitudinal direction corresponds to the length direction of the tie and local axis 1 in the model. The radial and tangential directions correspond to the local axes 2 and 3 of the

local polar coordinate system in the model, respectively. Since the lateral pushing on the bridge girder is transferred to the rails through the timber ties, which are anchored to the bridge girder every fourth tie, the mechanical properties of the timber, at least in the length direction, needs to be considered. By considering recommendations in the previous research (Ganesh Babu and Sujatha 2010, Green et al. 1999), the following material properties are employed in SAP2000 model: modulus of elasticity $E_1=1378$ ksi, $E_2=137.8$ ksi and $E_3=68.9$ ksi, Poisson's ratio $\nu_{12}=0.35$, $\nu_{13}=0.38$ and $\nu_{23}=0.41$, and shear modulus $G_{12}=144$ ksi, $G_{13}=132$ ksi and $G_{23}=14$ ksi where 1, 2 and 3 correspond to the numbers of local axes.

In the actual bridge, the rails were fixed to the timber ties with tie plates and cut spikes. Since there is almost no relative translational or rotational movement between the rails and ties in the lateral direction, these connections are simulated as fixed connections in the model.

3.2.1.5 Ballast

The rail track and guardrail track were laid in ballast at the embankment zone off the end of the bridge. The resistance of the ballast to the rail-tie structure lateral displacement consists of the friction forces between the stone aggregate and the bottom and the two long sides' surfaces of the ties and the pressure the ballast provides against the front-end surface of the ties.

In the model, the restraint of the ballast against the lateral movement of the ties is modeled as a spring link between the ties and the embankment by using the link element in SAP2000. The spring stiffness of this link under lateral load is defined based on Kerr's (1980) study as shown in **Figure 3.4**. This ballast embankment zone is modeled as a length of 6.1 m (20-ft) off the end of the bridge to consider the influence of ballast resistance on the lateral movement of the rail track on the embankment.

3.2.1.6 Bridge girders

The steel deck-plate girders are modeled with corresponding cross-section properties and self-weight to represent the real structure. The three-dimensional frame element is used. The mesh size is 1.5 ft. On the main spans, the track system was fixed to the bridge girder every fourth timber tie with hook bolts which restrict the translational and rotational movement of the ties from beneath the girder top flange

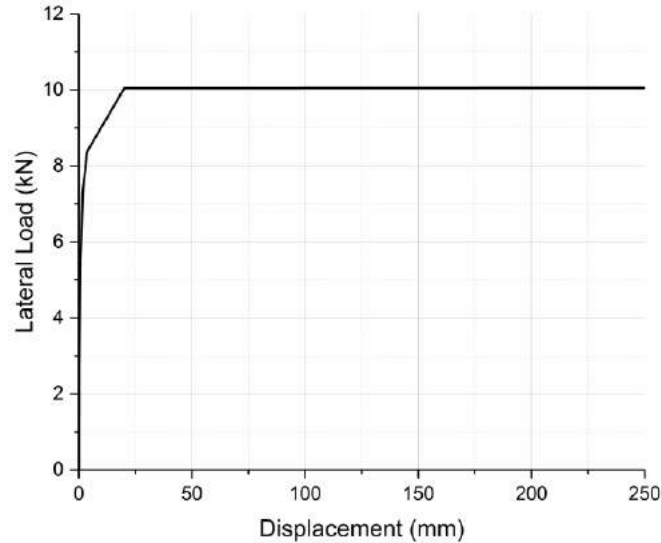


Figure 3.4 Stiffness of Ballast under Lateral Load in Modeling (after Kerr, 1980)

Thus, the connections between the track system and the bridge girder are simulated as fixed connections by using the rigid link element in SAP2000. These rigid link elements are connected to the bridge girder through the rigid link elements in the horizontal plane that simulate the width of the girder member.

3.2.1.7 Bearings

As stated in Uppal et al.'s report (2000), the girders rested on flat-plate bearings that were supported by concrete piers. The connection between each bearing and the pier consists of two anchor bolts with a nominal diameter of 38 mm (1.5-in.).

The bearings are modeled as spring links in the pushing direction between the girders and substructure by using the link element in SAP2000. The stiffness of these spring links is determined based on the testing at pier 17 in the report (Uppal et al. 2000). In the testing, the rail tracks were cut and discontinuous at both ends of span 18. The span was pushed laterally at one end, pier 17. The pushing load versus the displacement of the girder end is shown in the upper part of **Figure 3.5**. The bearings on the pushing end were almost the only resistance to the lateral load except the small rotation resistance provided by the bearings on the other end, pier 18. Thus, in this study the stiffness of the spring link in the model is consistent with the force-displacement results in Uppal et al.'s testing, as shown in the lower part of **Figure 3.5**.

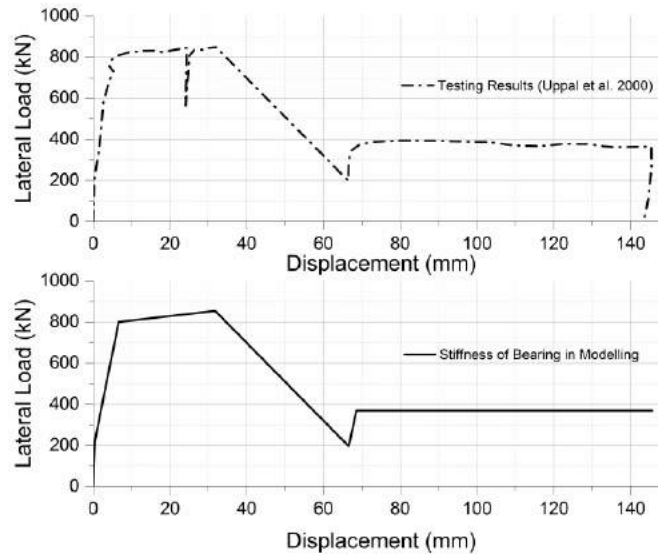


Figure 3.5 Stiffness of Bearing under Lateral Load in Testing and in Modelling for the Cincinnati Bridge

3.2.1.8 Substructures

Piers 16, 17, 18 and the abutment provided support to the spans studied here. Based on Uppal et al.'s report (2000), the piers and the abutment have very short height and relatively large cross-section areas (shown in **Figure 3.6**). Thus, the substructures are modeled as rigid ground supports to the bearings on top. This is modeled in SAP2000 by using three link elements: a vertical one to simulate the substructure and two horizontal ones to simulate the width of the top of the substructure which connect to the link elements simulating the aforementioned bearings. The two horizontal link elements are rigid in all six degrees-of-freedom. The stiffnesses of the vertical link element in the six degrees-of-freedom are configured as fixed for this Cincinnati Bridge study. They are changed in the *Discussion* section where the influence of the stiffness of the substructure members on the bridge behavior is investigated.

3.2.2 Modeling for Maragakis et al. (2001) testing

3.2.2.1 Introduction of the testing and continuities of rail track along the bridge in the modeling

Maragakis et al. (2001) tested a railroad bridge with two simple-supported spans that was located in California (referred to as the California Bridge). The bridge consisted of a



Figure 3.6 Typical Pier Condition in the Cincinnati Bridge (Uppal et al. 2000)

ballasted steel deck girder superstructure and a concrete two-column bent pier. As shown in **Figure 3.7**, the track structure of the west span, i.e., the rails, ties and ballast as well as the ballast pan, was cut completely free at the west abutment and the central pier. The east abutment was left in its as-built condition with the ties, rails, ballast, and ballast pan intact. The lateral force was applied to the bridge directly onto the lower portion of the girder at both abutments. Force-displacement diagrams were obtained at both ends of the bridge. The modeling consideration of the bridge system components and their connections is discussed below.

3.2.2.2 Rail track components and rail joints

AREMA standard rail with 168 kg/m (113 lb/ft) unit weight and Grade 50 steel was used as the rail track in the California Bridge. There is no guardrail for this ballasted bridge. The material properties of the rail steel in the model are the same with the Cincinnati Bridge model. The model configuration for the ties and the ballast are the same as the Cincinnati Bridge model. The rail joints are assumed to be located at the middle between the bridge girder ends and their adjacent abutments. The model configuration of the partial fixity release at rail joints is the same as the Cincinnati bridge model.

3.2.2.3 Bearings

The ballasted girder spans were supported by high seat type steel rocker bearings. The bearings are again modeled as a spring link that provides a lateral connection between the girder and the pier by using the link element in SAP2000. The spring stiffness of this connection is modeled with a nonlinear force-displacement curve based on the testing results of the west span in Maragakis et al. (2001). The load-displacement curves that were obtained in the testing as well as used in the model are shown in **Figure 3.8**.

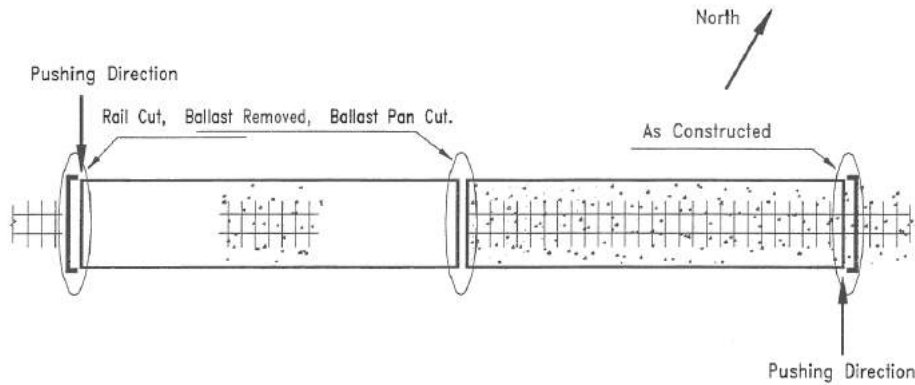


Figure 3.7 Plan-view Layout of Lateral Push Tests of the California Bridge (Maragakis et al. 2001)

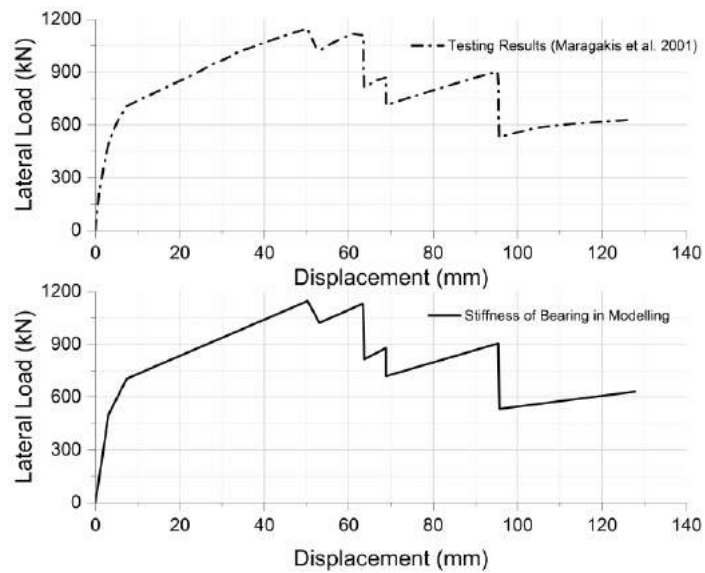


Figure 3.8 Stiffness of Bearing under Lateral Load in Testing and in Modeling for the California Bridge

3.2.2.4 Substructures

The bridge girders were supported on two abutments and one center concrete pier. The abutments are modeled as rigid ground supports to the superstructure. The center pier was modeled as a plain concrete continuum with a compressive strength of 4000 psi by using frame element in SAP2000. The modulus of elasticity was 24.9 GPa (3605 ksi) (ACI 2014), Poisson's ratio 0.2, and a nonlinear stress-strain curve for unconfined concrete (Mander et al. 1988; Computers & Structures Inc. 2016) were used as shown in **Figure 3.9**. The three-dimensional frame element in SAP2000 is used and the element size is 0.84 m (2.76 ft.) for this 7 m (23 ft.) high pier.

3.3 Results and Model Verification

3.3.1 Natural frequencies and modal analysis

A modal analysis was conducted for the California bridge model in SAP2000. **Table 3.1** tabulates the first three natural frequencies and mode types of SAP2000 analysis and the experimental results for the rail intact and rail cut cases. The fundamental frequencies in numerical analysis for the rail intact and rail cut cases are 5.39 Hz and 5.25 Hz. Both are oriented in the transverse direction. The second and third natural frequencies for the rail intact case in SAP2000 are 7.55 Hz and 8.74 Hz. They lie vertically and longitudinally, respectively. For the rail cut case, the second and third natural frequencies in SAP2000 are 6.74 Hz and 7.71 Hz. They are also in vertical and longitudinal directions, respectively.

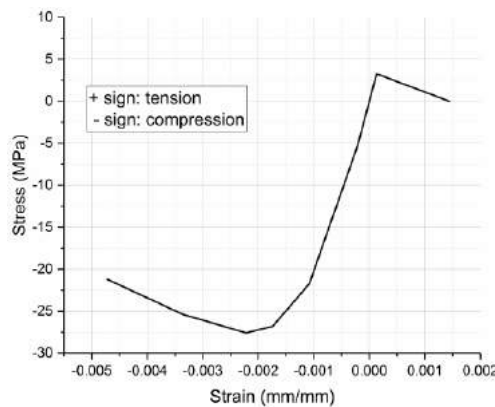


Figure 3.9. Constitutive Law of Plain Concrete in Modeling

Table 3.1 Frequencies and Mode Types of First Three Vibration Modals

Modal Number	Numerical Results		Experimental Results (Maragakis et al. 1998)	
	Natural Frequency (cycle/sec.)	Mode Type	Natural Frequency (cycle/sec.)	Mode Type
1	5.39 (5.25)	Transverse	4.93 (4.80)	Transverse
2	7.55 (6.74)	Vertical	6.06 (5.55)	Vertical
3	8.74 (7.71)	Longitudinal	6.56 (5.95)	Longitudinal

Note: Numbers without and with parentheses are results of rail intact and rail cut cases respectively.

Compared with the experimental results, the fundamental frequencies of the numerical analysis is 9.3% and 9.4% higher than the testing results for rail intact and rail cut cases, respectively. The differences between the model analysis and testing results increase for the second and third natural frequencies. Since the transverse, or lateral, direction is the research objective in this study, which is identical with the fundamental frequency direction, it would be reasonable to use the proposed model scheme for the following nonlinear static loading study in the lateral direction.

3.3.2 Load-displacement curve

Nonlinear static analyses, using the nonlinear material constitutive law for the steel and concrete and the nonlinear spring link element for the bearings and ballast, were implemented in SAP2000 (Computers & Structures Inc. 2016). This was done to simulate the behavior of the bridge structures under lateral pushing load at span ends in the experiments. In the analyses, the lateral load was applied directly at the span end of the superstructure girder to align with the field testing configuration. Both the force-load and the displacement-load can be applied in SAP2000. In this study, the force-load method was used for the ascending portion in order to capture the initial portion of the load-displacement curve, which has relatively high stiffness. The force load was increased gradually with an increment of 222.4 kN (50 kips) until it approached the ultimate load, where the increment was decreased to 44.5 kN (10 kips) or 4.45 kN (1 kip). The ultimate load is defined as the force load just before the condition of non-convergence in the SAP2000 model. This non-convergence may be caused by the non-injective characteristic; one ordinate value has more than one corresponding abscissa value on the curve, of the nonlinear load-displacement property for the link element of bearings and ballast and the nonlinear constitutive law of the steel material corresponding to the post-

peak, or downward, part of the curve. The post-ultimate portion of the load-displacement curve is obtained by applying the displacement-load. The increment of displacement-load is 2.54 mm (0.1 in.).

3.3.2.1 *Span 16 at abutment of the Cincinnati Bridge*

The rail track structure is continuous at both ends of this span. One end is connected to the ballasted embankment, and the other end is connected to the adjacent span 17, as shown in **Figure 3.1**. The results of load versus lateral displacement are plotted as a dashed line with triangle markers in **Figure 3.10**. The curves show nonlinear characteristics, due primarily to the nonlinear property of the links. From 0 to 890 kN (200 kips, point A in **Figure 3.10**), the curve consists of two portions with the slope decreasing at 222.4 kN (50 kips). The secant stiffness before 890 kN (200 kips) reaches 147 kN/mm (839 kip/in.). After 890 kN (200 kips) the stiffness drops significantly. The ultimate load is 1010 kN (227 kips) at a displacement of 31.3 mm (1.23 in.). By comparison span 18 @ pier 17 which had rail discontinuous at both span ends (the diamond marker in **Figure 3.10**) has a secant stiffness of 121 kN/mm (692 kip/in.) at yield point B in **Figure 3.10** and an ultimate load of 854 kN (192 kips). This indicates for open-deck bridges the continuous rail track structure benefits the bridge system in terms of the ultimate lateral pushing resistance and the secant stiffness before yielding (yielding is defined at the point after it the displacement increases rapidly in this study). This coincides with the conclusions of Otter et al's (1999b) study.

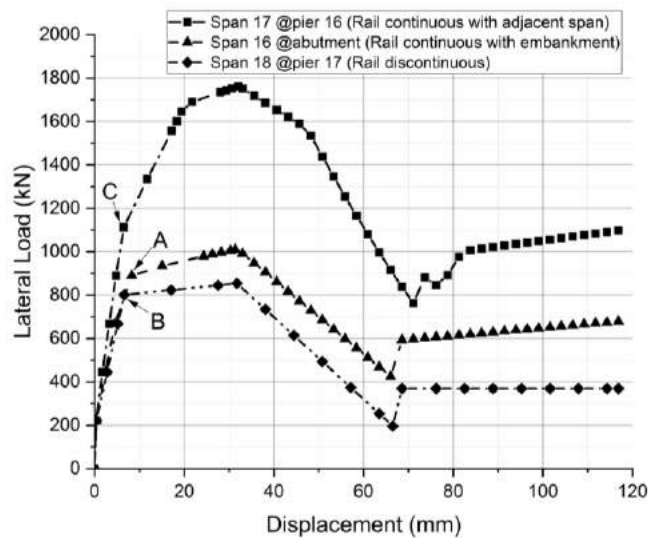


Figure 3.10 Load vs. Displacement of Modeling Results (Cincinnati Bridge)

The results of model analysis and experiment are compared in **Figure 3.11**. The model results match the experimental results on the ascending portion, especially in the initial part before 889.6 kN (200 kips). The modeling results have a greater ultimate load and corresponding displacement than the testing results. This may be caused by the over-estimation of the bearing lateral capacity in the model due to the difference of the deterioration level of the bearing-pier connection between different spans which will be discussed later.

3.3.2.2 Span 17 at pier 16 of the Cincinnati Bridge

Referring to **Figure 3.1**, one end of span 17 was continuous to the adjacent span 16 while at the other end, the rails and guiderails were cut and discontinuous with adjacent span 18. The pairs of lateral pushing loads and corresponding displacement results are plotted with the square marker line in **Figure 3.10**. The curve shows nonlinearity, caused primarily by the nonlinear property of the link elements. Similar to the results of span 16, from 0 to 1112 kN (250 kips, point C in **Figure 3.10**), the curve consists of two portions of linear increase with slope decreasing after 222.4 kN (50 kips). From 1112 kN (250 kips) to the ultimate load of 1761 kN (396 kips), the lateral displacement of bridge system increases severely as the pushing load increases. The secant stiffness at 1112 kN (250 kips) is 171 kN/mm (976 kip/in.) which is larger than the secant stiffness of 121 kN/mm (692 kip/in.) for span 18 @ pier 17 which had rail discontinuous at both span ends (referring to the diamond marker line in **Figure 3.10**). This shows the contribution of the rail track on the lateral pushing resistance both in ultimate load and secant stiffness before yielding that coincides with the findings in Otter et al (1999b).

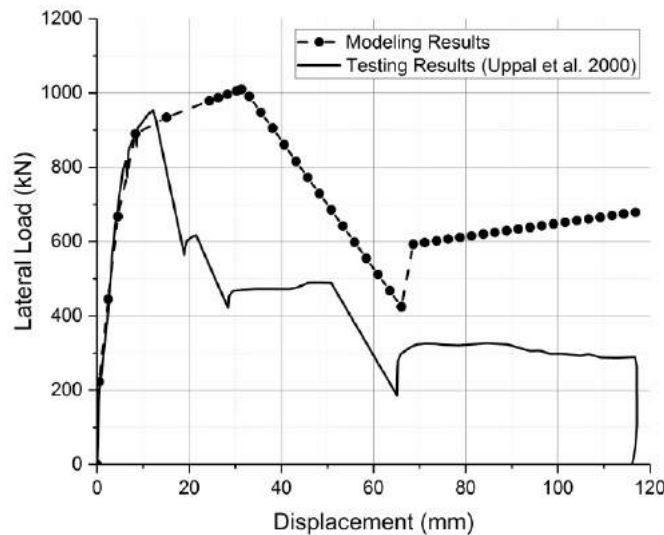


Figure 3.11 Comparison of Experimental and Modeling Results (Span 16 @ abutment, Cincinnati Bridge)

The modeling and testing results are compared in **Figure 3.12**. Note that in the experiment the lateral loading was forced to stop at 1357 kN (305 kips), referring to the peak point at about 30.5 mm (1.2 in.) displacement in **Figure 3.12**, because of the “incipient failure of the deteriorated surface concrete of the pier” reported in Otter et al.’s report (1999b). At that time, the anchor bolts of the bearing and the span were in good condition and should have been able to provide more lateral resistant capacity. This does not coincide with the assumption of rigid substructure in the aforementioned modeling analysis. However, the testing result curve also consisted of two portions before reaching the “ultimate state.” The load at yield point, about 1023 kN (230 kips), is close to the model result 1112 kN (250 kips).

3.3.2.3 East Span at abutment of the California Bridge

For the east span of the California Bridge, the rail track structure was intact at the connection between the east span, with ballast track, and the ballast embankment. Similar SAP2000 analysis and loading pattern with the Cincinnati Bridge were implemented. The load versus displacement results are plotted in dot-dash line with box markers in **Figure 3.13**. The yield point is around 667 kN (150 kips). The secant stiffness at 667 kN (150 kips) is 143 kN/mm (817 kip/in.) compared with the secant stiffness of 102 kN/mm (583 kip/in.) for the west span which has rail discontinuously (as shown in dash line in **Figure 3.11**). The lateral displacement rapidly increases as the pushing load increases. The

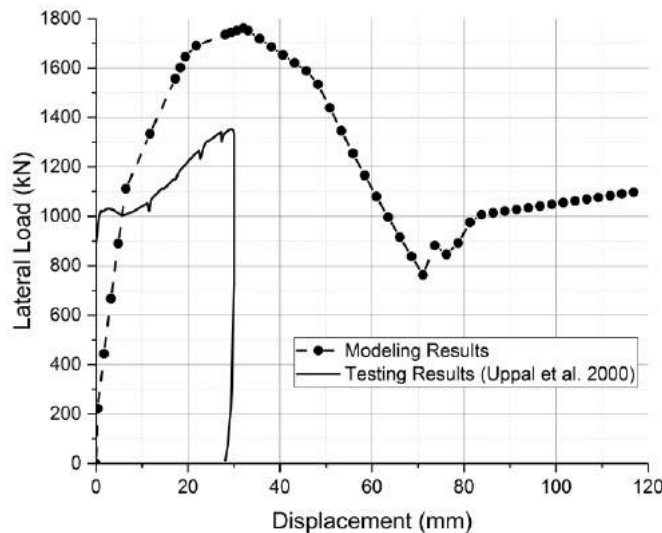


Figure 3.12 Comparison of Experimental and Modeling Results (Span 17 @ pier 16, Cincinnati Bridge)

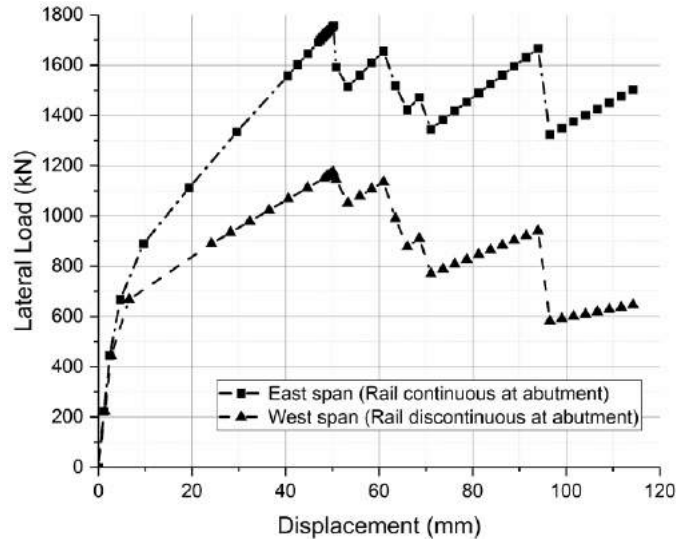


Figure 3.13 Load vs. Displacement of Modeling Results (California Bridge)

ultimate load is 1757 kN (395 kips) at a lateral displacement of 50.3 mm (1.98 in), while the ultimate capacity of the west span is 1174 kN (264 kip) at a displacement of 50.3 mm (1.98 in.). It indicates that for the ballasted bridge the rail track structure provides contribution to the secant stiffness before yield and ultimate resistance to the lateral pushing load, which coincides with the findings by Maragakis et al (2001).

The model results and experimental data are compared in **Figure 3.14**. The model results provide a reasonable prediction to the experiment before the ultimate state in the testing. The modeling has a relatively higher ultimate capacity than the testing result. This may be caused by the over-estimation on the bearing capability in the model due to the variation of the deterioration of bearings and their connections with the substructure.

3.4 Discussion

In the modeling analysis for the Cincinnati Bridge, a rigid substructure is assumed, which means infinite stiffness in displacement and rotation for the substructure. This assumption can be appropriate for a very short substructure, like the piers in the Cincinnati Bridge (**Figure 3.7**). However, it may not be appropriate to represent the behavior of bridges with taller piers.

A parametric analysis of the Cincinnati Bridge was carried out to determine the influence of the lateral and rotational substructure stiffness on the displacement behavior of the bridge, stress level in rail and failure modes under ultimate lateral loading. The

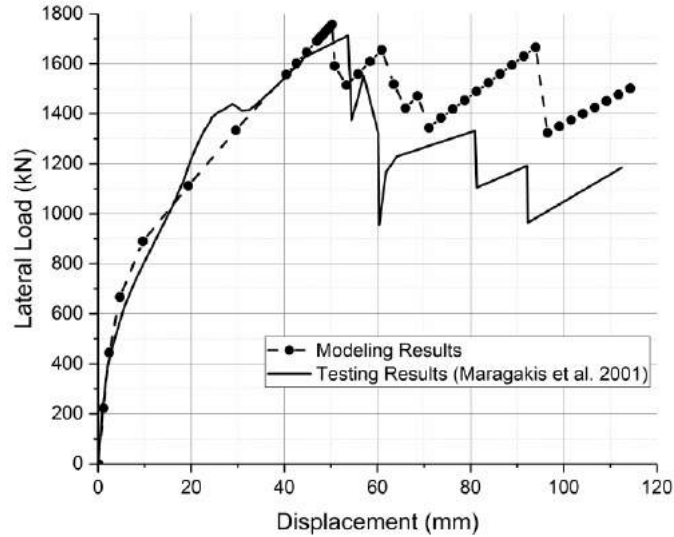


Figure 3.14 Comparison of Experimental and Modeling Results (East span, California Bridge)

parametric study focuses on the ascending portion of the load-displacement curve, especially the secant stiffness, and the post-ultimate portion of the curve is not examined.

3.4.1 Influence of lateral stiffness of substructure

3.4.1.1 Open-deck girder bridge

In order to explore the influence of the substructure’s lateral stiffness on the behavior of an open-deck girder bridge with continuous rail structure under lateral load at the end of the span, the lateral deformation stiffness of the “Link” element that simulates the substructure in SAP2000 model was varied from infinite (the same model for Span 17 of Cincinnati Bridge aforementioned) to 175 kN/mm (1000 kip/in.), 87.6 kN/mm (500 kip/in.), 35.0 kN/mm (200 kip/in.) and 17.5 kN/mm (100 kip/in.). **Figures 3.15** and **3.16** plot the behavior of lateral load versus displacement at the end of span and the stress level in rail under different levels of pier lateral stiffness. The influence of the lateral stiffness of substructure on the secant stiffness of the bridge system is tabulated in **Table 3.2** and illustrated in **Figure 3.17**. The secant stiffness is defined as the slope of the straight line between original point and the yield point in the load-displacement figures.

As shown in **Figure 3.15** and **Table 3.2**, as the pier stiffness decreases from infinite to 17.5 kN/mm (100 kip/in.), the secant stiffness of the bridge system decreases. This implies that at the initial phase of loading before system yielding, the lateral stiffness of

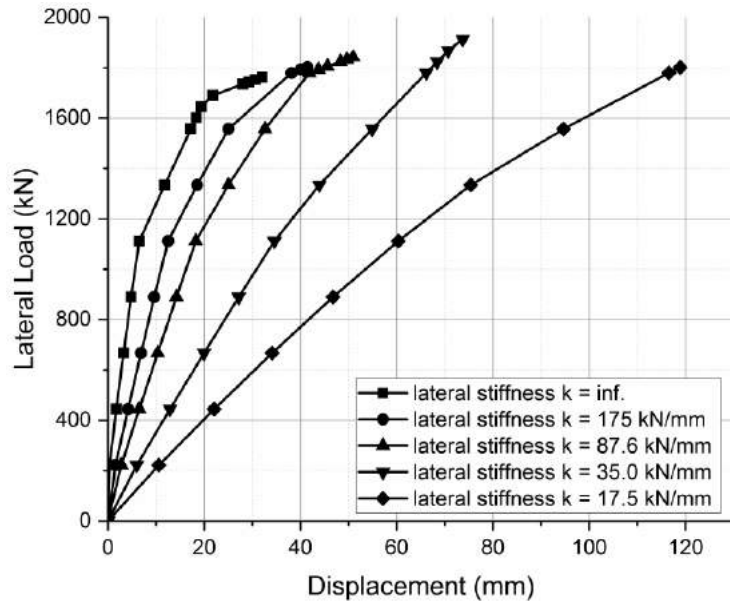


Figure 3.15 Influence of Lateral Stiffness of Substructure on Load vs. Displacement (open-deck bridge)

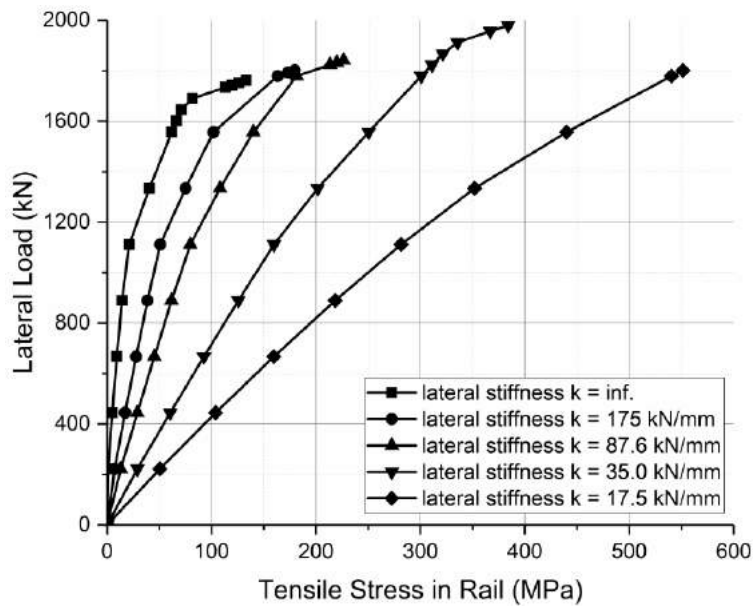


Figure 3.16 Influence of Lateral Stiffness of Substructure on Tensile Stress in Rail (Open-deck Bridge)

Table 3.2 Influence of Substructure Lateral Stiffness on System Secant Stiffness for Open-deck Bridge Models

Lateral Stiffness of Substructure (kN/mm)	infinite	175	87.6	35.0	17.5
Secant Stiffness of Bridge System (kN/mm)	171	89.0	60.9	32.2	17.7

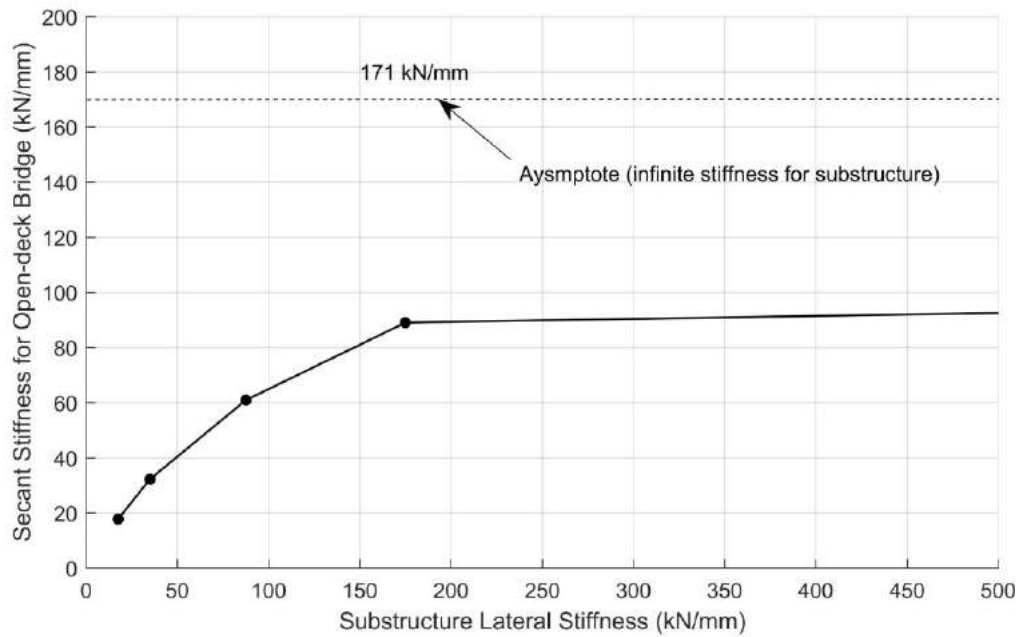


Figure 3.17 Relationship between Substructure Lateral Stiffness and Secant Stiffness for Open-deck Bridge System

the substructure plays an important role in the performance of the bridge system.

Figure 3.16 shows that the stress level in the rail steel increases with the decrease of the lateral stiffness of the substructure. It indicates that the rail picks up more of the load as the pier stiffness decreases. The model with the smallest pier stiffness fails by the failure of rail steel (the tensile stress reaches the ultimate stress of 551 MPa).

Figure 3.18 shows that as the lateral stiffness of the substructure decreases most of the total lateral displacement changes from being the local displacement of bearings to the lateral displacement of the substructure. The failure of the bridge system is governed by the bearing capacity for a stiffer substructure and by the rail steel failure for a substructure with less lateral stiffness.

3.4.1.2 Ballast bridge

Similar to the analysis for the open-deck girder bridge, a parametric study is performed for the ballasted deck bridge. The model for Span 17 of the Cincinnati Bridge was used and the load-displacement property of the Link element between rail and girder was changed to the one shown in **Figure 3.4** that was used to simulate the lateral displacement behavior of the ballasted structure. The analytic results are plotted in **Figures 3.19** and **3.20** to show the influence of the lateral stiffness of the substructure on the load-displacement behavior of bridge structure and the stress level within the rail steel, respectively. The influence of the lateral stiffness of substructure on the secant stiffness of the bridge system is tabulated in **Table 3.3** and illustrated in **Figure 3.21**.

Above a load of 890 kN (200 kips), the stiffness of the structure is similar and mostly independent of the substructure stiffness. The behavior of each model at ultimate load is controlled by the lateral displacement capacity of the bearing while independent of the lateral stiffness of the pier. This is verified by **Figure 3.22** in which the relative displacement between the top of the bearing and the top of the substructure for the models reaches 31.8 mm (1.25 in.) which identifies the maximum lateral displacement capacity of bearing. As shown in **Figure 3.20**, none of the rail steel in the models reaches the ultimate tensile stress. This can be explained by the ballast between the rail track structure and bridge girder. The ballast does not transfer much of the displacement from the bridge girder and the bearing to the track structure. The rail track structure is able to “float” on the ballast and has smaller lateral displacement and a smaller stress level during lateral loading in comparison with open-deck bridges.

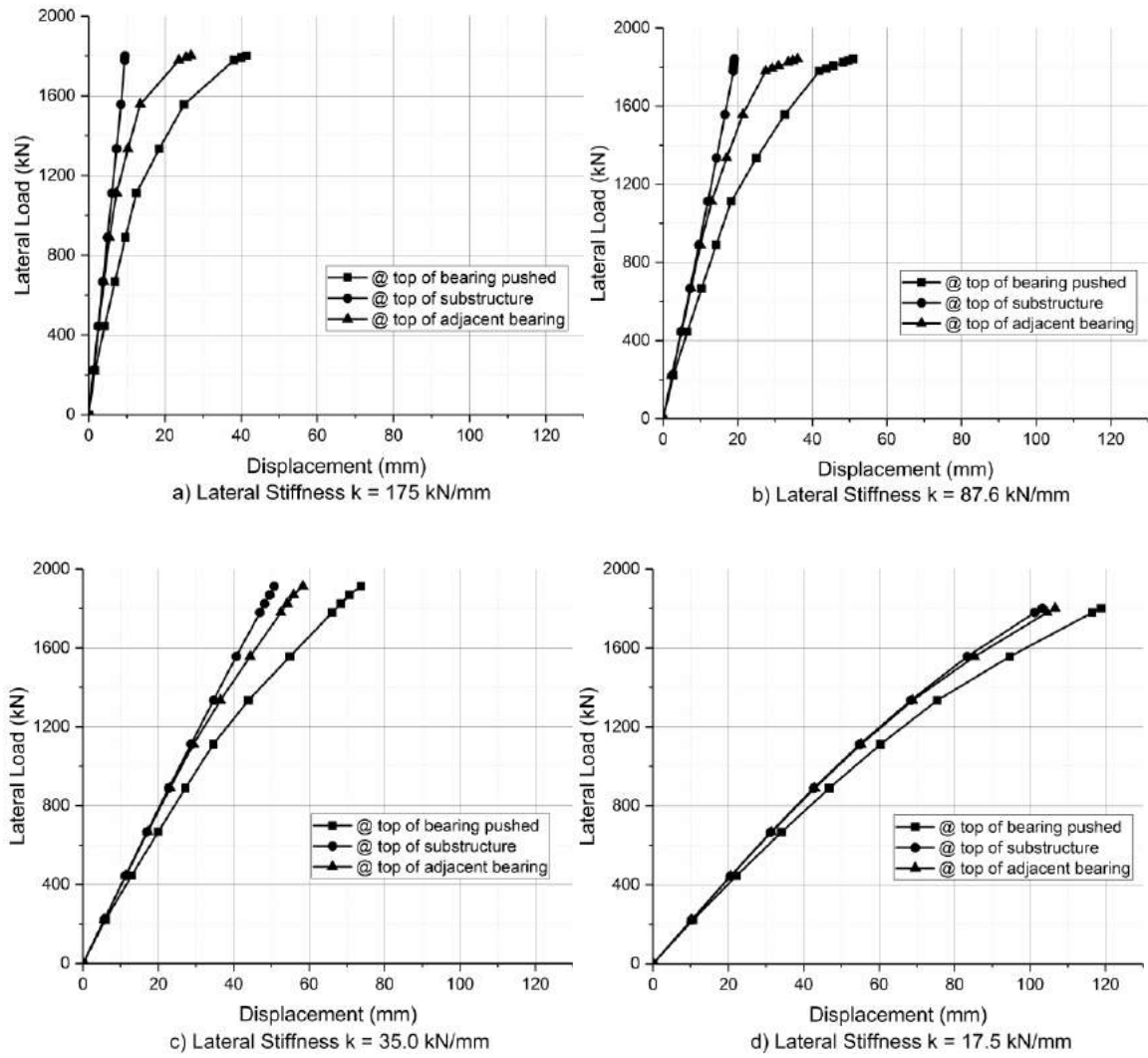


Figure 3.18 Influence of Lateral Stiffness of Substructure on Displacement at Different Position (Open-deck Bridge)

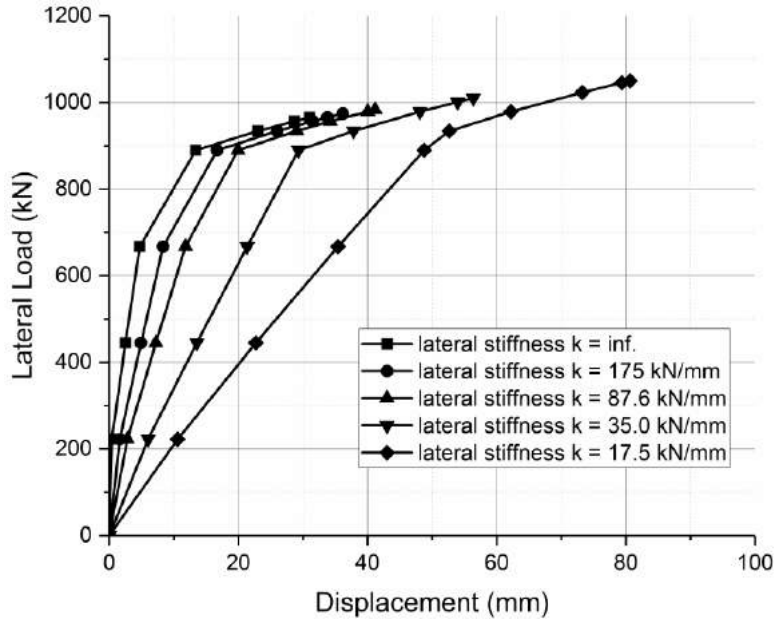


Figure 3.19 Influence of Lateral Stiffness of Substructure on Load vs. Displacement (Ballast Bridge)

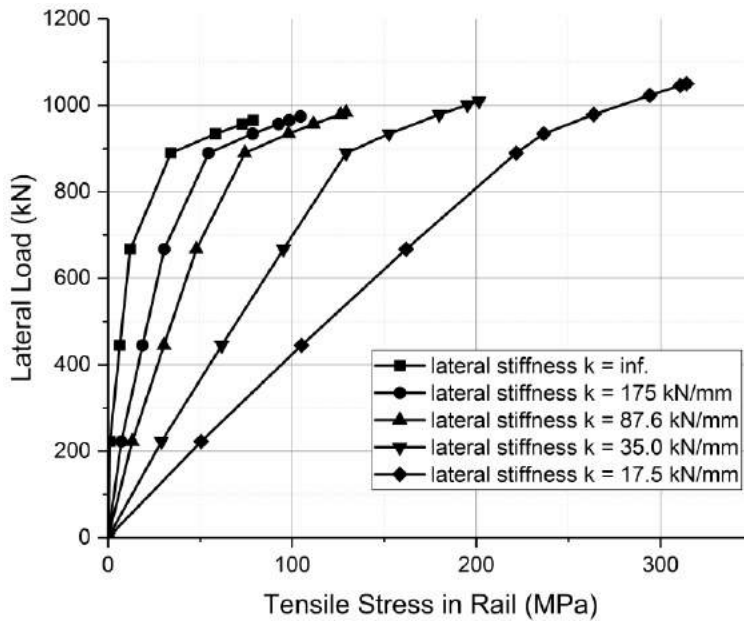


Figure 3.20 Influence of Lateral Stiffness of Substructure on Tensile Stress in Rail (Ballast Bridge)

Table 3.3 Influence of Substructure Lateral Stiffness on System Secant Stiffness for Ballast Bridge Models

Lateral Stiffness of Substructure (kN/mm)	infinite	175	87.6	35.0	17.5
Secant Stiffness of Bridge System (kN/mm)	141	79.9	56.5	31.2	18.8

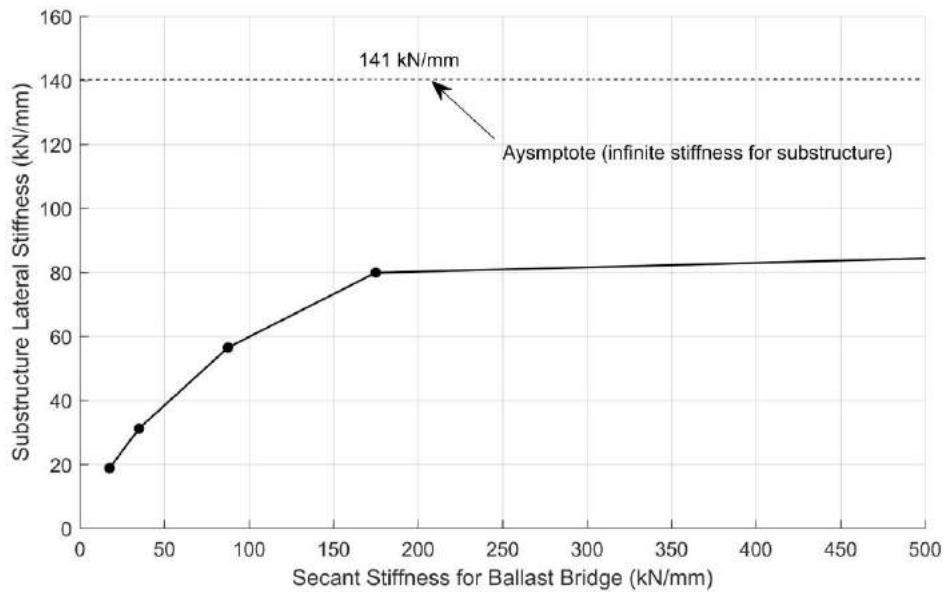


Figure 3.21 Relationship between Substructure Lateral Stiffness and Secant Stiffness for Ballast Bridge System

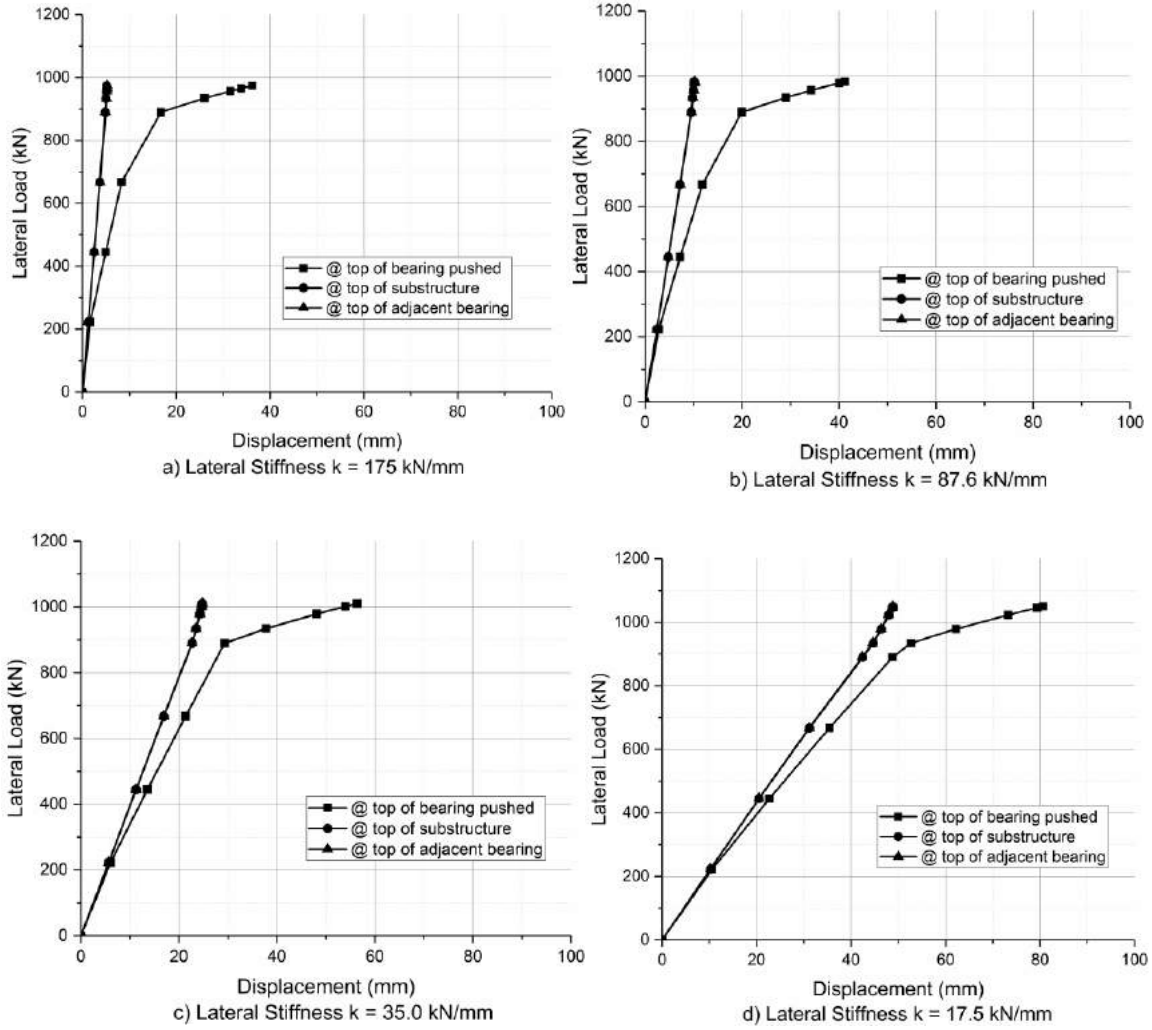


Figure 3.22 Influence of Lateral Stiffness of Substructure on Displacement at Different Position (Ballast Bridge)

3.4.2 Influence of rotational stiffness of substructure

3.4.2.1 Open-deck girder bridge

The torsional stiffness of the substructure may influence the displacement performance of a bridge under lateral loading, as shown in **Figure 3.23**. Based on the model of the Cincinnati Bridge's Span 17, a parametric study was performed that varied the torsional stiffness of the substructure from infinite to 565 kN-m/rad (5000 kip-in./rad) and 226 kN-m/rad (2000 kip-in./rad). The results for the load-displacement at the end of span and load-stress in rail are plotted in **Figures 3.24** and **3.25**. The influence of the rotational stiffness of the substructure on the secant stiffness of the bridge system is tabulated in **Table 3.4** and illustrated in **Figure 3.26**.

As shown in **Figure 3.24** and **Table 3.4**, the change of rotational stiffness has almost no impact on the stiffness of the bridge. The stress in the rail steel is only about 20% of the ultimate strength of 552 MPa. On the other hand, the failure of the models is all due to excessive displacement, reaching the maximum displacement at the ultimate load for bearing 31.8 mm (1.25 in.), **Figure 3.27**. Also, in the same figure, the rotation of the pier top causes the bearings at the same pier to move in the opposite direction (yield negative in displacement in **Figure 3.27**). As long as the load increases, these two bearings turn to move in the same direction with load due to the existence of the rail track structure.

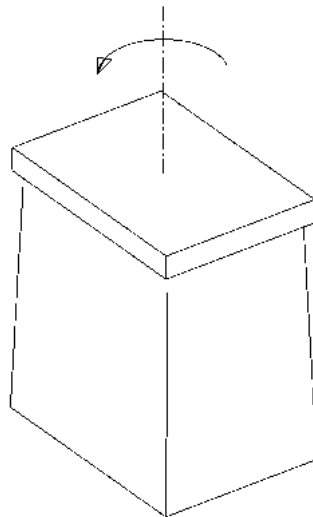


Figure 3.23 Torsion with Respect to Pier Centerline Axis

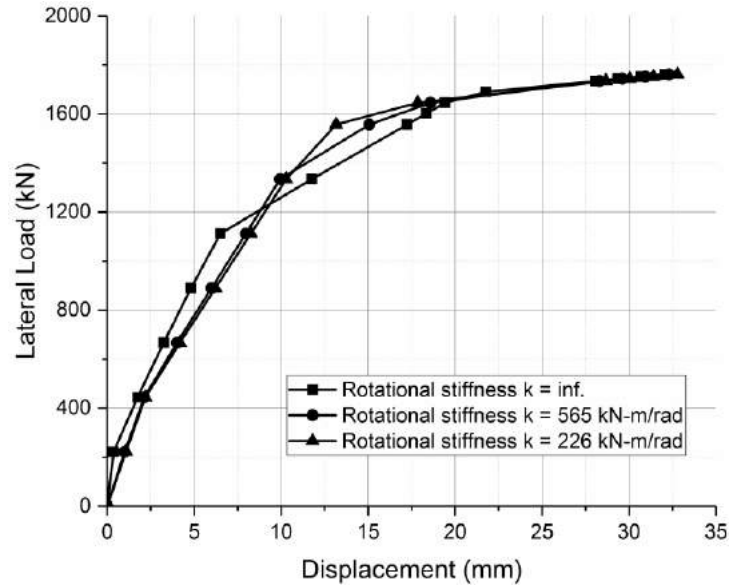


Figure 3.24 Influence of Torsional Stiffness of Substructure on Load vs. Displacement (Open-deck Bridge)

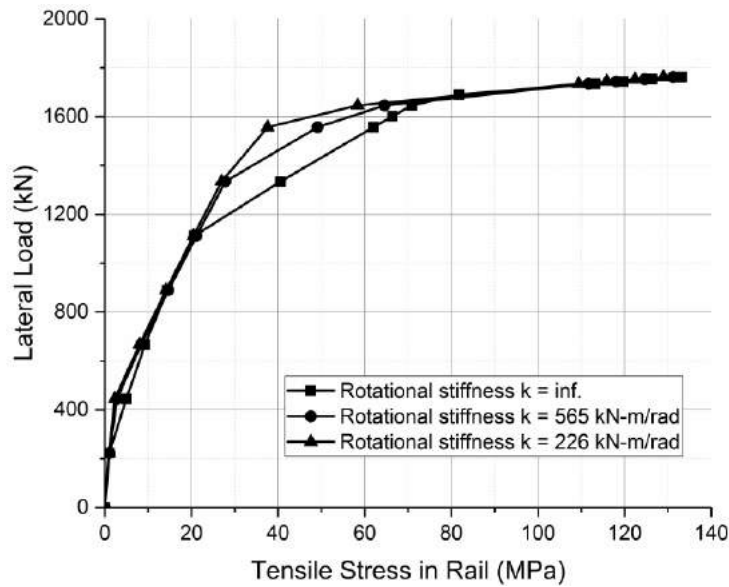


Figure 3.25 Influence of Torsional Stiffness of Substructure on Tensile Stress in Rail (Open-deck Bridge)

Table 3.4 Influence of Substructure Rotational Stiffness on System Secant Stiffness for Open-deck Bridge Models

Torsional Stiffness of Substructure (kN-m/rad.)	infinite	565	226
Secant Stiffness of Bridge System (kN/mm)	171	140	135

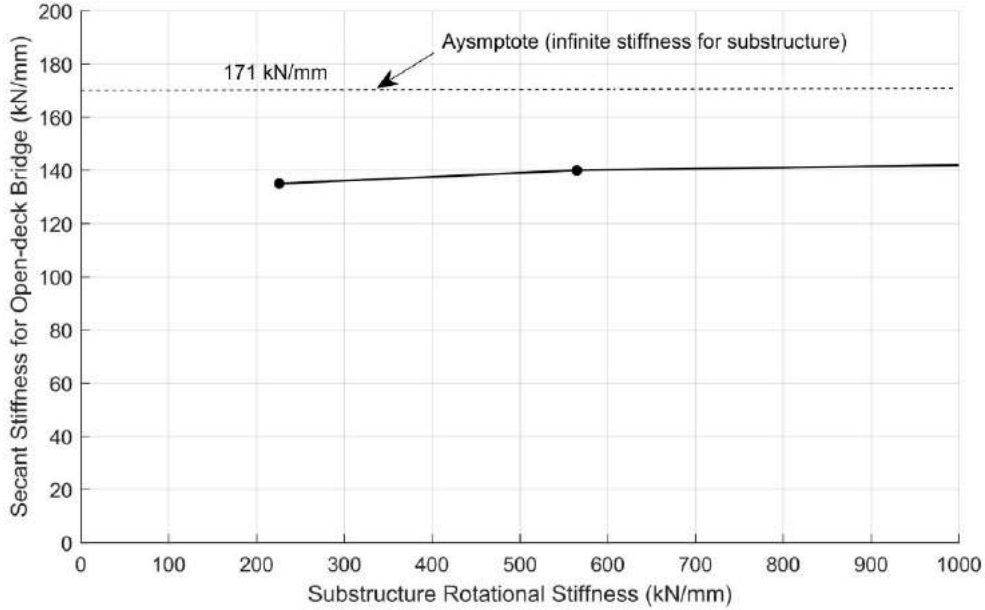


Figure 3.26 Relationship between Substructure Rotational Stiffness and Secant Stiffness for Open-deck Bridge System

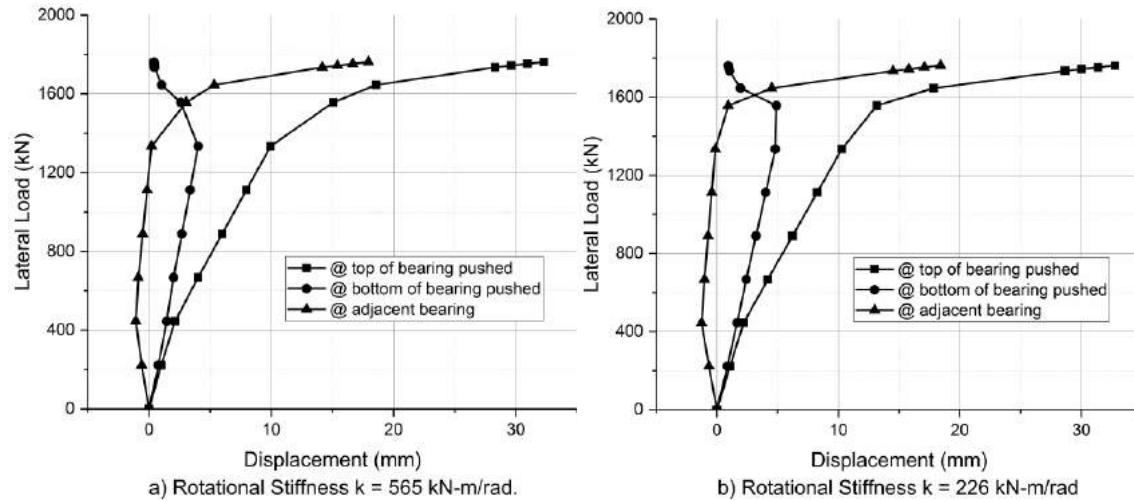


Figure 3.27 Influence of Rotational Stiffness of Substructure on Displacement at Different Position (Open-deck Bridge)

3.4.2.2 Ballast bridge

A similar parametric study was carried out on how torsional stiffness influences the substructure of ballast bridges. The torsional stiffness varied from infinite to 565 kN-m/rad (5000 kip-in./rad) and then 226 kN-m/rad (2000 kip-in./rad). The results of load-displacement and load-tensile stress level in rail are plotted in **Figures 3.28** and **3.29**. The influence of the rotational stiffness of the substructure on the secant stiffness of the bridge system is tabulated in **Table 3.5** and illustrated in **Figure 3.30**.

Figures 3.28 and **3.29** and **Table 3.5** show that the pier torsional stiffness affects the lateral stiffness of the bridge structure, its ultimate load, and corresponding displacement at ultimate load. As the rotational stiffness of the substructure decreases, the lateral stiffness of the bridge structure system decreases; at the same time, the ultimate load and the corresponding displacement at the ultimate load increase. **Figure 3.31** shows that the structure reaches its ultimate state due to excessive lateral deformation, over 30.8 mm or 1.25 in. (referring to the peak in **Figure 3.5**), of the bearing. These phenomena can be explained by the existence of ballast between the rail track and bridge girder. The ballast transfers little of the pier displacement to the rail track on the top. Thus, no excessive tensile force is generated in the rail track with the increase of lateral load on the bearing. The majority of the lateral displacement of the bridge system comes from the rotation of the pier top. The rail contributed little to the lateral stiffness and capacity of the bridge.

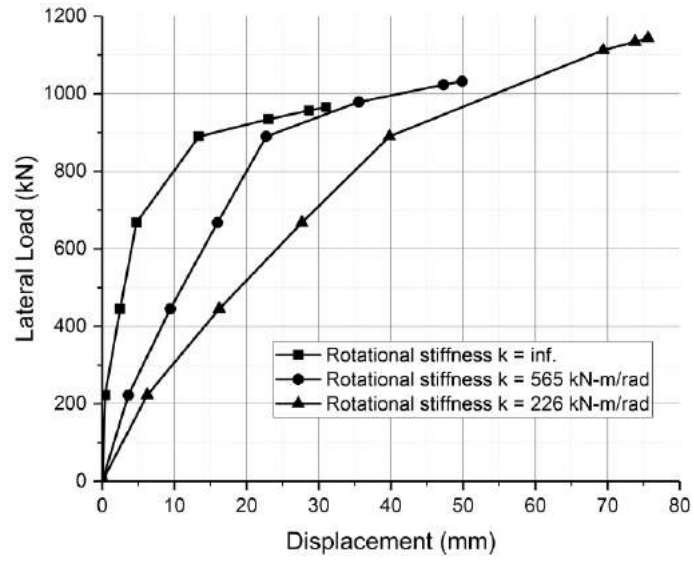


Figure 3.28 Influence of Torsional Stiffness of Substructure on Load vs. Displacement (Ballast Bridge)

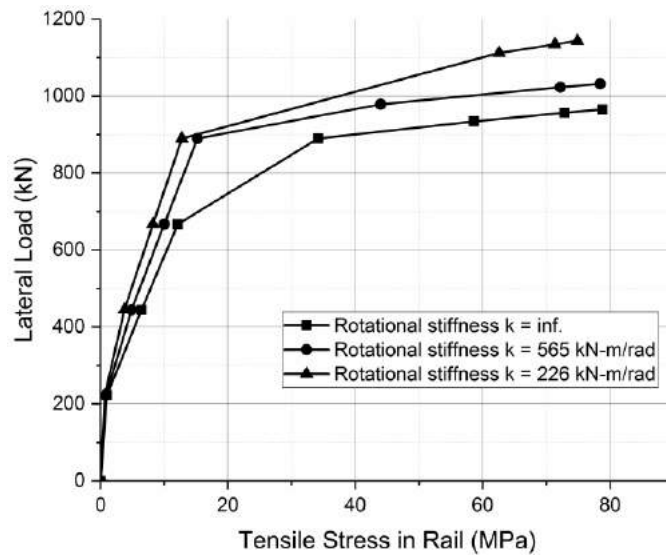


Figure 3.29 Influence of Torsional Stiffness of Substructure on Tensile Stress in Rail (Ballast Bridge)

Table 3.5 Influence of Substructure Rotational Stiffness on System Secant Stiffness for Ballast Bridge Models

Torsional Stiffness of Substructure (kN-m/rad.)	infinite	565	226
Secant Stiffness of Bridge System (kN/mm)	141	41.7	24.1

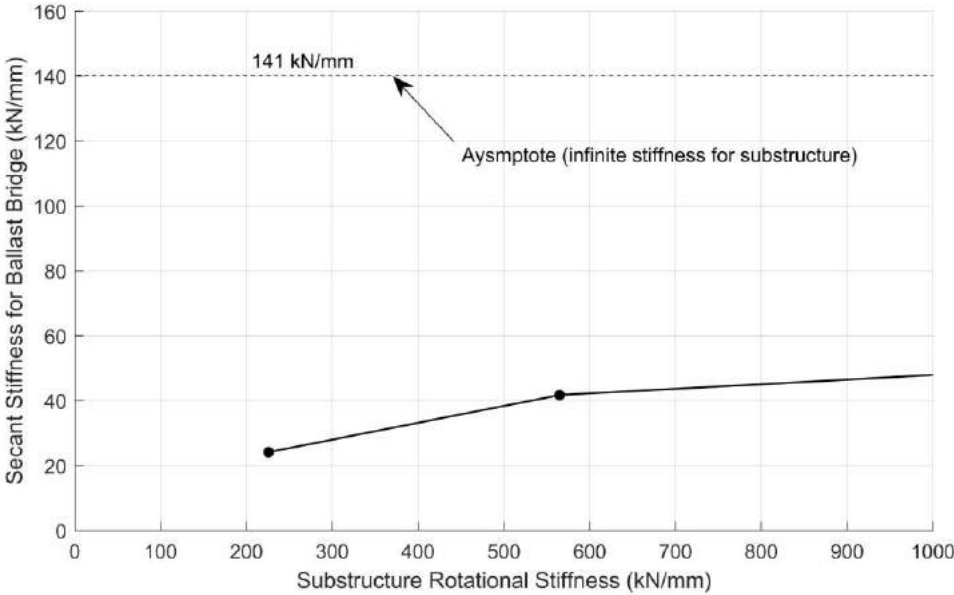


Figure 3.30 Relationship between Substructure Rotational Stiffness and Secant Stiffness for Ballast Bridge System

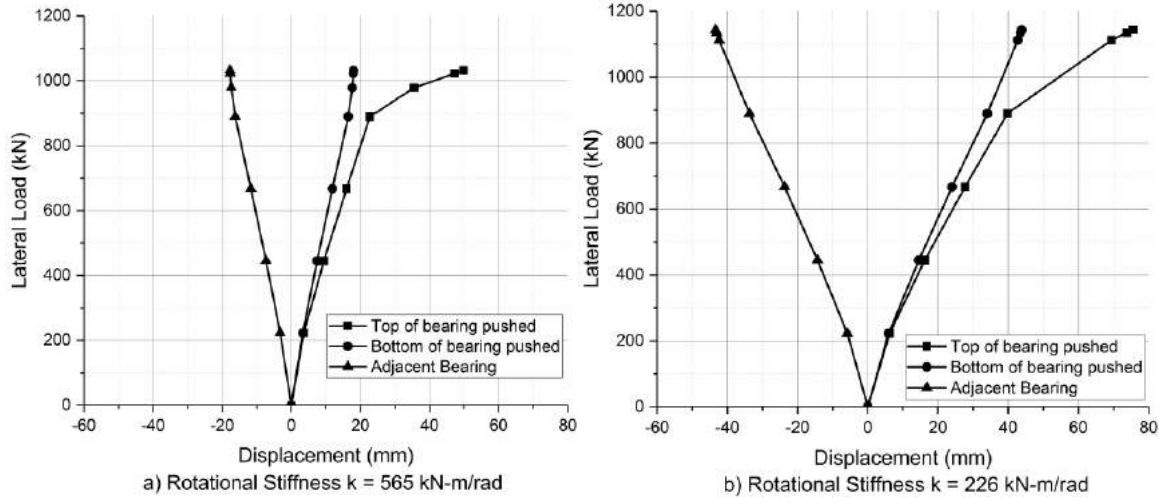


Figure 3.31 Influence of Rotational Stiffness of Substructure on Displacement at Different Position (Ballast Bridge)

3.5 Conclusions

To find out how the rail track influenced the lateral behavior of a railroad bridge system under lateral load at the end of the span, we implemented a nonlinear three-dimensional model analyses for both the ballast bridge and the open-deck girder bridge in SAP2000, and we validated the results based with the experimental research reported in the literature. Several conclusions were drawn:

- (1) The SAP2000 model scheme proposed in this study, which used the link element to simulate the behavior of bearings and ballast, reached a reasonable agreement with the previous full-scale field experimental results on both open-deck and ballast railroad bridges regarding the fundamental frequency and mode type and the force-displacement behavior before the ultimate state.
- (2) For the open-deck girder bridge model, the secant stiffness of the bridge system increased with the increase of the lateral stiffness of the substructure. The model with greater pier stiffness had less ultimate displacement. We found that the failure of the bridge system was governed by the bearing capacity for a stiffer substructure and by the rail steel failure for a substructure with less lateral stiffness.
- (3) For open-deck bridges, the rotational stiffness of the substructure had little impact on the secant lateral stiffness of the bridge system. The stress of rail steel remains at a low level. The cause of the ultimate state is the excessive bearing deformation.

- (4) For ballast bridges, the secant stiffness of the bridge system increases when the lateral stiffness of the substructure increases. Because of the ballast between the rail track and bridge girder, the lateral displacement and tensile stress of the rail steel remain small. The bridge system reaches the ultimate state when the bearing reaches the lateral displacement capacity.
- (5) For ballast bridge models, as the rotational stiffness of the substructure decreases, the secant lateral stiffness of the bridge structure system also decreases. Meanwhile, the ultimate load and the corresponding system lateral displacement at ultimate state increases. The bridge system reaches the ultimate state because of the excessive lateral deformation of the bearing.
- (6) We obtained a range of secant stiffness for both open-deck and ballasted bridges with the rail intact between each span under the lateral pushing load. We will conduct further investigation into the seismic performance of the substructure by simplifying the restraining effect of the rail track structure as a spring with a range of stiffness identified in this study.

4. SHAKING TABLE EXPERIMENT RESULTS AND DISCUSSION

4.1 Introduction

Housner (1963) initiated the research on the analytical solution of the rocking behavior of freestanding rigid blocks under various ground motions. Numerous additional studies examined the assumptions in Housner's research and then went on to extend the research to include multiple modes (Ishiyama, 1982, Shenton, 1996), multiple bodies (Psycharis, 1990; Wittich and Hutchinson, 2017), three dimensions (Konstantinidis and Makris, 2007), and flexibility of the body and interface (Chatzis and Smyth, 2011).

However, little research has been conducted on the dynamic behavior of a rigid body with horizontal restraint. The only research we found was conducted by Giresini and Sassu (2017). Their study looked at the dynamic behavior of horizontally restrained blocks that represent masonry/concrete wall façades subjected to out-of-plane constraints (e.g., flexible roof/floor, perpendicular wall panel, and an anti-overturn retrofit device). The major contribution of their study is the expansion of conventional knowledge on the rocking behavior of freestanding rigid blocks and consideration of horizontally restraining boundary conditions. However, the paper considered only the pure rocking behavior of slender blocks (height/thickness > 5) and ignored other possible modes such as sliding and rocking-sliding, which would be applicable for non-slender blocks such as bridge piers. The paper also only considered single-body motion and ignored the possibility of multi-body motion behavior. Finally, there was no experimental validation of the analytical models.

4.2 Testing Program

In this study, a series of rigid-body dynamic tests are conducted using a small-scale shaking table. The specimens are prismatic blocks. The major parameters in the test matrix design are stiffness of restraint spring (K), height/breadth (H/B) ratio of block, coefficient of friction between the specimen and base slab, ground excitations, coefficient of restitution (r) and single-body or stacked dual-body configurations (shown in **Figure 4.1**).

Considering the material of the specimens and the capability of the shake-table, the scale factors (value of model specimen/value of prototype) for the length and modulus of elasticity of the specimens and the acceleration of ground motions are adopted as 1/120, 1 and 1 respectively. Thus, the scale factors for mass, displacement response and acceleration response of the specimens are $(1/120)^3$, 1/120 and 1 respectively using the similitude law (Caccese and Harris, 1990; Harris and Sabnis, 1999).

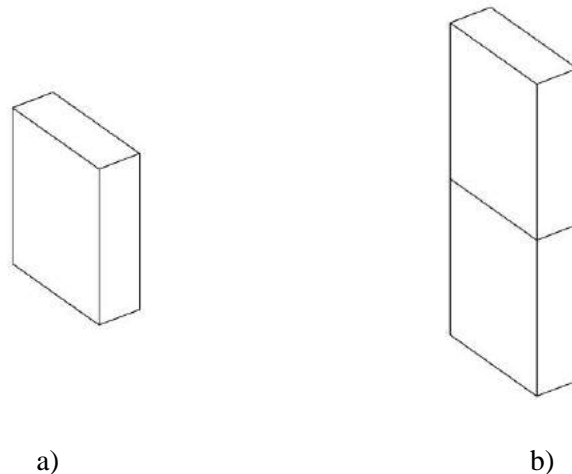


Figure 4.1 a) Single-body and b) Dual-body Prismatic Block Systems

The testing program and the components are as follows:

a. Shaking table:

A Quanser Shake Table II is employed in this testing. The payload area is 46 cm \times 46 cm (18.1 in. \times 18.1 in.). The maximum payload at 2.5 g table acceleration is 7.5 kg (16.5 lb.). The maximum travel is ± 7.6 cm (3 in.). The maximum velocity and acceleration capacity are 66.5 cm/s (26.2 in./s) and 2.5 g respectively with 7.5 kg (16.5 lb.) payload.

b. Instrumentation:

Instrumentation for the tests is summarized in **Table 4.1**. It is noted that in order to prevent the drag force on the specimens from the attached displacement sensors the video analysis method, by using Tracker 5.0.5 (Brown and Cox, 2009) (**Figure 4.2**), is adopted to obtain the position history of the specimens. Tracker 5.0.5 was validated by measuring the motion of shake table surface and comparing with the string potentiometer measurement. The shake table is heavy. The drag force of the string potentiometer on the table can be ignored. Two video recorders were deployed, one in front of the setup and the other one on top. The one on top is to observe any motion that occurred outside the investigated plane of the video recorder in front to capture any three-dimensional motion.

c. Frame for spring restraint

In order to apply a spring restraint to the top of the specimen, a special frame is designed and attached to the shaking-table surface (**Figure 4.3**). Based on the payload of the table

Table 4.1 Instrumentation List

Instrument	Objectives	Quantity
Camera	Observe the setup and specimen failure modes	1
Video recorder	Observe the motion history for video analysis	2
String potentiometer	Monitor the horizontal displacement history of shake-table	2
Accelerometer	Monitor the horizontal acceleration history of specimens and shake-table	2
NI DAQ	Data acquisition and conditioning; data storage	1

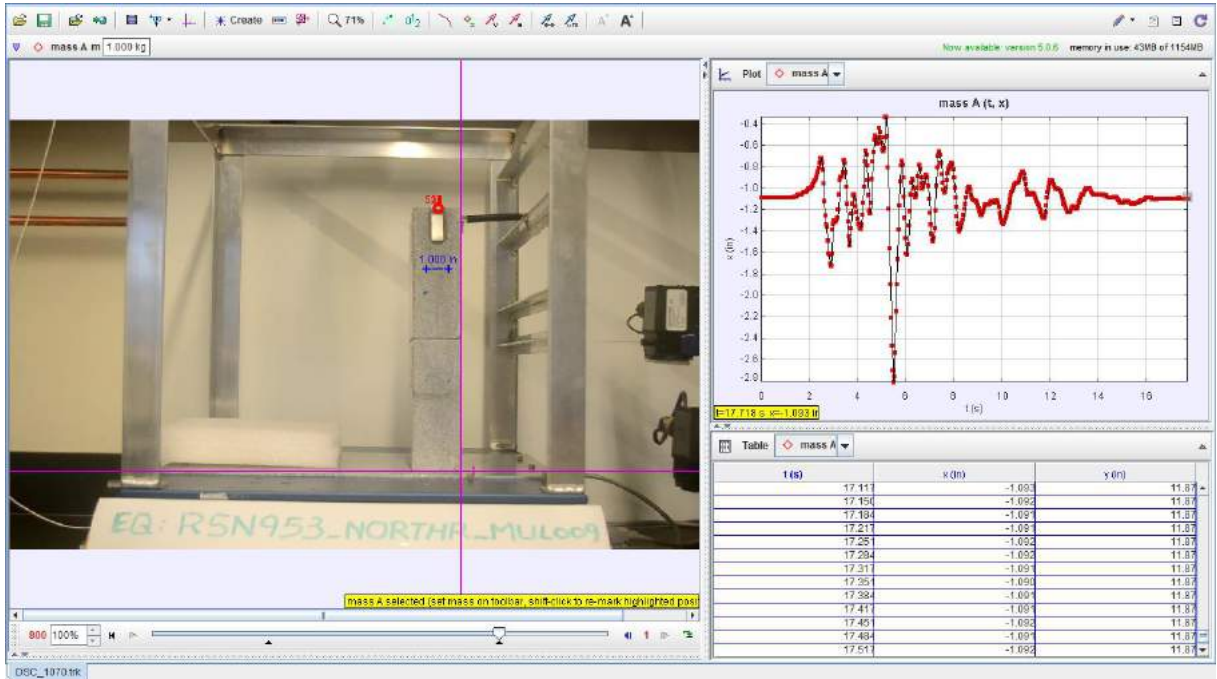


Figure 4.2 Example application of Tracker 5.0.5 in this study

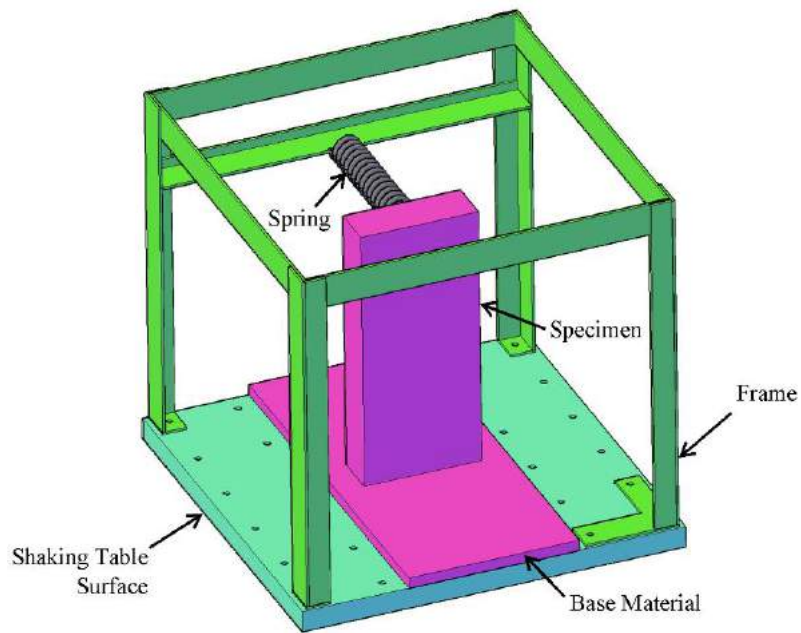


Figure 4.3 Frame for Spring Restraint Attachment and Testing Setup

and the height of specimens, the frame is designed as 425 mm (16.75 in.) height, 445 mm (17.5 in.) width and 451 mm (17.75 in.) depth. It is built with 3.2 mm (1/8 in.) thick aluminum plates. Based on a structural analysis using SAP2000, the maximum lateral deformation in the direction of shaking of this frame under 1.0 g table acceleration generated potential energy equivalent to approximately 0.7% of the kinetic energy of specimen which has ignorable impact on the measurement of the actual displacement of the specimen.

d. Testing specimens

Granite is used in the small shaking table tests because of its strength, allowing one block to be used for multiple tests. The geometric characteristics of the stone block specimens are tabulated in **Table 4.2**. Aluminum was selected as the base material.

e. Spring stiffness

Using similitude law (Caccese and Harris, 1990; Harris and Sabnis, 1999), the scale ratio of spring stiffness between the model and the real structure can be obtained following force equilibrium and scale ratio just obtained before:

Table 4.2 Geometries of Blocks

Specimen number	Dimensions mm (in.) H × B1 × B2	Weight kg (lb)	Slenderness ratio		Note
			H / B1	H / B2	
1	152 × 57 × 152 (6 × 2.25 × 6)	3.4 (7.5)	2.7	1	For dual-body tests
2	152 × 57 × 152 (6 × 2.25 × 6)	3.4 (7.5)	2.7	1	For single-body & dual-body tests
3	203 × 76 × 203 (8 × 3 × 8)	9.0 (19.9)	2.7	1	For single-body tests
4	406 × 51 × 152	8.9	8	2.7	For single-body tests

	(16 × 2 × 6)	(19.5)		
--	--------------	--------	--	--

Force equilibrium: Force provided by spring ($k\Delta$) = Inertial force of the block (ma)

Scale ratio of k = scale ratio of mass × scale ratio of acceleration / scale ratio of displacement = $[(1/120)^3 \times 1] / (1/120) = (1/120)^2$

Based on the analysis in Chapter 3, maximum equivalent stiffness of the railroad system is 171 kN/mm. Therefore, the corresponding model spring stiffness is taken as 11.9 N/mm and used for the spring selection.

f. Test matrix

The test matrix is tabulated in **Table 4.3**. We considered three types of earthquake records, near fault with a pulse, near fault without a pulse, and far field. The ground motion history records were downloaded from PEER Ground Motion database (Ancheta et al., 2014). Their ground acceleration time histories and FFT power spectra are plotted in **Figures 4.4, 4.5, and 4.6**.

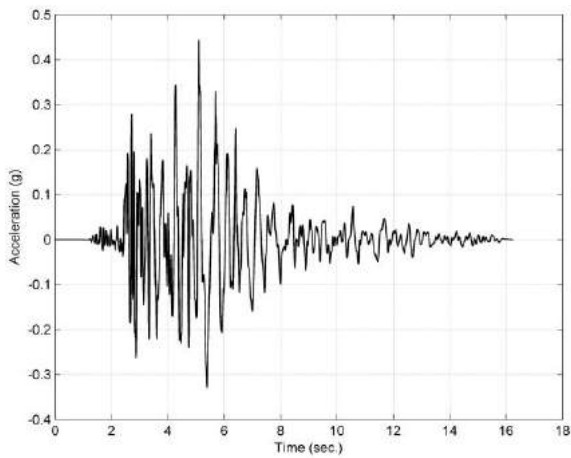
g. Coefficient of friction

The coefficient of friction between granite specimen and aluminum base was the measurement per ASTM G115 standard (2018). The test set up is illustrated in **Figure 4.7**. A digital force gauge (Mark M7-10) was used to apply a push load to the bottom part of the specimen. The force and displacement time histories were obtained by the force gauge and string potentiometer. And the static and dynamic coefficients of friction were calculated following ASTM G115.

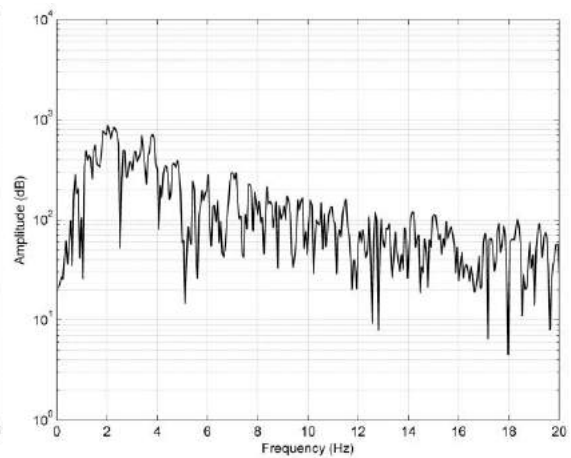
Table 4.3 Test Matrix

Specimen #	H/B	Horizontal restraint	Ground motion
1	2.7	No restraint/	Sine waves (varied of amplitudes (1 cm, 2 cm and 3 cm) and frequencies [0.5 Hz to 4.5 Hz with 0.1 Hz increment toward failure])
	1.0	Restraint (k =11.9 /mm)	
3	2.7		Earthquake record in PEER database:

	1.0		(Far field: NORTHR_MUL009
4	8.0		Near fault with a pulse: IMPVALL_E06140
	2.7		Near fault without a pulse: GAZLI_GAZ000)
1+2 stacked	5.6		
	2.0		
2	2.7	No restraint	Free rocking (for measurement of coefficient of restitution, discussed in Chapter 5)



a)



b)

Figure 4.4 a) Ground Acceleration Time History and b) FFT Power Spectrum of NORTHR_MUL009 Record

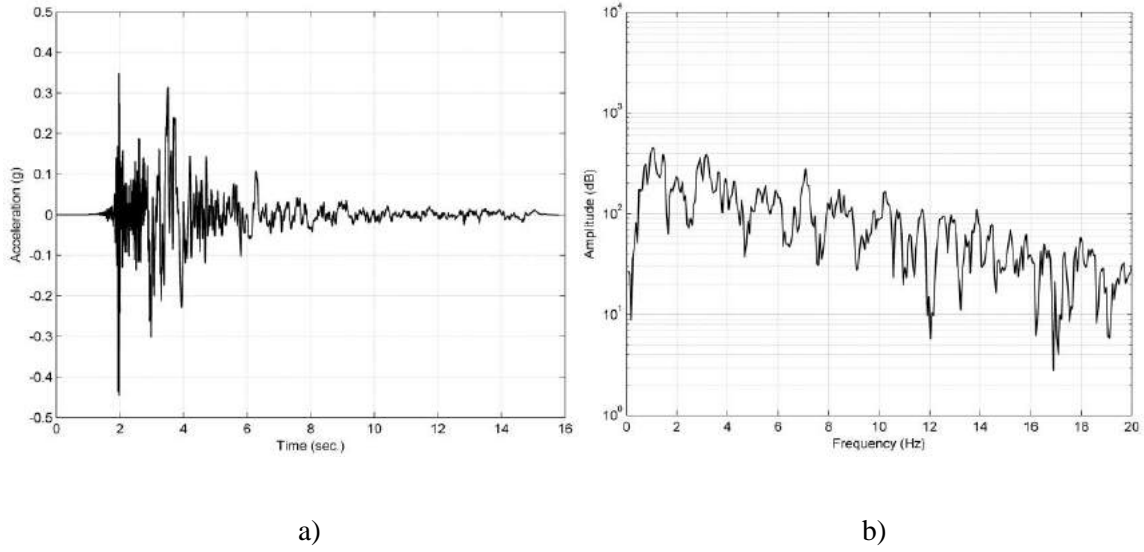


Figure 4.5 a) Ground Acceleration Time History and b) FFT Power Spectrum of IMPVALL_E06140 Record

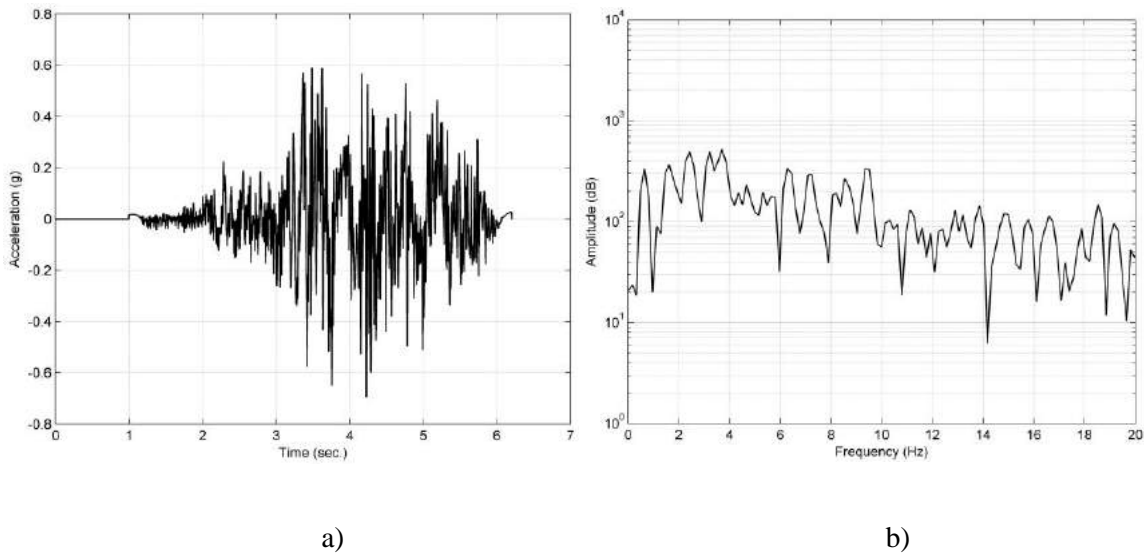


Figure 4.6 a) Ground Acceleration Time History and b) FFT Power Spectrum of GAZLI_GAZ000 Record

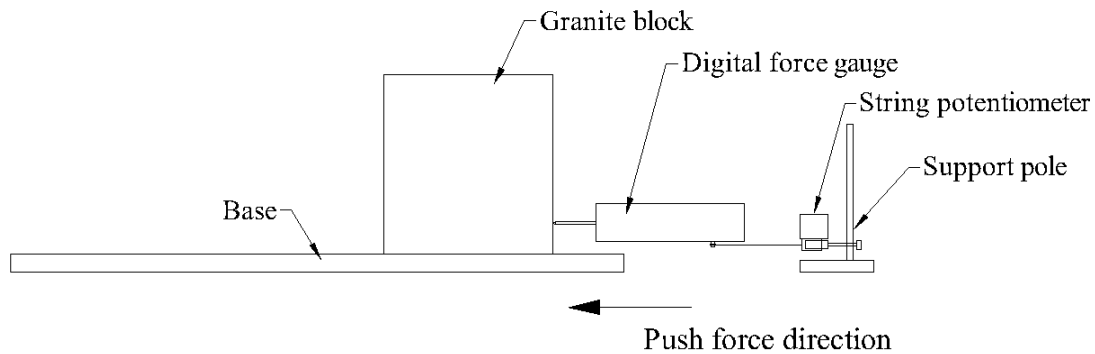


Figure 4.7 Coefficient of Friction Measurement Setup

4.3 Testing Result and Discussion

4.3.1 Coefficient of friction

The force and displacement data were synchronized to have the same start time. The force-displacement curve data are plotted in **Figure 4.8**. Per ASTM G115, the static coefficient of friction is 0.552, and the dynamic coefficient of friction is 0.505.

4.3.2 Failure mode under sinusoidal input

This study investigated the failure modes of single-body specimens without restraint under sinusoidal ground motion inputs. The input set includes sinusoidal waves with various amplitudes and frequencies. The slenderness ratio H/B , weight of the specimens and the characteristics of the shake inputs were considered in the test design. The testing results are tabulated in **Table 4.4**.

The results indicated that the failure mode was directly related to the slenderness ratio H/B and the weight of the specimens, and the maximum acceleration of the ground input. Sliding failure occurred for the specimens with slenderness ratio of 1.0. Rocking overturning failure occurred for the specimens with slenderness ratio larger than 1.0, i.e. 2.7 and 8.0. For the specimens with the same slenderness ratio, slightly larger maximum ground acceleration was needed to trigger the failure of the heavier specimen. For the specimens with the same weight, larger maximum ground acceleration was needed to trigger the failure of the specimen with a smaller slenderness ratio. It was also observed that either amplitude or critical frequency of the ground shake input is not the only factor that triggers the failure. The failure is due to the critical acceleration of ground input that is generated by the combination of amplitude and frequency of the input.

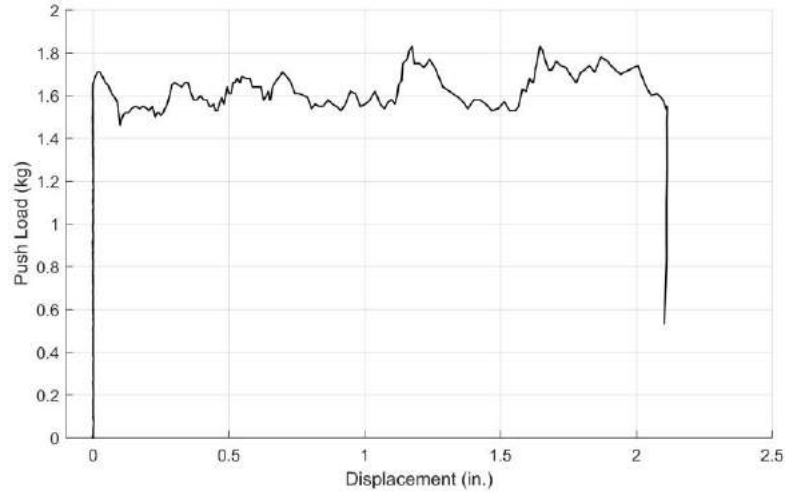


Figure 4.8 Force-displacement Data for Coefficient of Friction Measurement

Table 4.4 Failure Mode Results of Single-body Specimens without Restraint under Sinusoidal Waves

Specimen number (weight in lb)	H/B	Amplitude (m)	Critical frequency (cycle/sec)	Maximum ground acceleration (g)	Failure mode
2 (7.5)	1.0	0.01	4.5	0.659	sliding
		0.02	3.0	0.686	sliding
		0.03	2.4	0.701	sliding
	2.7	0.01	2.9	0.436	rocking overturning
		0.02	2.1	0.431	rocking overturning
		0.03	1.7	0.438	rocking overturning
3 (19.9)	1.0	0.01	4.4	0.828	sliding
		0.02	3.2	0.880	sliding
		0.03	2.9	0.996	sliding

	2.7	0.01	3.0	0.506	rocking overturning
		0.02	2.1	0.504	rocking overturning
		0.03	1.8	0.626	rocking overturning
4 (19.5)	2.7	0.01	2.6	0.313	rocking overturning
		0.02	2.1	0.393	rocking overturning
		0.03	1.7	0.356	rocking overturning
	8.0	0.01	1.5	0.196	rocking overturning
		0.02	1.1	0.187	rocking overturning
		0.03	0.7	0.112	rocking overturning

4.3.3 Restraining effect

The restraining effect of the spring on the rigid motion can be observed (see **Figure 4.9**) by using a dual-body system testing as an example. The system was subjected to a far-field earthquake record NORTHHR_MUL009. This showed that the displacement response at the top of the spring restrained specimen (solid line) is almost identical with the ground motion input, which proves the benefit of the restraining effect on the seismic behavior of the rigid body structures. On the other hand, the specimen without the spring restraint (dot-dash line) failed at about four seconds due to the excessive acceleration.

4.4 Conclusions

A set of shaking table tests was conducted on the single-body and dual-body prismatic block systems. Several parameters were considered in the testing design, such as the slenderness ratio and weight of the specimens, the horizontal restraint condition at the top of the specimens, the various ground motion inputs, etc. The following conclusions were drawn:

1. The failure modes of the single-body specimens without horizontal restraint included sliding and rocking overturning. They were directly related to the slenderness ratio H/B and the weight of the specimen, and the maximum acceleration of the ground input. Specimens with smaller slenderness ratio or larger weight required larger maximum ground acceleration to cause the failure.

2. For the rigid-body system, either amplitude or critical frequency of the ground shake input is not the only factor that triggers the failure. The failure is due to the critical acceleration of ground input that is generated by the combination of amplitude and frequency of the input.

3. The benefit of the restraint effect on the dynamic behavior of the prismatic rigid body structures was confirmed in the shake table test.

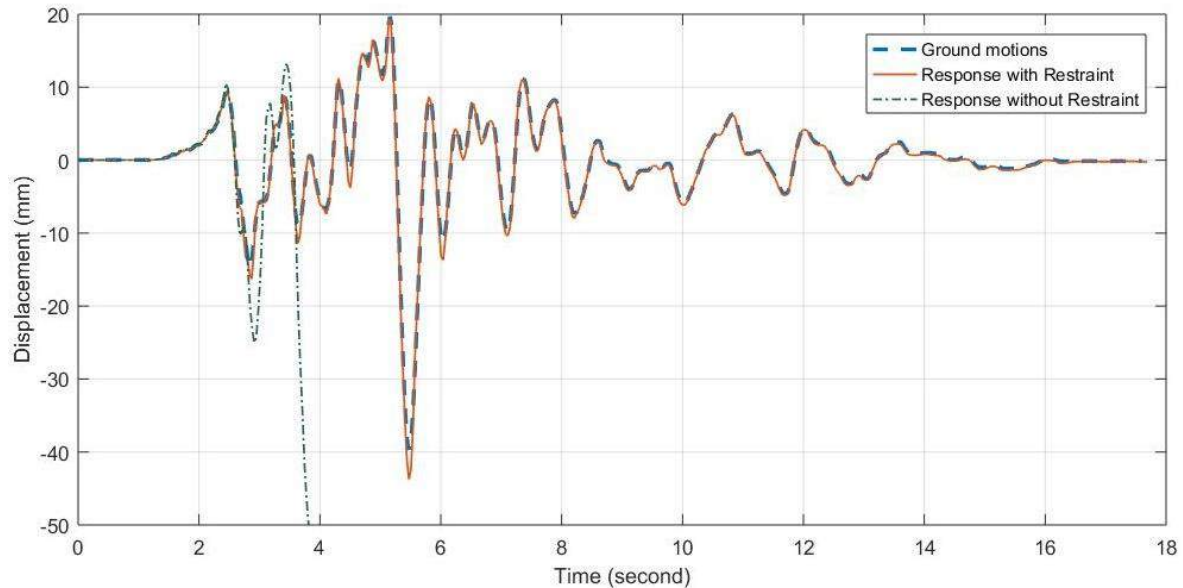


Figure 4.9 Response Time-history Comparison for X-direction Tip Displacement of Dual-body System w/ and w/o Horizontal Restraint under Earthquake NORTHR_MUL009, 1 in.=25.4 mm

5. CONTRIBUTIONS AND RECOMMENDATIONS

Following is a summary of the contributions of this study:

1. We collected and investigated 4,315 seismic performance records of railroad bridges. In total, five URM and nine URC pier damage records were found. This indicates that the URM and URC railroad bridge piers had superior performance in the past earthquakes.
2. Based on observations of damages to URM and URC railroad bridge piers damages caused by earthquakes, we found that these types of piers are prone to sliding and rocking, which are typical for rigid body motions. Other failure modes are (1) integral displacement in horizontal or vertical directions or integral tilting; (2) coping stones being loosened, displaced, or torn; (3) anchorage failure between bearings and piers.

3. The track system contributed to the superior performance of railroad bridges due to its ability to restrain horizontal movement of the superstructure during earthquakes. We propose a numerical modeling scheme that considers the nonlinear properties of the ballast and bearings as well as steel and concrete materials, which has been validated by previous field full-scale testing. The model was used to obtain equivalent spring stiffness of the rail track system. Other findings include:

(1) For open-deck girder bridge models, the secant stiffness of the bridge system increases with the increase of the lateral stiffness of substructure. The model with greater pier stiffness has less ultimate displacement. We found that the failure of the bridge system is governed by the bearing capacity for a stiffer substructure and by the rail steel failure for a substructure with less lateral stiffness.

(2) For open-deck bridges, the rotational stiffness of the substructure has little impact on the secant lateral stiffness of the bridge system. The stress of rail steel remains at a low level. The cause of ultimate state is the excessive bearing deformation.

(3) For ballast bridges models, the secant stiffness of the bridge system increases when the lateral stiffness of the substructure increases. Ballast between the rail track and bridge girder causes the lateral displacement and tensile stress of the rail steel to remain small. The bridge system reaches the ultimate state when the bearing reaches the lateral displacement capacity.

(4) For ballast bridges, as the rotational stiffness of the substructure decreases the secant lateral stiffness of the bridge structure system also decreases. Meanwhile, the ultimate load and corresponding system lateral displacement at ultimate state increases. The bridge system reaches the ultimate state because of excessive lateral deformation of the bearing.

4. We conducted a small-scale shaking table experimental study that investigated the dynamic response of prismatic rigid body specimens with a spring restraint on top. Several parameters were considered in the test matrix such as stiffness of the restraint spring, height-to-breadth ratio, ground excitations, and single-body or multi-body configuration. Results showed that

(1) The failure modes of the single-body specimens without horizontal restraint were sliding and rocking overturning. They were directly related to the slenderness ratio h/b and the weight of the specimen, and the maximum acceleration of the ground input. Specimens with smaller slenderness ratios or greater weight required larger maximum ground acceleration to cause the failure.

(2) For the rigid-body system, either amplitude or critical frequency of the ground shake input was not the only factor that triggers the failure. The failures were due to the critical acceleration of ground input generated by the combination of amplitude and frequency of the input.

(3) The benefit of the restraint effect on the dynamic behavior of the prismatic rigid body structures was confirmed in the shake table test.

There are several recommendations for future study on this topic and they are summarized below:

1. We recommend the large-scale or full-scale experiment studies using either the shaking table method or the quasi-static cyclic loading method. A preliminary testing design for a large-scale quasi-static cyclic load experiment is attached in Appendix B.
2. Like the rail track system, the performance of the bridge bearings influences the railroad bridge seismic performance. The authors recommend conducting a related study to investigate the mechanism of existing types of railroad bridge bearings subject to the dynamic load. The preliminary literature review on this topic is summarized in Appendix C.

REFERENCES

- AASHTO (1941). "*Standard Specifications for Highway Bridges.*" AASHTO (American Association of State Highway and Transportation Officials), Washington, DC.
- AASHTO (1991). "*AASHTO Guide Specifications for Seismic Isolation Design.*" AASHTO (American Association of State Highway and Transportation Officials), Washington, DC.
- AASHTO (2011). "*AASHTO Guide Specifications for LRFD Seismic Bridge Design.*" American Association of State Highway Transportation Officials (AASHTO), Washington, DC.
- AASHTO (2017). "*AASHTO LRFD bridge design specifications, customary U.S. units.*" AASHTO (American Association of State Highway and Transportation Officials), Washington, DC.
- Abé, M., and Shimamura, M. (2014). "Performance of Railway Bridges during the 2011 Tōhoku Earthquake." *Journal of Performance of Constructed Facilities*, 28(1), 13-23.
- ACI. (2014). Building Code Requirements for Structural Concrete and Commentary. *ACI 318-14*, American Concrete Institute, Farmington Hills, MI.
- ACI, Saiidi, M. S., Stroh, S., and Pantazopoulou, V. J. (2003). "Seismic analysis and design of concrete bridge systems." *ACI 341.2R-97-R03*, American Concrete Institute, Farmington Hills, MI.
- ACI, Valluvan, R., and Sritharan, S. (2007). "Seismic evaluation and retrofit techniques for concrete bridges." *ACI 341.3R-07*, American Concrete Institute (ACI), Farmington Hills, MI.
- America's Library (2015). "First U.S. Railway Chartered to Transport Freight and Passengers February 28, 1827 ",
<http://www.americaslibrary.gov/jb/nation/jb_nation_train_1.html>.
- Ancheta, T. D., Darragh, R. B., Stewart, J. P., Seyhan, E., Silva, W. J., Chiou, B. S.-J., Wooddell, K. E., Graves, R. W., Kottke, A. R., Boore, D. M., Kishida, T., and Donahue, J. L. (2014). "NGA-West2 Database." *Earthquake Spectra*, 30(3), 989-1005.
- AREMA (1907). "*Manual for railway engineering.*" American Railway Engineering Maintenance-of-Way Association, Chicago, IL.

- AREMA (2018). "Manual for railway engineering." American Railway Engineering Maintenance-of-Way Association, Lanham, MD.
- ASCE, and FEMA (2000). "Prestandard and commentary for the seismic rehabilitation of buildings." *FEMA 356*, Federal Emergency Management Agency (FEMA), Washington, D.C.
- ASTM A499 (2015). Standard Specification for Steel Bars and Shapes, Carbon Rolled from "T" Rails. *ASTM A499*, ASTM International, West Conshohocken, PA.
- ASTM G115-10 (2018), Standard Guide for Measuring and Reporting Friction Coefficients. *ASTM G115-10*, ASTM International, West Conshohocken, PA
- ATC (1983). "Seismic retrofitting guidelines for highway bridges." *FHWA/RD-83/007*, Applied Technology Council (ATC), Redwood City, Calif.
- ATC MCEER Joint Venture, and NCHRP (2003). "Recommended LRFD guidelines for the seismic design of highway bridges." *MCEER/ATC-49*, Applied Technology Council (ATC); Multidisciplinary Center for Earthquake Resistant Engineering Research (MCEER), Redwood City, CA; Buffalo, N.Y.
- Baker, I. O. (1909). *A treatise on masonry construction*, J. Wiley & Sons, New York.
- Brown, D., and Cox, A.J. (2009). "Innovative uses of video analysis." *Phys. Teacher*, 47, 145–150.
- Buckle, I. G., FHWA, and MCEER (2006). "Seismic retrofitting manual for highway structures." *FHWA-HRT-06-032*, Multidisciplinary Center for Earthquake Engineering Research (MCEER), Buffalo, NY.
- Byers, W. G. (1996). "Railroad bridge behavior during past earthquakes." *Proc., 14th Structures Congress*, ASCE, UNITED ENGINEERING CENTER, 345 E 47TH ST, NEW YORK, NY 10017-2398, 175-182.
- Byers, W. G. (2003). "Earthquake Damage to Railroads."
<<http://nisee.berkeley.edu/byers/browse.html>>.
- Byers, W. G. (2004). "Behavior of Railway Bridges and Other Railway Infrastructure in Three Strong to Great Earthquakes in 2001." *Transportation Research Record: Journal of the Transportation Research Board*, 1863(-1), 37-44.
- Byers, W. G. (2004). "Railroad Lifeline Damage in Earthquakes." *Proc., 13th World Conference on Earthquake Engineering*. Vancouver, B.C., Canada.

- Caccese, V., and Harris, H. G. (1990). "Earthquake Simulation Testing of Small-Scale Reinforced Concrete Structures." *Structural Journal*, 87(1).
- Computers & Structures Inc. (2016). *CSI Analysis Reference Manual for SAP2000®, ETABS®, SAFE® and CSiBridge®*, Computer and Structures, Inc., Berkeley, CA.
- Cook, S., Kennedy, D., and Cavaco, J. (2006). Seismic Screening Methodology for Railroad Bridges. *Proc., AREMA 2006 Annual Conference*. Louisville, KY.
- Day, K., and Barkan, C. (2003). "Model for Evaluating Cost-Effectiveness of Retrofitting Railway Bridges for Seismic Resistance." *Transportation Research Record: Journal of the Transportation Research Board*, 1845(1), 203-212.
- Derleth, C. (1907). *Design of a railway bridge pier*, Engineering News Pub. Co.
- Doe, B. E., Uppal, A. S., Otter, D. E., and Oliva-Maal, D. (2001). "Seismic Resistance Tests on an Open-Deck Steel Bridge." *Technology Digest 01-007*, Association of American Railroads, Transportation Technology Center, Inc., Pueblo, Colorado, pp. 4.
- Dong, R. G., Sankar, S., and Dukkipati, R. V. (1994). A Finite Element Model of Railway Track and its Application to the Wheel Flat Problem. *Proceedings of the Institution of Mechanical Engineers, Part F: Journal of Rail and Rapid Transit*, 208(1), pp. 61-72.
- Durda, D. D., Movshovitz, N., Richardson, D. C., Asphaug, E., Morgan, A., Rawlings, A. R., and Vest, C. (2011). "Experimental determination of the coefficient of restitution for meter-scale granite spheres." *Icarus*, 211(1), 849-855.
- Duryea, E., and ASCE (1907). *The Effects of the San Francisco Earthquake of April 18th, 1906, on Engineering Construction: Reports of a General Committee and of Six Special Committees of the San Francisco Association of Members of the American Society of Civil Engineers*, American Society of Civil Engineers.
- Foutch, D. A., and Yun, S. Y. (2001). "Seismic Evaluation of a Steel Truss Railway Bridge." *KEERC-MAE Joint Seminar on Risk Mitigation for Regions of Moderate Seismicity*. University of Illinois at Urbana-Champaign.
- Ganesh Babu, K., and Sujatha, C. (2010). Track Modulus Analysis of Railway Track System Using Finite Element Model. *Journal of Vibration and Control*, 16(10), pp. 1559-1574.




- Giresini, L., and Sassu, M. (2017). "Horizontally restrained rocking blocks: evaluation of the role of boundary conditions with static and dynamic approaches." *Bulletin of Earthquake Engineering*, 15(1), 385-410.
- Goldsmith, W. (1960). *Impact: the theory and physical behaviour of colliding solids*, E. Arnold, London.
- Green, D. W., Winandy, J. E., and Kretschmann, D. E. (1999). Mechanical properties of wood. *Wood handbook: wood as an engineering material (General technical report FPL; GTR-113)*, USDA Forest Service, Forest Products Laboratory, Madison, WI. pp. 4.1-4.45.
- Harris, H. G., and Sabnis, G. M. (1999). *Structural Modeling and Experimental Techniques*, CRC-Press.
- Housner, G. W. (1963). "The behavior of inverted pendulum structures during earthquakes." *Bulletin of the Seismological Society of America*, 53(2), 403-417.
- International Correspondence Schools (1908). *Bridge piers and abutments*, International Textbook Company, the United States.
- Kerr, A. D. (1980). An improved analysis for thermal track buckling. *International Journal of Non-Linear Mechanics*, 15(2), pp. 99-114.
- Ketchum, M. S. (1921). *Structural engineers' handbook: data for the design and construction of steel bridges and buildings*, McGraw-Hill Book Co., Inc., New York; London.
- Mander, J. B., Priestley, M. J. N., and Park, R. (1988). Theoretical Stress-Strain Model for Confined Concrete. *Journal of Structural Engineering*, 114(8), pp. 1804-1826.
- Maragakis, E., Douglas, B. M., Haque, S., and Sharma, V. (1996). Full-Scale Resonance Tests of a Railway Bridge. *Proc., 14th Structures Congress*, American Society of Civil Engineers, New York, NY, pp. 183-190.
- Maragakis, E., Douglas, B., Chen, Q., and Sandirasegaram, U. (1998). Full-Scale Tests of a Railway Bridge. *Transportation Research Record: Journal of the Transportation Research Board*, 1624(1), pp. 140-147.
- Maragakis, E., Douglas, B., and Chen, Q. (2001). "Full-Scale Field Failure Tests of Railway Bridge." *Journal of Bridge Engineering*, 6(5), 356-362.


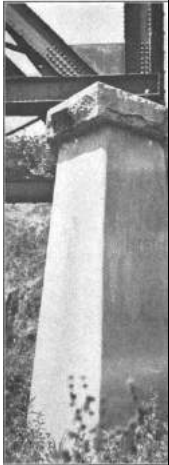
- MATLAB Version 2018. *The Language of Technical Computing*. The Mathworks, Inc.: Natick, MA, 2018.
- McCulloch, D. S., and Bonilla, M. G. (1970). *Effects of the earthquake of March 27, 1964, on the Alaska Railroad*, U.S. Government Printing Office, Washington D.C.
- Moreu, F., and LaFave, J. M. (2012). "Current research topics: Railroad bridges and structural engineering." *Newmark Structural Engineering Laboratory*. University of Illinois at Urbana-Champaign.
- Ni, Y. (2005). "The Revision of the Code for the Seismic Design of Railway Engineering and Its Influence on Railway Bridge Piers (in Chinese)." *Railway Standard Design*, 2005(11), 82-84.
- NRA China (2009). "Code for Seismic Design of Railway Engineering (in Chinese)." *GB50111-2006 (2009 Edition)*, National Railway Administration (NRA) of the People's Republic of China, Beijing, China.
- NRA China (2014). "Code for Design of High-speed Railway (in Chinese)." *TB10621-2014*, National Railway Administration (NRA) of the People's Republic of China, Beijing, China.
- Nutt, R. V., Caltrans, and ATC (2000). "Improved seismic design criteria for California bridges: resource document." *ATC 32*, Applied Technology Council (ATC), Redwood City, Calif.
- Otter, D. E., Uppal, A. S., and Joy, R. (1999a). "Seismic Resistance Tests on an Open-Deck Steel Bridge." *Technology Digest No. 99-028*, Association of American Railroads, Transportation Technology Center, Inc., Pueblo, Colorado.
- Otter, D. E., Uppal, A. S., and Joy, R. (1999b). Measuring Seismic resistance on an open-deck steel bridge. *Railway Track and Structures* (Nov.), pp. 13-16.
- Priestley, J. N., Seible, F., and Calvi, G. M. (1996). *Seismic Design and Retrofit of Bridges*, Wiley, New York, NY.
- Prucz, Z., and Otter, D. E. (2002). "Railroad Bridge Performance in Past Earthquakes." *Proc., AREMA 2002 Annual Conference*.
- Rodrigue, J.-P. (2015). "The Geography of Transport Systems." <<https://people.hofstra.edu/geotrans/eng/ch3en/conc3en/usrail18402003.html>>.


- Sandirasegaram, U. (1997). "Full-scale Field Resonance Tests of a Railway Bridge." Master of Science in Civil Engineering, University of Nevada, Reno.
- Sharma, V., Choros, J., Maragakis, E. M., and Byers, W. G. "Seismic Performance of Railway Bridges." *Proc., the Structures Congress XII '94*, 24-28.
- Solomon, B. (2008). *North American railroad bridges*, Voyageur Press, St. Paul, MN.
- Tyrrell, H. G. (1911). *History of bridge engineering*, The author, Chicago, IL.
- U.S. Govt. Accountability Office (2007). "*Railroad bridges and tunnels federal role in providing safety oversight and freight infrastructure investment could be better targeted: report to congressional requesters.*" U.S. Govt. Accountability Office, Washington, D.C.
- Uppal, A. S., Joy, R., and Otter, D. E. (2000). "Seismic Resistance Tests on an Open-Deck Steel Bridge." *Report No. R-939*, Association of American Railroads, Transportation Technology Center, Inc., Pueblo, Colorado, pp. 27.
- Uppal, A. S., Otter, D. E., and Doe, B. E. (2001). "Longitudinal Resistance Test on an Open Deck Steel Bridge." *Report No. R-949*, Association of American Railroads, Transportation Technology Center, Inc., Pueblo, Colorado, pp. 45.


APPENDICES



**APPENDIX A. SUMMARY OF RECORDED DAMAGES OF URM AND URC RAILROAD
BRIDGE PIERS IN PAST EARTHQUAKES**


Earthquake			Bridge			Structural Damages, Description about Piers	Photos
Date	Id.	Magnitude	Id.	Pier Material	Pier No.		
1891-10-28	Mino-Owari, Japan	8.39	Kisogawa Railroad Bridge	brick	No Detail	<ul style="list-style-type: none"> • Crack at arch in brick pier 	
1895-10-31	Charleston, MO	6.60	Illinois Central Railroad Cairo Bridge over the Ohio River	stone	No Detail	<ul style="list-style-type: none"> • Cracking of joints in a bridge pier • Bands were probably installed as a repair or retrofit after the earthquake 	
1897-06-12	Assam, India	8.50	Manshai Bridge, Eastern Bengal State Railway.	brick	No Detail	<ul style="list-style-type: none"> • No detail description 	



Earthquake			Bridge			Structural Damages, Description about Piers	Photos
Date	Id.	Magnitude	Id.	Pier Material	Pier No.		
1906-04-18	San Francisco, CA	8.25	Pajaro River Bridge	plain concrete	General	<ul style="list-style-type: none"> • The Pajaro River railroad bridge was damaged severely caused by crossing fault line. • Dislocated bridge supported by falsework. 	 
as above	as above	as above	as above	plain concrete	Pier 1 (East abutment)	<ul style="list-style-type: none"> • Wing-wall crack • Settlement 	No Photo
as above	as above	as above	as above	plain concrete	Pier 2	<ul style="list-style-type: none"> • Coping stone displace 	



Earthquake			Bridge			Structural Damages, Description about Piers	Photos
Date	Id.	Magnitude	Id.	Pier Material	Pier No.		
as above	as above	as above	as above	plain concrete	Pier 3	<ul style="list-style-type: none"> • Move horizontally • Settle and raise • Coping stone loosen • 2 horizontal cracks in pier (construction joint or “the line marking the end of day’s work”) 	
as above	as above	as above	as above	plain concrete	Pier 4	<ul style="list-style-type: none"> • Move horizontally • Twist slightly • Raise • 1 horizontal crack in pier (construction joint or “the line marking the end of day’s work”), and move relatively between upper 	No Photo


Earthquake			Bridge			Structural Damages, Description about Piers	Photos
Date	Id.	Magnitude	Id.	Pier Material	Pier No.		
						and lower portion	
as above	as above	as above	as above	plain concrete	Pier 5	<ul style="list-style-type: none"> • Move horizontally • Settle • Break along a horizontal line close to the ground surface, and move relatively between upper and lower portion • Coping stone (header) torn by the relative movement between substructure and pier 	




Earthquake			Bridge			Structural Damages, Description about Piers	Photos
Date	Id.	Magnitude	Id.	Pier Material	Pier No.		
as above	as above	as above	as above	plain concrete	Pier 6 (West abutment)	<ul style="list-style-type: none"> • Move horizontally 	
1925-06-29	Santa Barbara, CA	6.83	Dos Pueblos viaduct on Southern Pacific Railroad near Naples, California.	stone	West end	<ul style="list-style-type: none"> • The piers are shown as repaired after the shock. • The cracks between individual stones were packed with cement mortar and then the entire pier was encased in a 12-inch thick jacket of reinforced concrete. 	

Earthquake			Bridge			Structural Damages, Description about Piers	Photos
Date	Id.	Magnitude	Id.	Pier Material	Pier No.		
as above	as above	as above	as above	stone	No Detail	<ul style="list-style-type: none"> • Shear-off along a horizontal line, and move relatively between upper and lower portion • The pier was repaired by driving wooden wedges into the crack, then packing it with cement mortar. • The entire pier was encased in a 12-inch jacket of reinforced concrete. 	



Earthquake			Bridge			Structural Damages, Description about Piers	Photos
Date	Id.	Magnitude	Id.	Pier Material	Pier No.		
1948-06-28	Fukui, Japan	7.30	Kuzuryu River Bridge	plain concrete	General	<ul style="list-style-type: none"> This was a single track bridge spanning the Kuzuryu River and located about 1500 ft. west of the Nakatsuno highway bridge. It consisted of 10 concrete piers supporting 11 spans, each consisting of 2 parallel plate girders on which the rail structure rested. 	
as above	as above	as above	as above	plain concrete	Pier 7	<ul style="list-style-type: none"> Braced by the felled girders, this pier was still standing in an inclined position. The prime cause of failure was the lack of 	



Earthquake			Bridge			Structural Damages, Description about Piers	Photos
Date	Id.	Magnitude	Id.	Pier Material	Pier No.		
						continuity in the pier construction.	
as above	as above	as above	as above	plain concrete	No Detail	<ul style="list-style-type: none"> Sheared-off pier top. The prime cause of failure was the lack of continuity in the pier construction 	
as above	as above	as above	as above	plain concrete	Pier 2 from the south	<ul style="list-style-type: none"> The top of the 2nd pier from the south sheared off cleanly and horizontally, the top portion being displaced to the southwest. 	


Earthquake			Bridge			Structural Damages, Description about Piers	Photos
Date	Id.	Magnitude	Id.	Pier Material	Pier No.		
as above	as above	as above	as above	plain concrete	N.C.	<ul style="list-style-type: none"> • The anchorage of the girders to the piers appeared stronger than in the other bridges that failed, but close inspection showed that the anchor rods were very small. • The anchor bolts pulled out of the pier as the girders were displaced to the south. • Failure was due to instability of pier foundations, lack of necessary pier reinforcement 	

Earthquake			Bridge			Structural Damages, Description about Piers	Photos
Date	Id.	Magnitude	Id.	Pier Material	Pier No.		
						and weak anchorages.	
as above	as above	as above	Kanazu Bridge (over the Takeda River)	brick	Center	<ul style="list-style-type: none"> The center pier failed by shearing off on a horizontal line. 	
1960-05-22	Chile	9.50	Llanquihue railway bridge	concrete	Center	<ul style="list-style-type: none"> Tilted Looking west at center pier, showing bearing separation. 	 

Earthquake			Bridge			Structural Damages, Description about Piers	Photos
Date	Id.	Magnitude	Id.	Pier Material	Pier No.		
1964-03-27	Prince William Sound, Alaska	9.24	Bridge 14.5	concrete	North end of No. 6 span	<ul style="list-style-type: none"> Fixed end bearing lifted from pier at north end of 6th span of Bridge 14.5. Anchor bolt pulled free of concrete. In adjacent expansion bearing, nested rollers were driven to the extreme position. 	
1976-07-28	Tangshan, China	8.00	Ji Channel Bridge	plain concrete	No Detail	<ul style="list-style-type: none"> Bridges located on silty clay and silty-sandy clay, such as Ji Channel Bridge, suffered serious damage. 	

Earthquake			Bridge			Structural Damages, Description about Piers	Photos
Date	Id.	Magnitude	Id.	Pier Material	Pier No.		
as above	as above	as above	Dou River Bridge	plain concrete	No Detail	<ul style="list-style-type: none"> • Bridges located on silty clay and silty-sandy clay, such as the Dou River Bridge, suffered serious damage. • The top of the piers sheared off horizontally, the top portion tilted and was braced by the superstructure 	
1978-06-12	Miyagiken-oki, Japan	7.70	Eaigawa Bridge	plain concrete	No Detail	<ul style="list-style-type: none"> • Constructed in 1941, the Eaigawa Bridge was a deck girder bridge separated for each line of a double track. • An oval pier supported by a well foundation 	

Earthquake			Bridge			Structural Damages, Description about Piers	Photos
Date	Id.	Magnitude	Id.	Pier Material	Pier No.		
						was cut at the concrete construction joint, and was dislocated as much as 30 cm. in an orthogonal direction, causing a large track deformation.	
1989-10-17	Loma Prieta, CA	7.10	Bridge 119.67	concrete pier with stones cap	Pier 3	<ul style="list-style-type: none"> • Shift between the cap stones and concrete stem; • tipped 6 inches to the west 	
1991-04-22	Costa Rica	7.60	Rio Matina Rail Bridge	concrete	N.C.	<ul style="list-style-type: none"> • The location of the pier with respect to the old connection on the girder shows horizontal displacement of 1.17 m. and 	

Earthquake			Bridge			Structural Damages, Description about Piers	Photos
Date	Id.	Magnitude	Id.	Pier Material	Pier No.		
						settlement of 0.12 m.	
2011-3-11	Tohoku, Japan	9.0	unknown bridge on Tohoku-Shinkansen railway line	brick	center	<ul style="list-style-type: none"> • Cracking along bed joint of masonry piers 	

APPENDIX B. PRELIMINARY QUASI-STATIC CYCLIC LOADING TESTING PLAN

B.1 Specimens

B.1.1 Material design properties

Limestone unit: density = 175 lb/3ft

Mortar: Lime mortar and cement mortar were commonly used in the masonry works in 1910s. Compared with lime mortar, cement mortar was usually employed in laying stone masonry (Baker 1917). In Baker's book, a series of mortar proportions (ratio of cement and sand) was tabulated and a proportion of 1:2 or 1:3 for Portland cement was recommended in practice, as shown in **Table B.1**.

PROPORTIONS.	MORTAR PROPORTIONED BY WEIGHT.			
	Portland.		Natural.	
	Cement bbl.	Sand cu. yd.	Cement bbl.	Sand cu. yd.
1:0	7.59	0.00	8.05	0.00
1:1	4.24	0.63	4.99	0.56
1:2	2.89	0.87	3.54	0.79
1:3	2.17	0.97	2.70	0.91
1:4	1.69	1.01	2.12	0.95
1:5	1.38	1.02	1.74	0.98
1:6	1.11	1.04	1.49	1.00

Table B.1 Weigh Proportions of Cement and Sand for Mortar (Baker 1917)

Masonry:

Table B.2 Properties of Masonry Used for Specimen Strength Estimation

Compressive strength f_m' (psi)	6000
Initial elastic modulus E (psi)	1200000
Initial shear modulus G (psi)	480000
Fracture strength f_r' (psi)	40
Diagonal tensile strength f_{dt}' (psi)	197
Shear friction coefficient μ	0.5

Material supportive test

- i. Stone unit density: ASTM C97
- ii. Stone unit compressive strength: ASTM C170
- iii. Stone unit modulus of rupture: ASTM C99

- iv. Mortar block compressive strength: ASTM C109
- v. Masonry prism compressive strength: ASTM C1314
- vi. Masonry prism elastic modulus: ASTM E111
- vii. Masonry prism flexural bond strength: ASTM C1072
- viii. Masonry assemblage diagonal tensile strength: ASTM E519
- ix. In situ masonry mortar joint shear strength: ASTM C1531
- x. Masonry prism dynamic properties: ASTM C215

B.1.2 Dimensions

Specimen: Height = 144 in., Width = 54 in., Thickness = 18 in. (14175 lb.)

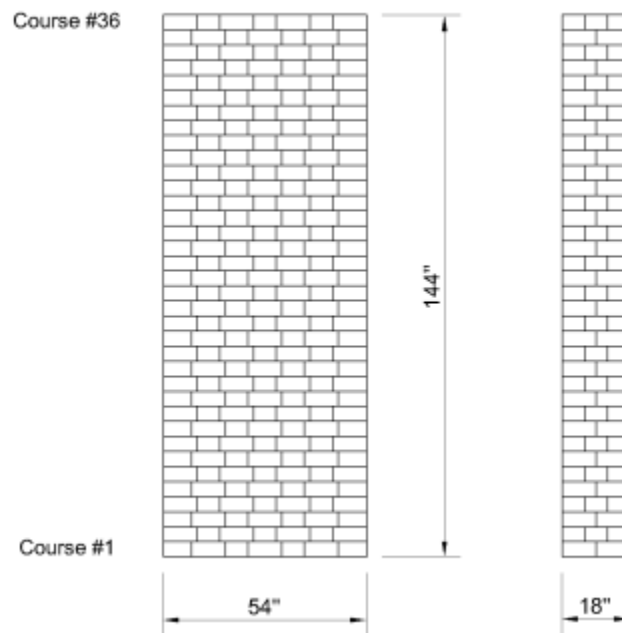


Figure B.1 Elevation and Lateral View of Specimen

Stone unit:

Table B.3 Types of Stone Units

Type	Dimension	Selfweight	Quantity per specimen
1	9 in. x 6 in. x 4 in.	20 lb.	527
2	9 in. x 7.5 in. x 4 in.	27 lb.	68

Type 1	Type 1	Type 1	Type 1	Type 1	Type 1	Type 1
Type 1		Type 1		Type 1		Type 1
Type 1	Type 1	Type 1	Type 1	Type 1	Type 1	Type 1

Figure B.2 Unit Layout in Courses with Even Numbers

Type 2	Type 1	Type 1	Type 1	Type 1	Type 1	Type 2
	Type 1		Type 1		Type 1	
Type 2	Type 1	Type 1	Type 1	Type 1	Type 1	Type 2

Figure B.3 Unit Layout in Courses with Odd Numbers

Courses: 36, Flemish bond

Mortar thickness: 3/8 in.

Testing matrix

Table B.4 Testing Matrix

Specimen	Load type	Load direction	Rail track	Retrofit method
1	monotonic	transverse	w/o	w/o
2	monotonic	longitudinal	w/o	w/o
3	cyclic	transverse	w/o	w/o
4	cyclic	longitudinal	w/o	w/o
5	cyclic	transverse	w/	w/o
6	cyclic	longitudinal	w/	w/o

7	cyclic	longitudinal	w/	w/
8	cyclic	transverse	w/	w/

Note: Loading direction shown in Figure B.4

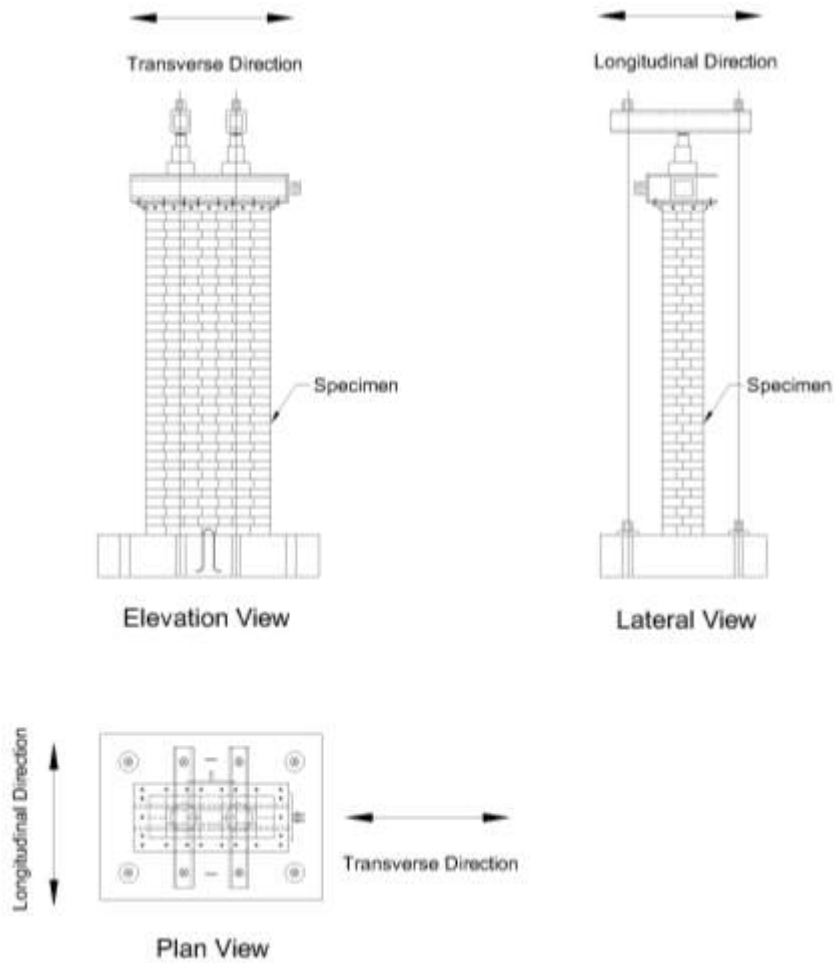
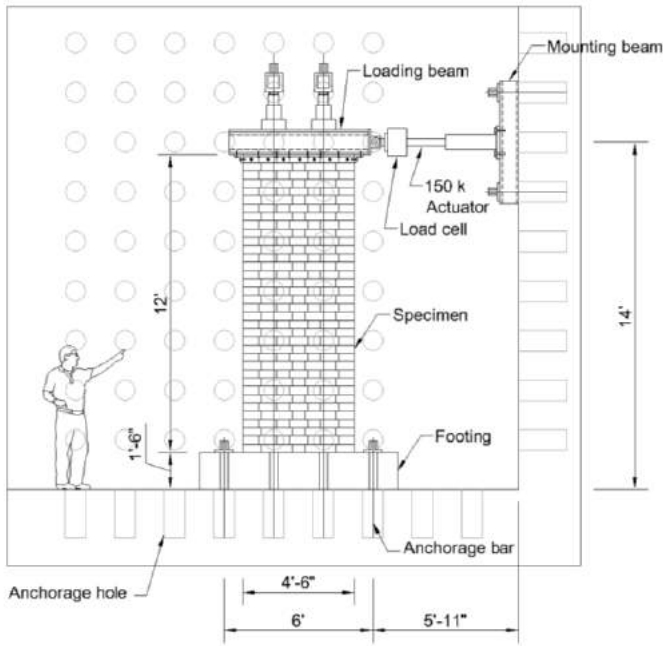
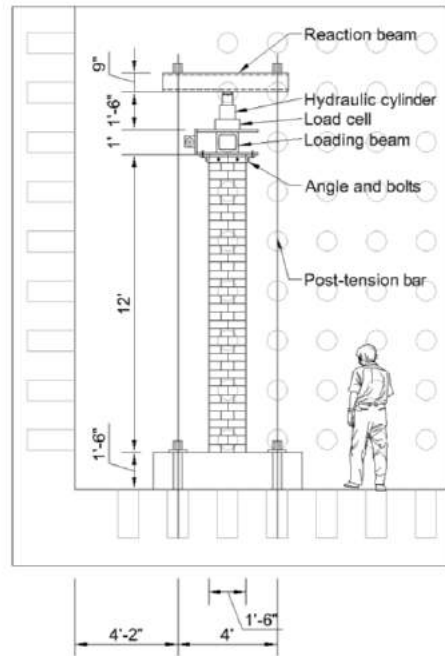


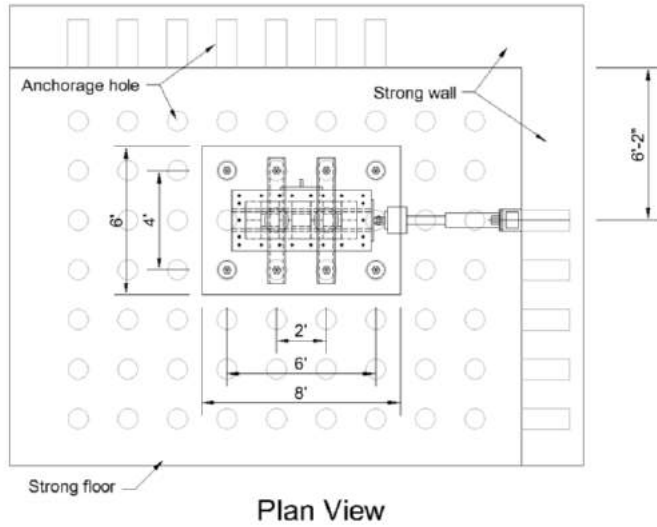
Figure B.4 Loading Direction



Elevation View

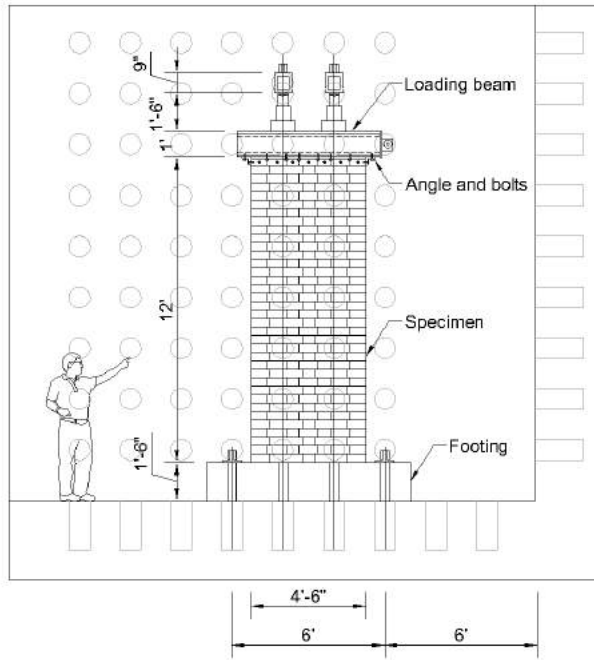


Lateral View

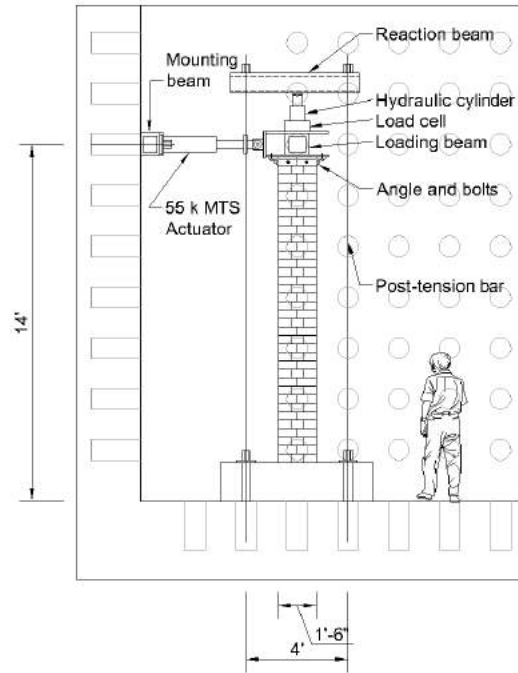


Plan View

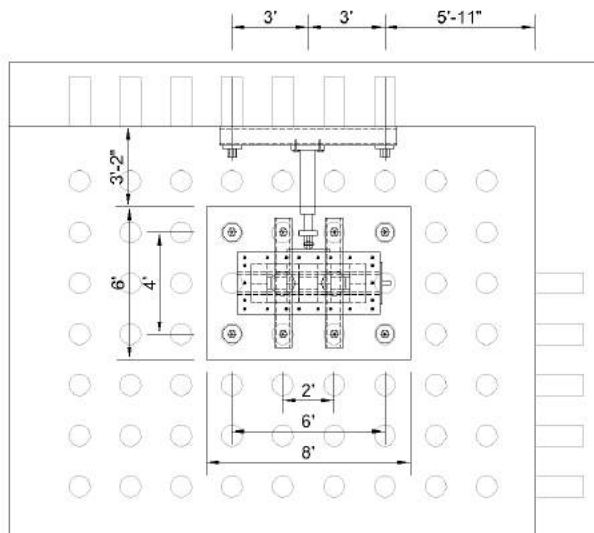
Figure B.5 Proposed Test Setup for Specimen 1 and 3



Elevation View

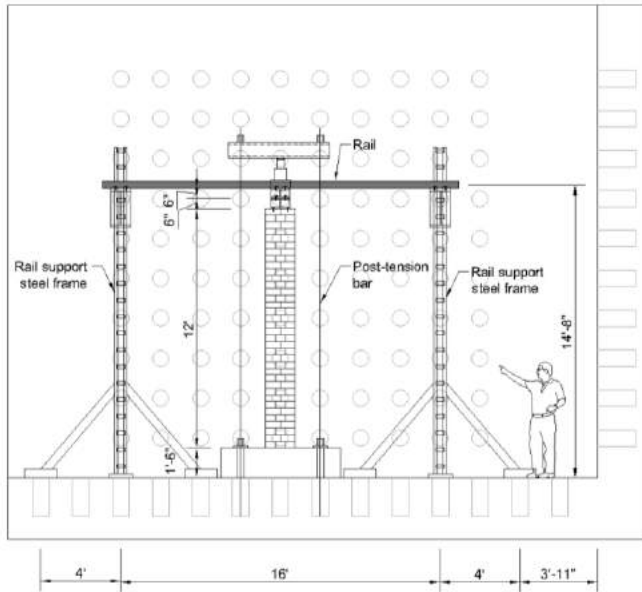


Lateral View

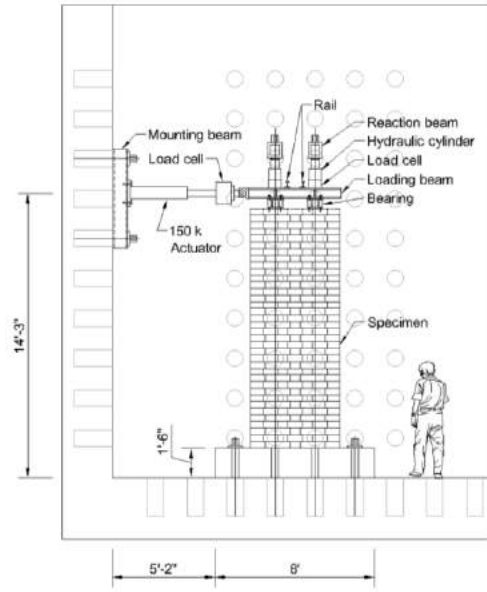


Plan View

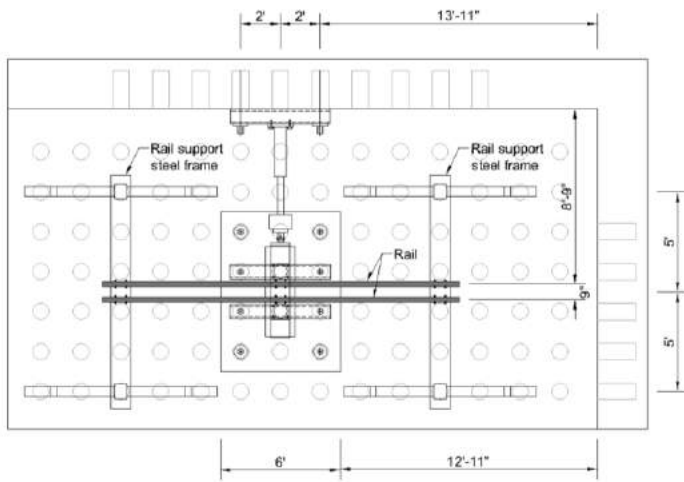
Figure B.6 Proposed Test Setup for Specimen 2 and 4



Elevation View

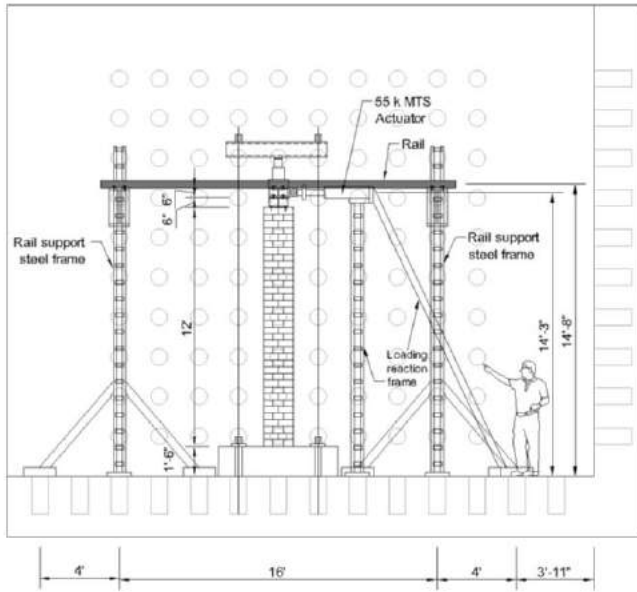


Lateral View

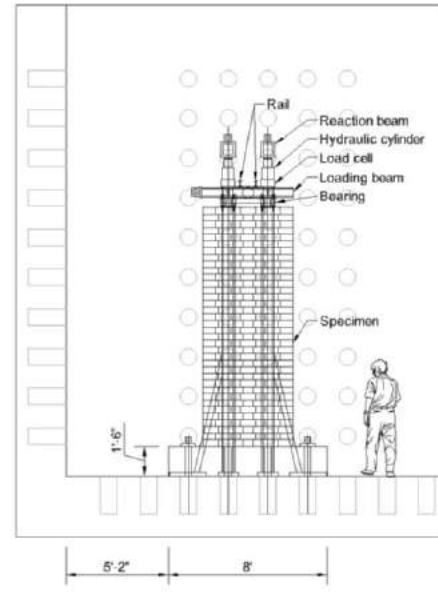


Plan View

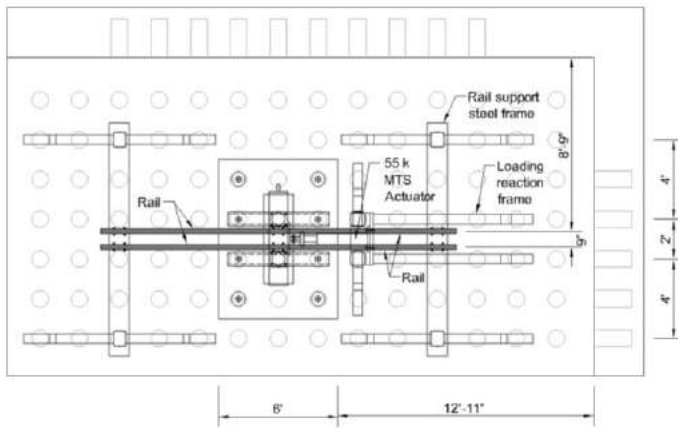
Figure B.7 Proposed Test Setup for Specimen 5



Elevation View



Lateral View



Plan View

Figure B.8 Proposed Test Setup for Specimen 6

Prediction of failure mode and strength of monotonic loading specimens

Table B.5 Estimated Failure Mode and Ultimate Strength of Specimen 1 and 2

Specimen	Failure mode and corresponding shear load		
	ACI530/TMS 402 (2012)	FEMA 356 (2000)	Effective pier model (Li et al., 2005)
1	Toe crushing, 155.8 k	Toe crushing, 50.5 k	Rocking/Toe crushing, 54.2 k
2	Toe crushing, 52.0 k	Toe crushing, 16.8 k	Rocking/Toe crushing, 18.1 k

Note: Axial load ratio = 0.05

B.2 Lateral Loading System

- Actuators: 55 k MTS actuator (longitudinal loading) and 150 k actuator (transverse loading)
- Load cell: 150 k compression/tension load cell
- Loading beam
- Reaction steel frame
- Strong wall
- Strong floor

B.3 Vertical Loading System

- Hydraulic cylinders: 60 ton and 36 ton ENERPAC hydraulic cylinder
- Load cells: two 100 k compression load cell
- Reaction steel frame
- Strong floor
- Post-tension bars

B.4 Bearing System

- Bearings

Anchor bolts -swedged anchor bolts with 3/4" in. diameter and 1 feet length are proposed to use.

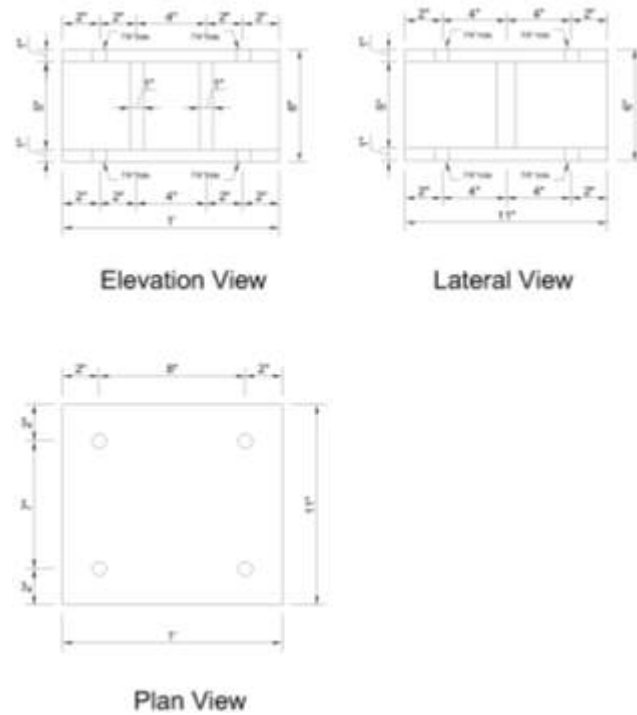


Figure B.9 Proposed Bearing for Specimen 5 and 6

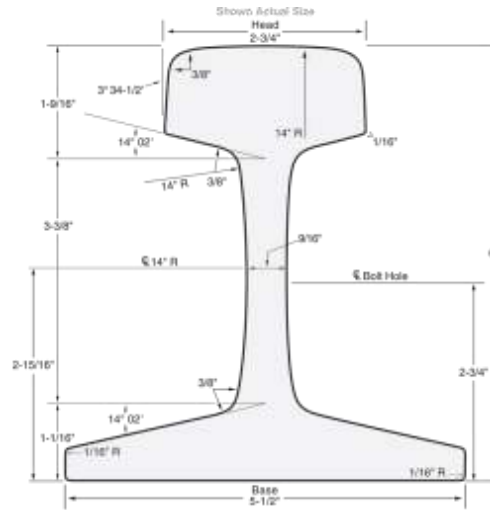
B.5 Rail System

- Rail tracks

The most commonly used rail is shown as **Figure B.10**. However, it may be excessively strong for this testing. Steel I beam which has smaller size and the same yield and ultimate tensile strength is proposed, as shown in **Figure B.11**.

- Spikes

The rail-spike system (**Figure B.12**) and the rail-fastening system (**Figure B.13**) are both used in the U.S. railroad system. During the period when the masonry railroad bridges were prevailing, the rail-spike system was the most commonly used. Spikes (carbon steel 6 3/4" Railroad Spikes) are proposed to be used in this testing as a connection between rail and rail support system.



Rail Type: 100 RA	Area in ² : 9.64
Section Number: 10020	Section Modulus in ³ : Head: 15.04
Nominal Weight: 100 lbs/yd	Base: 17.78
Standard Length: 39'	Moment of Inertia in ⁴ : 48.94
Standard Drilling: 2-11/16" X 5-1/2" with 1-3/16" dia. holes	
Joint Bar Length: 22'	
Joint Bar Weight: 54 lbs/pr with hardware: 62 lbs/pr	
Track Bolt: 1" X 5-1/2"	

Figure B.10 Dimension of commonly used rail (S-10020)
[\(http://harmersteel.com/catalog/tee-rails/100-lbyd-ara-a-rail/\)](http://harmersteel.com/catalog/tee-rails/100-lbyd-ara-a-rail/)

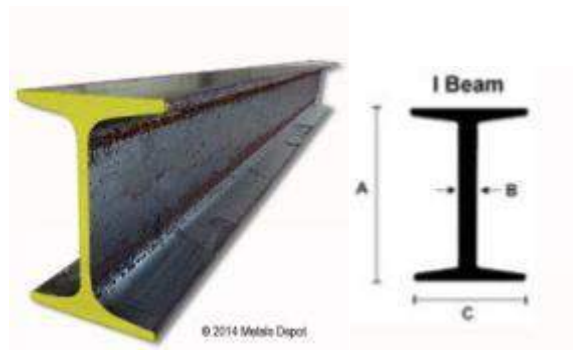


Figure B.11 A36/A572-50 Steel I Beam S 3 x 5.7 lb. (3.00" x .170" x 2.33")
<http://www.metalsdepot.com/products/hrsteel2.phtml?page=steel%20beam>

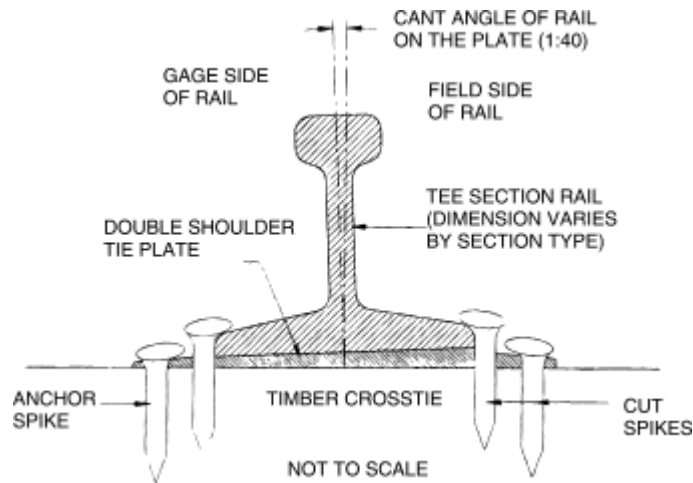


Figure B.12 Layout of common used rail-spike system

(http://www.allenrailroad.com/consulting/Railroad_Glossary.htm)

ASTM A499-89/Grade 50: tensile strength of 80 ksi min, yield strength of 50 ksi min.

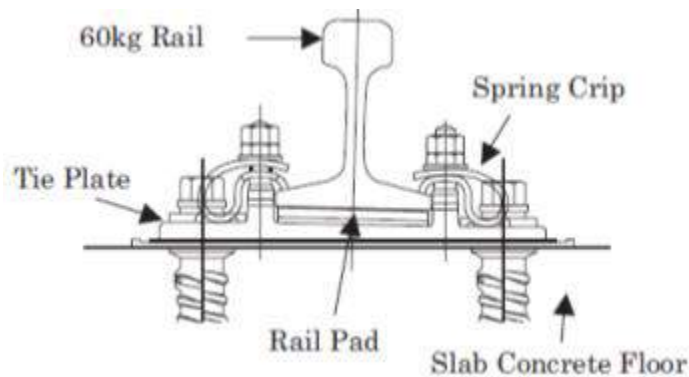


Figure B.13 Layout of commonly used rail-fastening system

- Rail support steel frame
- Strong floor

B.6 Footing and Anchorage System

- Reinforced concrete footings: thickness 1.5 ft x width 8 ft. x depth 6 ft (~10.8 kips or ~5 tons)
- Anchor bars: 1-3/8" diameter Dywidag steel bars
- Strong floor

B.7 Instrument System

The proposed instrument layout for the specimens is shown from **Figure B.14** to **Figure B.17**. It includes the following types of sensor. And the estimated quantities of each type sensor are listed from **Table B.6** to **Table B.9**.

- LVDT
- String potentiometer
- Strain gages
- DEMEC
- DAQ
- Camera and video recorder

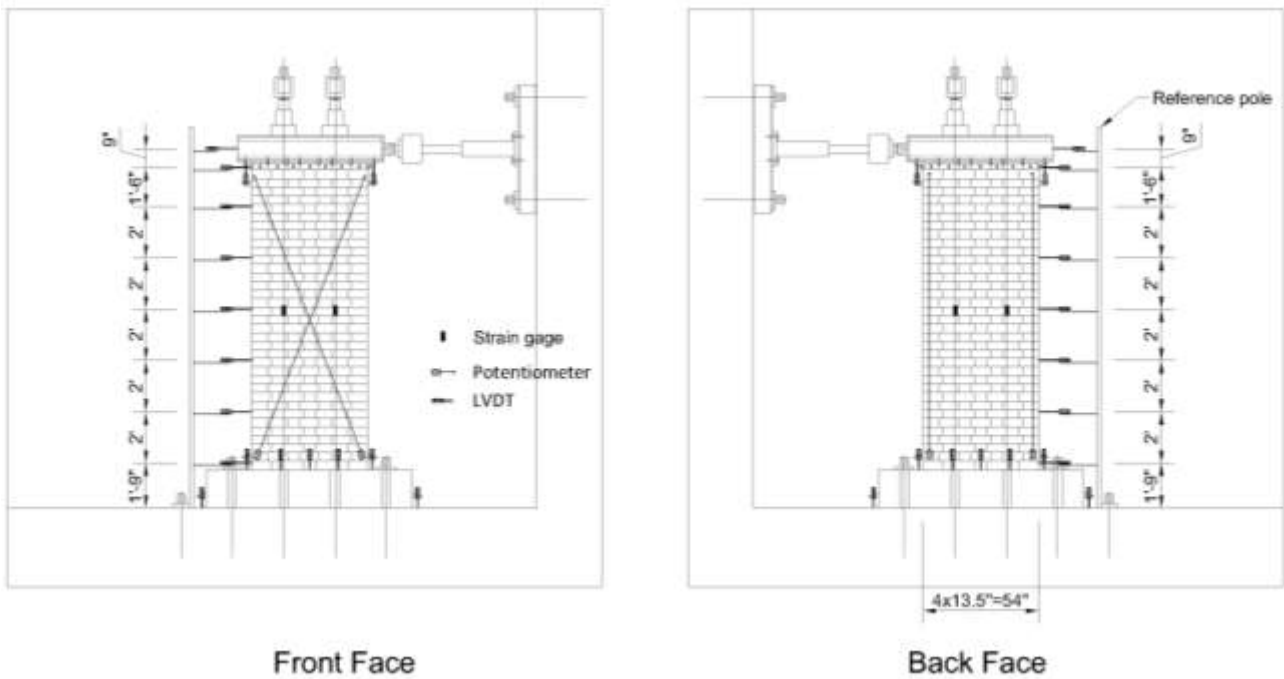


Figure B.14 Instrument Layout of Specimen 1 and 3

Table B.6 Instrument List (Specimen 1 and 3)

Instrument	Specification	Quantity
Stain gage	350 ohm quarter bridge	4
Potentiometer	50 in. measurement range	4

LVDT	± 3 in. measurement range	6
LVDT	± 1 in. measurement range	14

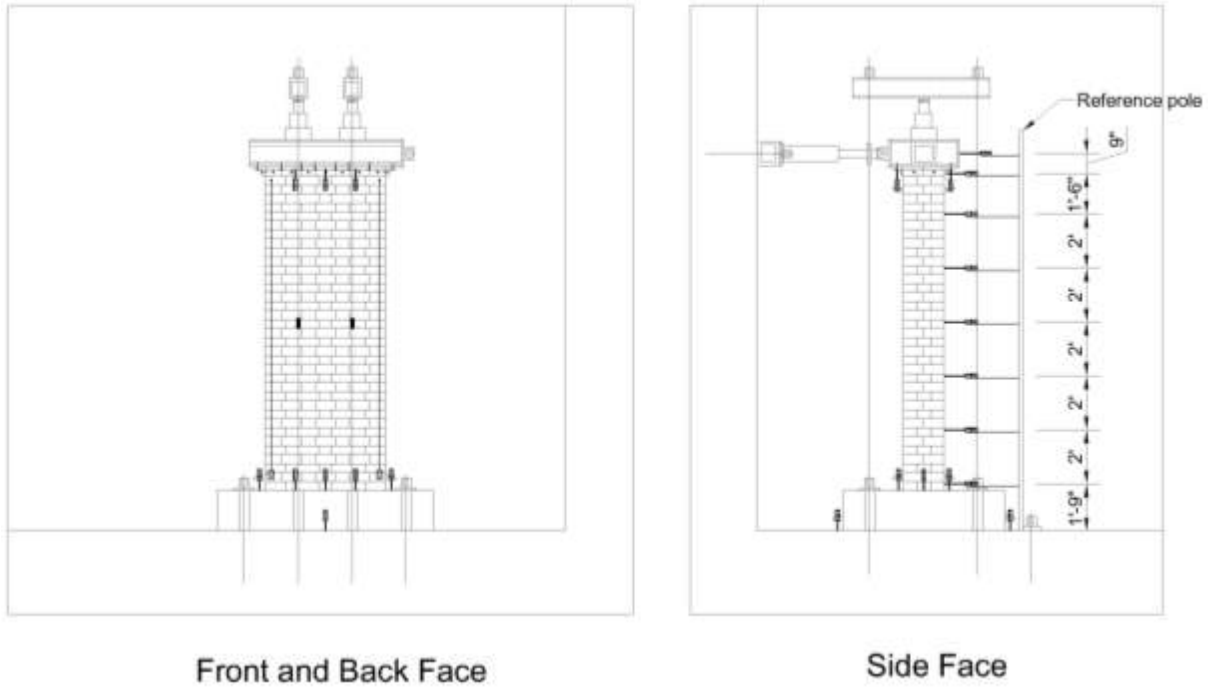


Figure B.15 Instrument Layout of Specimen 2 and 4

Table B.7 Instrument List (Specimen 2 and 4)

Instrument	Specification	Quantity
Stain gage	350 ohm quarter bridge	4
Potentiometer	50 in. measurement range	4
LVDT	± 3 in. measurement range	6
LVDT	± 1 in. measurement range	18

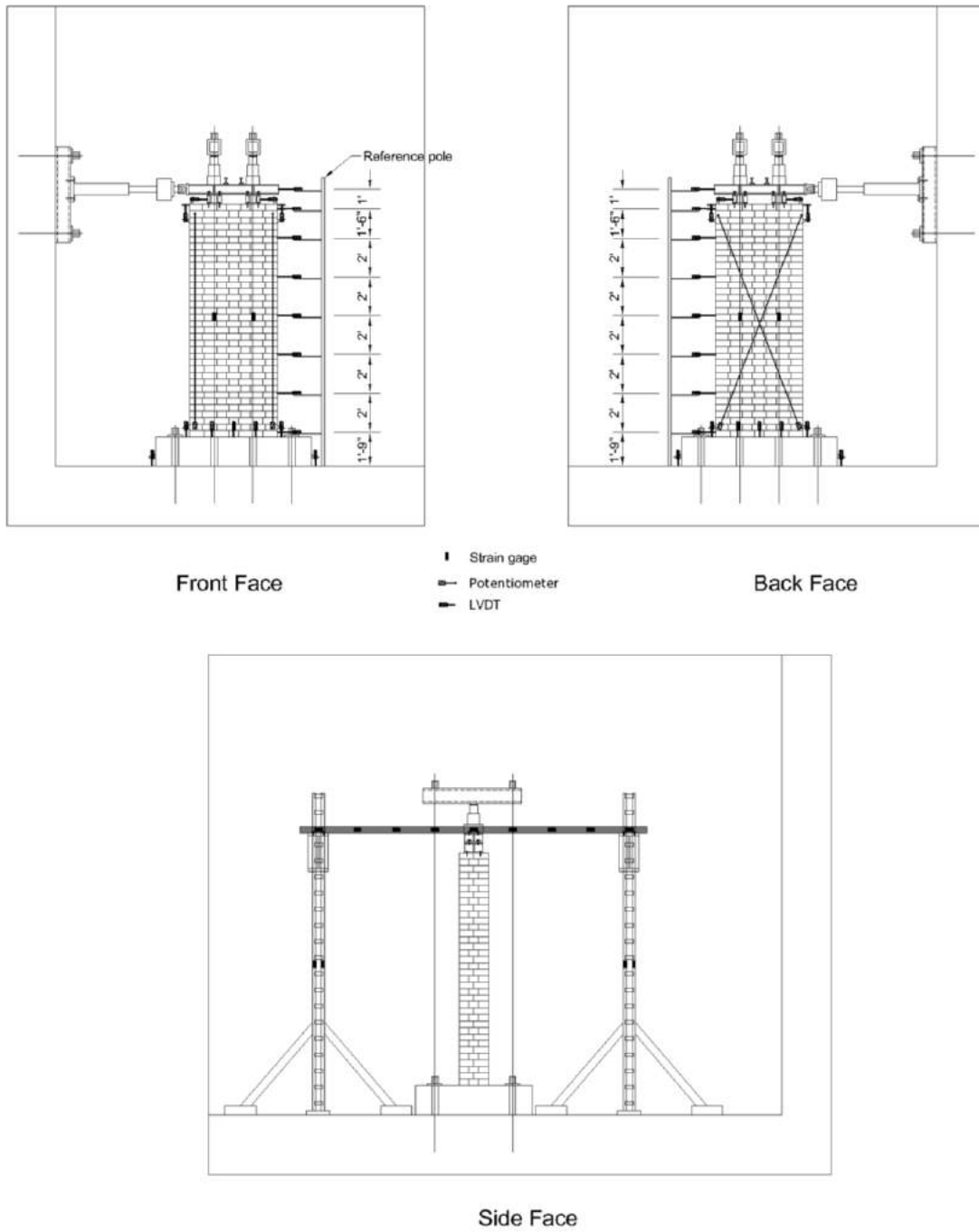


Figure B.16 Instrument Layout of Specimen 5

Table B.8 Instrument List (Specimen 5)

Instrument	Specification	Quantity
Stain gage	350 ohm quarter bridge	30
Potentiometer	50 in. measurement range	4
LVDT	± 3 in. measurement range	6
LVDT	± 1 in. measurement range	16

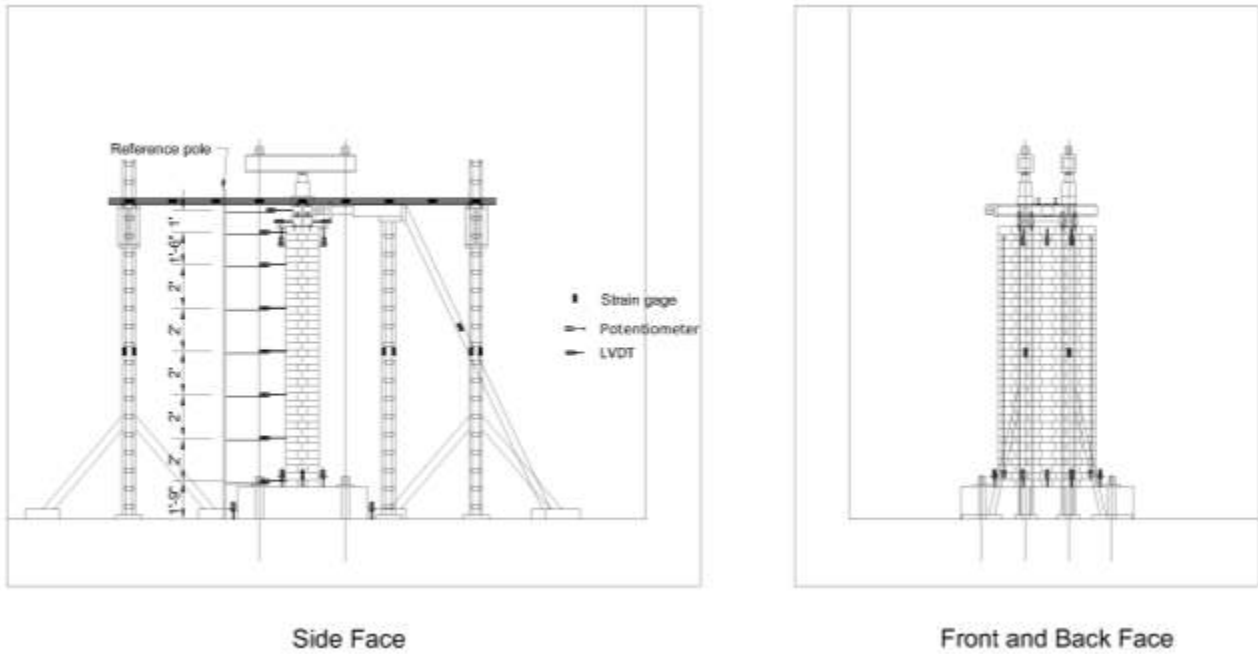


Figure B.17 Instrument Layout of Specimen 6

Table B.9 Instrument List (Specimen 6)

Instrument	Specification	Quantity
Stain gage	350 ohm quarter bridge	36
Potentiometer	50 in. measurement range	4
LVDT	±3 in. measurement range	6
LVDT	±1 in. measurement range	22

B.8 Loading Protocol

Proposed loading protocol is designed by conforming to FEMA 461 (Interim Testing Protocols or Determining the Seismic Performance Characteristics of Structural and Nonstructural Components). Detail considerations are listed below:

- a. At the lowest damage state at least six cycles must have been executed.
- b. The number of steps is generally equal or larger than 10.
- c. Each step consists of two cycles.
- d. Each cycle in the same step has the same amplitude.
- e. The amplitude a_{i+1} of the step $i+1$ is given by the following equation: $a_{i+1} = 1.4 a_i$

Thus, in this test, the ratios of the targeted deformation amplitude in each step to the targeted maximum deformation amplitude are proposed as shown in **Table B.10**. And the corresponding loading history diagram is shown in **Figure B.18**. The maximum deformation amplitude will be obtained in the monotonic tests.

Table B.10 Targeted Deformation Amplitude in Each Step

Step S_i	S1	S2	S3	S4	S5	S6	S7	S8	S9	S10	S11	S12	S13
a_i/a_{max}	0.018	0.025	0.035	0.048	0.068	0.095	0.133	0.186	0.26	0.364	0.51	0.714	1

Note: a_i – targeted amplitude of deformation at the i th step (in)

a_{max} – targeted maximum amplitude of deformation (in)

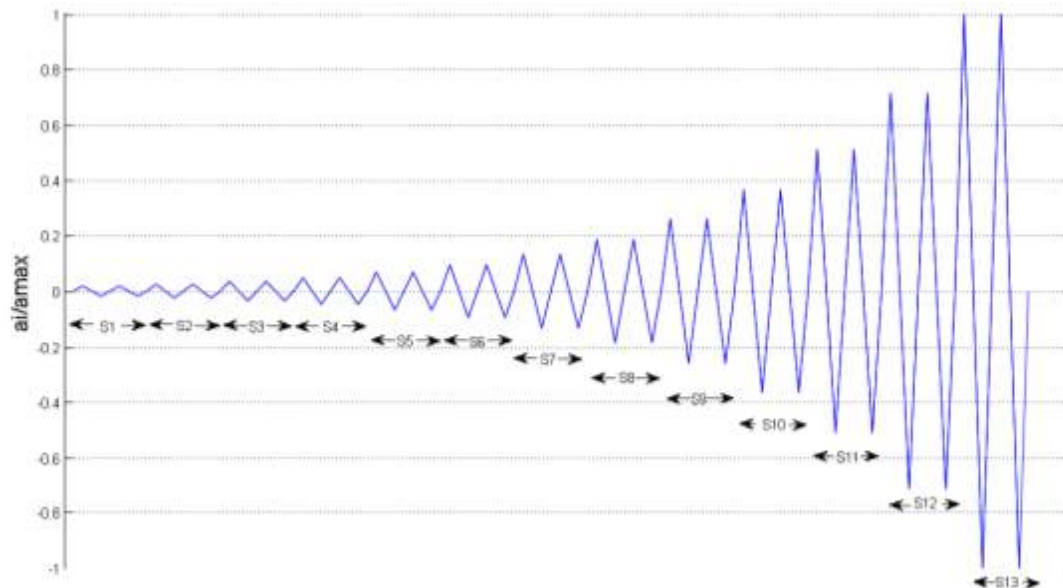


Figure B.18 Proposed Loading History

If the specimen has not reached the final damage state at a_{max} , the amplitude shall be increased further by the constant increment $0.3 a_{max}$.

B.9 Prototype Pier

The Illinois Central Railroad Cairo Bridge was constructed in 1889 and experienced rehabilitation from 1949 to 1952. The piers of this bridge represent most of the railroad piers built from 1880 to 1930. The bridge drawings are accessible from a report about the rehabilitation project aforementioned (Modjeski and Masters 1953).

The elevation and lateral views of a pier of this bridge are shown in **Figure B.19**. The height of the pier is 177 feet. The width varies from 35 feet (at the top) to 60 feet (at the base). The thickness is various from 12 feet (at the top) to 24 feet (at the base).

The layout of the masonry courses is shown in **Figure B.20**. The dimension of single stone unit is 84 in. (length) by 56 in. (depth) by 24 in. (thickness).

The sample test data of the compressive strength of material are shown in **Table B.11**. The average compressive strength of stone samples is 7176 psi. The average compressive strength of mortar samples is 4243 psi.

The bearing used for this bridge is shown in **Figure B.21** and **Figure B.22**. Four swedged anchor bolts with a 1-1/2 in. diameter and 4.5 feet in length were used for each bearing in the Cairo Railroad Bridge.

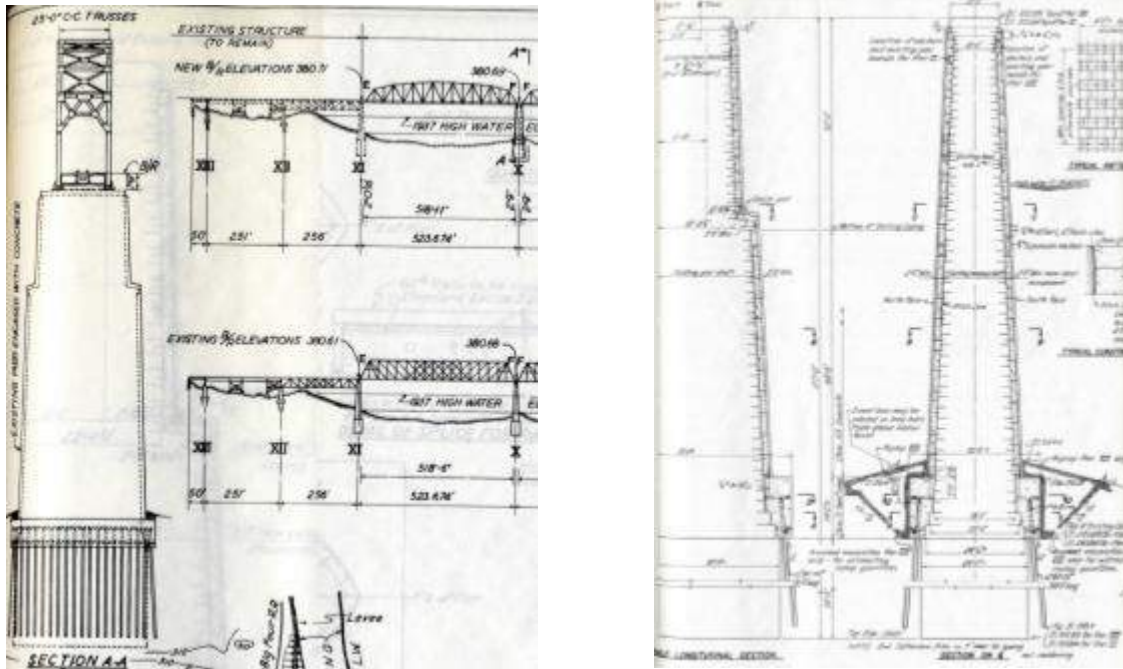


Figure B.19 Elevation and Lateral Views of a Pier of Cairo Railroad Bridge

REFERENCES

- Baker, I. O. (1917). *A treatise on masonry construction*, J. Wiley & Sons, New York.
- FEMA (2000). *Prestandard and Commentary for the Seismic Rehabilitation of Buildings*, FEMA 356, Federal Emergency Management Agency.
- FEMA (2007). *Interim Protocols for Determining Seismic Performance Characteristics of Structural and Nonstructural Components Through Laboratory Testing*, FEMA 461, Federal Emergency Management Agency.
- Modjeski and Masters (1953). *Final report on reconstruction, Illinois Central Railroad Cairo bridge over the Ohio River*, Modjeski and Masters, Harrisburg, PA.
- The Masonry Society, ACI, and ASCE (2013). "Building Code Requirements and Specification for Masonry Structures and Companion Commentaries." *ACI 530/530.1-13*, Boulder, Co.; Farmington Hills, Mi.; Reston, Va.
- Yi, T., Moon F.L., Leon, R.T. and Kahn L.F. (2005). Effective pier model for the nonlinear in-plane analysis of individual URM piers. *The Masonry Society Journal*, 23.

**APPENDIX C. SUMMARY OF PREVIOUS EXPERIMENTAL STUDIES ON
BRIDGE BEARING**

No.	Reference	Bearing Type	Model ratio	Material	Specimens	Loading
1	Steelman et al. (2013)	Steel low-profile fixed bearings in Highway bridges (ILDOT bearings)	1:1	M270 Grade 36 steel	1 with weak anchors under longitudinal loading 1 with weak anchors under transverse loading 1 with weak pintles under longitudinal loading 1 with weak pintles under transverse loading	Horizontal quasi-static cyclic loading
2	Fan and McCormic (2014)	Steel rocker and bolster bearings with corrosion in old highway bridges in MI	1:1	ASTM A36 steel	4 with different corrosion-level under longitudinal loading 4 with different corrosion-level under transverse loading	Monotonic loading
					6 with different corrosion-level under longitudinal loading 6 with different corrosion-level under transverse loading	Horizontal quasi-static cyclic loading
3	Mander et al. (1996)	Steel low-type sliding bearings, high-type rocker bearings, low-type fixed bearings and high-type fixed bearings	1:1	Not found	43 bearing specimens	Horizontal quasi-static cyclic loading

No.	Reference	Bearing Type	Model ratio	Material	Specimens	Loading
		retrieved from two old highway bridges in NY				
4	Hite et al. (2008)	Steel pedestals in highway bridges (GADOT bearings)	1:1	ASTM A36 steel	2 short pedestals (0.5 m height) with longitudinal and transverse loading direction 4 long pedestals (0.85 m height) with longitudinal and transverse loading direction and different anchor bolts layout	Horizontal quasi-static cyclic loading
5	Barker and Hartnagel (1998)	Old steel rocker bearings (Missouri Type D bearings) in an as-received condition obtained from two bridges in MO	1:1	Not found	4 specimens, 2 of them with one anchor bolt layout, 2 of them with another bolt layout	Monotonic loading
					11 specimens, they are varied with corrosion levels and anchor bolts layout	Horizontal quasi-static cyclic loading
6	Maragakis et al. (2001)	Steel high-seat-type rocker bearings in a ballasted railroad bridge in CA	1:1	Not found	1 full-scale two-span ballasted railroad bridge with four steel high-seat-type rocker bearings at both ends of abutment-bridge connections	Monotonic loading to the abutment-bridge connections at both ends

REFERENCES

- Barker, M., and Hartnagel, B. (1998). "Longitudinal Restraint Response of Existing Bridge Bearings." *Transportation Research Record: Journal of the Transportation Research Board*, 1624, 28-35.
- Fan, X. (2014). "Characterization of the Cyclic Behavior of Corroded Steel Bridge Bearings and their Influence on Seismic Bridge Performance." Ph.D. Dissertation, University of Michigan.
- Hite, M., DesRoches, R., and Leon, R. (2008). "Full-Scale Tests of Bridge Steel Pedestals." *Journal of Bridge Engineering*, 13(5), 483-491.
- Mander, J. B., Kim, D. K., Chen, S. S., and Premus, G. J. (1996). "Response of Steel Bridge Bearings to Reversed Cyclic Loading." *Technical Report NCEER-96-0014*, National Center for Earthquake Engineering Research, Buffalo, N.Y.
- Steelman, J., Filipov, E., Fahnestock, L., Revell, J., LaFave, J., Hajjar, J., and Foutch, D. (2013). "Experimental Behavior of Steel Fixed Bearings and Implications for Seismic Bridge Response." *Journal of Bridge Engineering*, 19(8), A4014007.

APPENDIX D. TEAM MEMBERS

Qiang Gui

PhD Student

The University of Tennessee

Dept. of Civil & Environmental Engineering

324 John D Tickle Bldg.

Knoxville, TN 37996-2313

Phone: (865)438-9043

E-mail: qgui@vols.utk.edu

Dr. Z. John Ma

Professor

The University of Tennessee

Dept. of Civil & Environmental Engineering

313 John D Tickle Bldg.

Knoxville, TN 37996 - 2313

Phone: (865) 974-7276

E-mail: zma2@utk.edu

Dr. Richard M. Bennett

Professor and Director of Engineering
Fundamentals

The University of Tennessee

Dept. of Civil & Environmental Engineering

207C Perkins Hall

Knoxville, TN 37996-4133

Phone: (865)974-9810

E-mail: rbennet2@utk.edu

Dr. David B. Clarke

Director, Research Associate Professor
The University of Tennessee

Center for Transportation Research

309 Conference Center Bldg.

Knoxville, TN 37996-4133

Phone: (865)974-1812

Fax: (865)974 -3889

E-mail: dclarke@utk.edu